



**NAVAL  
POSTGRADUATE  
SCHOOL**

**MONTEREY, CALIFORNIA**

**THESIS**

**VALIDATION OF HIGH FREQUENCY RADAR USED IN  
OCEAN SURFACE CURRENT MAPPING VIA IN-SITU  
DRIFTING BUOYS**

by

George Wright

September 2008

Thesis Advisor:

Jeffrey D. Paduan

Second Reader:

Mary L. Batteen

**Approved for public release; distribution is unlimited**

THIS PAGE INTENTIONALLY LEFT BLANK

<b>REPORT DOCUMENTATION PAGE</b>			<i>Form Approved OMB No. 0704-0188</i>
Public reporting burden for this collection of information is estimated to average 1 hour per response, including the time for reviewing instruction, searching existing data sources, gathering and maintaining the data needed, and completing and reviewing the collection of information. Send comments regarding this burden estimate or any other aspect of this collection of information, including suggestions for reducing this burden, to Washington headquarters Services, Directorate for Information Operations and Reports, 1215 Jefferson Davis Highway, Suite 1204, Arlington, VA 22202-4302, and to the Office of Management and Budget, Paperwork Reduction Project (0704-0188) Washington DC 20503.			
<b>1. AGENCY USE ONLY (Leave blank)</b>	<b>2. REPORT DATE</b> September 2008	<b>3. REPORT TYPE AND DATES COVERED</b> Master's Thesis	
<b>4. TITLE AND SUBTITLE</b> Validation of High Frequency Radar used in Ocean Surface Current Mapping via in-situ Drifter Buoys		<b>5. FUNDING NUMBERS</b>	
<b>6. AUTHOR(S)</b> George Wright		<b>8. PERFORMING ORGANIZATION REPORT NUMBER</b>	
<b>7. PERFORMING ORGANIZATION NAME(S) AND ADDRESS(ES)</b> Naval Postgraduate School Monterey, CA 93943-5000		<b>10. SPONSORING/MONITORING AGENCY REPORT NUMBER</b>	
<b>9. SPONSORING /MONITORING AGENCY NAME(S) AND ADDRESS(ES)</b> N/A		<b>11. SUPPLEMENTARY NOTES</b> The views expressed in this thesis are those of the author and do not reflect the official policy or position of the Department of Defense or the U.S. Government.	
<b>12a. DISTRIBUTION / AVAILABILITY STATEMENT</b> Approved for public release, distribution is unlimited		<b>12b. DISTRIBUTION CODE</b>	
<b>13. ABSTRACT</b> High frequency (HF) radar and its application to mapping ocean surface currents is a relatively new field of study in oceanography. Nevertheless, this scientific field produces real, tangible, accurate real-time results readily available to the military operational planner. The information gained through this process aids in the planning and execution of littoral operations via the development of the battle-space environment. Additionally, commercial use of this information can aide in the containment of coastal oil spills, efforts in search and rescue, and the execution of coastal engineering projects. Indeed, the utilization of High Frequency radar in the ocean environment has many beneficial qualities used by a wide variety of organizations. This study focuses on the validation aspects of High Frequency radar through the use of four drifters placed in-situ from 23-27 January 2008 on the Central California Coast from Monterey to San Francisco. A second experiment was conducted from 01-10 April 2008 involving 32 drifters placed west of the San Francisco Bay. Various statistical comparisons of radial current velocity data from 12 CODAR (Coastal Ocean Dynamics Application Radar) stations to the radial velocity data of each of the drifters will be analyzed.			
<b>14. SUBJECT TERMS</b> HF Radar, Ocean surface current, Validation, Drifter Buoys		<b>15. NUMBER OF PAGES</b> 110	
		<b>16. PRICE CODE</b>	
<b>17. SECURITY CLASSIFICATION OF REPORT</b> Unclassified	<b>18. SECURITY CLASSIFICATION OF THIS PAGE</b> Unclassified	<b>19. SECURITY CLASSIFICATION OF ABSTRACT</b> Unclassified	<b>20. LIMITATION OF ABSTRACT</b> UU

THIS PAGE INTENTIONALLY LEFT BLANK

**Approved for public release; distribution is unlimited**

**VALIDATION OF HIGH FREQUENCY RADAR USED IN OCEAN SURFACE  
CURRENT MAPPING VIA IN-SITU DRIFTING BUOYS**

George C. Wright  
Commander, United States Navy  
B.A., University of North Carolina at Chapel Hill, 1992

Submitted in partial fulfillment of the  
requirements for the degree of

**MASTER OF SCIENCE IN PHYSICAL OCEANOGRAPHY**

from the

**NAVAL POSTGRADUATE SCHOOL  
September 2008**

Author: George C. Wright

Approved by: Jeffrey D. Paduan  
Thesis Advisor

Mary L. Batteen  
Second Reader

Mary L. Batteen  
Chairman, Department of Oceanography

THIS PAGE INTENTIONALLY LEFT BLANK

## ABSTRACT

High frequency (HF) radar and its application to mapping ocean surface currents is a relatively new field of study in oceanography. Nevertheless, this scientific field produces real, tangible, accurate real-time results readily available to the military operational planner. The information gained through this process aids in the planning and execution of littoral operations via the description of the battle-space environment. Additionally, commercial use of this information can aid in the containment of coastal oil spills, efforts in search and rescue, and the execution of coastal engineering projects. Indeed, the utilization of High Frequency radar in the ocean environment has many beneficial qualities used by a wide variety of organizations.

This study focuses on the validation aspects of High Frequency radar through the use of four drifters placed in-situ from 23-27 January 2008 on the Central California Coast from Monterey to San Francisco. A second experiment was conducted from 01-10 April 2008 involving 32 drifters placed west of the San Francisco Bay. Various statistical comparisons of radial current velocity data from 12 CODAR (Coastal Ocean Dynamics Application Radar) stations to the radial velocity data of each of the drifters are analyzed.

CODAR type HF radar validated through the use of Lagrangian drifters is documented throughout this study. Specific results document a robust correlation between in-situ measurements and surface current velocity vectors produced via the CODAR system suite. With the exception of COMM data in the first experiment, the RMS differences of the measured patterns had a reasonable spread of between 9.0 cm/s to upwards of 19.124 cm/s. In the second experiment, RMS differences ranged from 9.8 cm/s to 15.9 cm/s.

THIS PAGE INTENTIONALLY LEFT BLANK

# TABLE OF CONTENTS

<b>I.</b>	<b>INTRODUCTION.....</b>	<b>1</b>
<b>A.</b>	<b>HIGH FREQUENCY RADAR.....</b>	<b>1</b>
<b>B.</b>	<b>EVALUATION OF CODAR SEASONDE HF RADAR ON THE CENTRAL CALIFORNIA COAST .....</b>	<b>2</b>
<b>1.</b>	<b>Use of Drifters in Validation Study .....</b>	<b>4</b>
<b>II.</b>	<b>DATA COLLECTION.....</b>	<b>7</b>
<b>A.</b>	<b>HIGH FREQUENCY RADAR.....</b>	<b>7</b>
<b>B.</b>	<b>DRIFTER.....</b>	<b>8</b>
<b>III.</b>	<b>DATA ANALYSIS AND RESULTS.....</b>	<b>11</b>
<b>A.</b>	<b>HIGH FREQUENCY RADAR COMPARED TO DRIFTER DATA .....</b>	<b>11</b>
<b>B.</b>	<b>EXPERIMENT NUMBER TWO RESULTS.....</b>	<b>13</b>
<b>1.</b>	<b>Scatter Plot of Radial Data.....</b>	<b>13</b>
<b>2.</b>	<b>Effect of Radar Angular Aspect .....</b>	<b>14</b>
<b>3.</b>	<b>Effect of Drifter and Radar Standard Deviation .....</b>	<b>15</b>
<b>4.</b>	<b>Effect of Temporal Quality .....</b>	<b>16</b>
<b>5.</b>	<b>Effect of Radar Point Distance to the Radar Site .....</b>	<b>18</b>
<b>6.</b>	<b>Effect of the Number of Drifters that Matched within the Two- Kilometer Filter.....</b>	<b>19</b>
<b>7.</b>	<b>Effect of RMS Distance of Matched Drifters within the Two- Kilometer Filter.....</b>	<b>19</b>
<b>8.</b>	<b>Effect of Drifter Standard Deviation.....</b>	<b>20</b>
<b>9.</b>	<b>Overall Summary of Combined Radar Site Data .....</b>	<b>20</b>
<b>C.</b>	<b>EXPERIMENT NUMBER ONE RESULTS.....</b>	<b>21</b>
<b>1.</b>	<b>Scatter Plot of Radial Data.....</b>	<b>21</b>
<b>2.</b>	<b>Effect of Radar Angular Aspect .....</b>	<b>22</b>
<b>3.</b>	<b>Effect of Drifter and Radar Standard Deviation .....</b>	<b>23</b>
<b>4.</b>	<b>Effect of Radar Point Distance to the Radar Site .....</b>	<b>24</b>
<b>5.</b>	<b>Effect of the Number of Drifters that Matched within the Two Kilometer Filter.....</b>	<b>24</b>
<b>6.</b>	<b>Effect of RMS Distance of Matched Drifters within the Two Kilometer Filter.....</b>	<b>25</b>
<b>7.</b>	<b>Effect of Drifter Standard Deviation.....</b>	<b>25</b>
<b>8.</b>	<b>Overall Summary of Combined Radar Site Data .....</b>	<b>25</b>
<b>IV.</b>	<b>SUMMARY .....</b>	<b>27</b>
<b>V.</b>	<b>APPENDIX.....</b>	<b>31</b>
	<b>LIST OF REFERENCES.....</b>	<b>85</b>
	<b>INITIAL DISTRIBUTION LIST .....</b>	<b>87</b>

THIS PAGE INTENTIONALLY LEFT BLANK

## LIST OF FIGURES

Figure 1.	The SeaSonde measurement system includes a transmit chassis and receive chassis. The MUSIC algorithm processes the radar returns to provide hourly radial velocity reports.....	31
Figure 2.	The HF radar antenna suite for the SeaSonde system off the California Coast, consisting of a crossed loop and monopole receive antenna (left) and a monopole transmit antenna (right). .....	31
Figure 3.	Plot of drifter tracks obtained during both experiments. The first experiment was conducted from 23-27 January 2008 using four drifters and is shown in blue. A second experiment was conducted from 1-10 April 2008 using 32 drifters and is shown in black. HF radar station locations and their 4 letter identifiers are shown as well. ....	32
Figure 4.	Deployment of the Pacific Gyre Microstar drifter. The surface float contains the telemetry system, antenna, batteries and sensors. Drifter positions are calculated by an onboard Global Positioning System (GPS) receiver that records and transmits a position every 10 minutes. ....	32
Figure 5.	Collapsible Nylon drogue shown with depth centered at approximately one meter.....	33
Figure 6.	Research vessel <i>Point Sur</i> (top left) was used in Experiment One. Research vessels <i>John H. Martin</i> (top right) and <i>Mussel Point</i> (bottom) were used during Experiment Two. All were used to deploy and retrieve the drifters. ....	33
Figure 7.	Representation of the spatial scale used in drifter/radial calculations. Section of FORT radial pattern shown in area of a majority of Experiment Two drifter tracks. A two kilometer filter (blue circle(s)) limits the closest drifter tracks to each respective radar point (red dot) used in velocity comparisons. Only four circular filters shown here to exhibit no gaps in coverage. ....	34
Figure 8.	Example of how a representative radar / drifter calculation was made. For each hourly radar point (only one 0200Z radar point highlighted/described here), drifter tracks corresponding to plus or minus 30 minutes and less than 2km away are captured (magenta points inside blue circle). This example has 14 total drifter matches. This process is done for each of the radar points in each hourly report, for each station. ....	34
Figure 9.	Representation of the drifter speeds shown during Experiment One. This experiment exhibited excellent angular aspects with a wide variety of speed regimes. Spatial coverage around a specific radar point was deficient here.....	35
Figure 10.	Representation of the drifter speeds shown during Experiment Two. This experiment exhibited excellent spatial coverage within a limited area with moderate speed regimes.....	35

Figure 11.	Typical measured radar patterns showing ocean coverage for DRAK, COMM, SLID and FORT, respectively. First experiment drifter tracks are shown in blue and second experiment drifter tracks are shown in magenta....	36
Figure 12.	Typical measured radar patterns showing ocean coverage for MONT, PILR, PESC and BIGC (ideal pattern), respectively. First experiment drifter tracks are shown in blue and second experiment drifter tracks are shown in magenta. ....	37
Figure 13.	Scatter Plot of Drifter Radial Velocity vs. Radar Radial Velocity for Radar Sites DRAK, COMM and SLID respectively (Second Experiment). Measured Radar Patterns are shown on the left and Ideal Radar Patterns are shown on the right. Dashed line represents one to one correlation and red solid line represents the linear least squares fit of the data. The standard deviation value refers to the best fit line. ....	38
Figure 14.	Scatter Plot of Drifter Radial Velocity vs. Radar Radial Velocity for Radar Sites FORT, MONT and PILR, respectively (Second Experiment). Measured Radar Patterns are shown on the left and Ideal Radar Patterns are shown on the right. Dashed line represents one to one correlation and red solid line represents the linear least squares fit of the data. The standard deviation value refers to the best fit line. ....	39
Figure 15.	Scatter Plot of Drifter Radial Velocity vs. Radar Radial Velocity for Radar Sites PESC and BIGC, respectively (Second Experiment). Bottom graph is a combined plot of all Radar Sites. Measured Radar Patterns are shown on the left and Ideal Radar Patterns are shown on the right. Dashed line represents one to one correlation and red solid line represents the linear least squares fit of the data. The standard deviation value refers to the best fit line. ....	40
Figure 16.	Correlation Coefficient and RMS difference plots vs. DRAK Radar Look Angle (top) and corresponding Drifter and Radial Standard Deviation plots vs. DRAK Radar Look Angle (middle). Bold lines represent measured data and thin lines represent ideal data. The lower plot indicates the number of drifter/radar point matches/observations that occurred vs. DRAK Radar Look Angle. The thin blue bar represents the measured pattern and the wide yellow bar represents the ideal pattern. Second experiment only. ....	41
Figure 17.	Correlation Coefficient and RMS difference plots vs. COMM Radar Look Angle (top) and corresponding Drifter and Radial Standard Deviation plots vs. COMM Radar Look Angle (middle). Bold lines represent measured data and thin lines represent ideal data. The lower plot indicates the number of drifter/radar point matches/observations that occurred vs. COMM Radar Look Angle. The thin blue bar represents the measured pattern and the wide yellow bar represents the ideal pattern. Second experiment only. ....	42
Figure 18.	Correlation Coefficient and RMS difference plots vs. SLID Radar Look Angle (top) and corresponding Drifter and Radial Standard Deviation plots vs. SLID Radar Look Angle (middle). Bold lines represent	

	measured data and thin lines represent ideal data. The lower plot indicates the number of drifter/radar point matches/observations that occurred vs. SLID Radar Look Angle. The thin blue bar represents the measured pattern and the wide yellow bar represents the ideal pattern. Second experiment only. ....	43
Figure 19.	Correlation Coefficient and RMS difference plots vs. FORT Radar Look Angle (top) and corresponding Drifter and Radial Standard Deviation plots vs. FORT Radar Look Angle (middle). Bold lines represent measured data and thin lines represent ideal data. The lower plot indicates the number of drifter/radar point matches/observations that occurred vs. FORT Radar Look Angle. The thin blue bar represents the measured pattern and the wide yellow bar represents the ideal pattern. Second experiment only. ....	44
Figure 20.	Correlation Coefficient and RMS difference plots vs. MONT Radar Look Angle (top) and corresponding Drifter and Radial Standard Deviation plots vs. MONT Radar Look Angle (middle). Bold lines represent measured data and thin lines represent ideal data. The lower plot indicates the number of drifter/radar point matches/observations that occurred vs. MONT Radar Look Angle. The thin blue bar represents the measured pattern and the wide yellow bar represents the ideal pattern. Second experiment only. ....	45
Figure 21.	Correlation Coefficient and RMS difference plots vs. PILR Radar Look Angle (top) and corresponding Drifter and Radial Standard Deviation plots vs. PILR Radar Look Angle (middle). Bold lines represent measured data and thin lines represent ideal data. The lower plot indicates the number of drifter/radar point matches/observations that occurred vs. PILR Radar Look Angle. The thin blue bar represents the measured pattern and the wide yellow bar represents the ideal pattern. Second experiment only. ....	46
Figure 22.	Correlation Coefficient and RMS difference plots vs. PESC Radar Look Angle (top) and corresponding Drifter and Radial Standard Deviation plots vs. PESC Radar Look Angle (middle). Bold lines represent measured data and thin lines represent Ideal data. The lower plot indicates the number of drifter/radar point matches/observations that occurred vs. PESC Radar Look Angle. The thin blue bar represents the measured pattern and the wide yellow bar represents the ideal pattern. Second experiment only. ....	47
Figure 23.	Correlation Coefficient and RMS difference plots vs. BIGC Radar Look Angle (top) and corresponding Drifter and Radial Standard Deviation plots vs. BIGC Radar Look Angle (middle). Thin lines represent ideal data. The lower plot indicates the number of drifter/radar point matches/observations that occurred vs. BIGC Radar Look Angle. The wide yellow bar represents the ideal pattern. Second experiment only. ....	48
Figure 24.	Plot of absolute value of (Drifter Radial Velocity minus Radar Radial Velocity) vs. weighted temporal quality of the DRAK Radar Data (top). The middle plot represents the cumulative RMS difference and cumulative	

	R <sup>2</sup> value vs. weighted temporal quality as you increase temporal values from left to right. The bottom plot includes the number of data points contained in each temporal increment and its associated cumulative percent of data. Second experiment only.....	49
Figure 25.	Plot of absolute value of (Drifter Radial Velocity minus Radar Radial Velocity) vs. weighted temporal quality of the COMM Radar Data (top). The middle plot represents the cumulative RMS difference and cumulative R <sup>2</sup> value vs. weighted temporal quality as you increase temporal values from left to right. The bottom plot includes the number of data points contained in each temporal increment and its associated cumulative percent of data. Second experiment only.....	50
Figure 26.	Plot of absolute value of (Drifter Radial Velocity minus Radar Radial Velocity) vs. weighted temporal quality of the SLID Radar Data (top). The middle plot represents the cumulative RMS difference and cumulative R <sup>2</sup> value vs. weighted temporal quality as you increase temporal values from left to right. The bottom plot includes the number of data points contained in each temporal increment and its associated cumulative percent of data. Second experiment only.....	51
Figure 27.	Plot of absolute value of (Drifter Radial Velocity minus Radar Radial Velocity) vs. weighted temporal quality of the FORT Radar Data (top). The middle plot represents the cumulative RMS difference and cumulative R <sup>2</sup> value vs. weighted temporal quality as you increase temporal values from left to right. The bottom plot includes the number of data points contained in each temporal increment and its associated cumulative percent of data. Second experiment only.....	52
Figure 28.	Plot of absolute value of (Drifter Radial Velocity minus Radar Radial Velocity) vs. weighted temporal quality of the MONT Radar Data (top). The middle plot represents the cumulative RMS difference and cumulative R <sup>2</sup> value vs. weighted temporal quality as you increase temporal values from left to right. The bottom plot includes the number of data points contained in each temporal increment and its associated cumulative percent of data. Second experiment only.....	53
Figure 29.	Plot of absolute value of (Drifter Radial Velocity minus Radar Radial Velocity) vs. weighted temporal quality of the PILR Radar Data (top). The middle plot represents the cumulative RMS difference and cumulative R <sup>2</sup> value vs. weighted temporal quality as you increase temporal values from left to right. The bottom plot includes the number of data points contained in each temporal increment and its associated cumulative percent of data. Second experiment only.....	54
Figure 30.	Plot of absolute value of (Drifter Radial Velocity minus Radar Radial Velocity) vs. weighted temporal quality of the PESC Radar Data (top). The middle plot represents the cumulative RMS difference and cumulative R <sup>2</sup> value vs. weighted temporal quality as you increase temporal values from left to right. The bottom plot includes the number of data points	

	contained in each temporal increment and its associated cumulative percent of data. Second experiment only.....	55
Figure 31.	Plot of absolute value of (Drifter Radial Velocity minus Radar Radial Velocity) vs. weighted temporal quality of the BIGC Radar Data (top). The middle plot represents the cumulative RMS difference and cumulative $R^2$ value vs. weighted temporal quality as you increase temporal values from left to right. The bottom plot includes the number of data points contained in each temporal increment and its associated cumulative percent of data. Second experiment only.....	56
Figure 32.	Plot of absolute value of (Drifter Radial Velocity minus Radar Radial Velocity) vs. distance of radar point from radar station for each radar station (North to South). The three kilometer spatial range separation of each radar station's data is evident in the vertical groupings of the data. Second experiment only.....	57
Figure 33.	Plot of absolute value of (Drifter Radial Velocity minus Radar Radial Velocity) vs. the # of drifters that matched within 2km of a radar point for each radar station (North to South). Vertical groupings at intervals of 7 are indicative of the predominance of having a full range of drifter data (+/- 30 min) per hourly radar point. Second experiment only. ....	58
Figure 34.	Plot of absolute value of (Drifter Radial Velocity minus Radar Radial Velocity) vs. the RMS distance of matched drifters within 2km of a radial point. Second experiment only. ....	59
Figure 35.	Plot of absolute value of (Drifter Radial Velocity minus Radar Radial Velocity) vs. the Standard Deviation of the radial velocities of the drifters that matched within 2km of a radar point. Second experiment only. ....	60
Figure 36.	Scatter Plot of combined measured radar data for the second experiment vs. various queries. Bottom chart includes density of points via use of a colorbar. ....	61
Figure 37.	Scatter Plot (with relative density of points) of combined measured radar data for the second experiment vs. various queries. ....	62
Figure 38.	Typical measured radar patterns showing ocean coverage for SCRZ, MLML, PPIN and NPGS, respectively. First experiment drifter tracks are shown red, green, blue and magenta.....	63
Figure 39.	Scatter Plot of Drifter Radial Velocity vs. Radar Radial Velocity for Radar Sites COMM, FORT and MONT, respectively (First Experiment – 23-27 January 2008). Measured Radar Patterns are shown on the left and Ideal Radar Patterns are shown on the right. Dashed line represents one to one correlation and red solid line represents the linear least squares fit of the data. The standard deviation value refers to the best fit line. ....	64
Figure 40.	Scatter Plot of Drifter Radial Velocity vs. Radar Radial Velocity for Radar Sites PESC, SCRZ and MLML, respectively (First Experiment – 23-27 January 2008). Measured Radar Patterns are shown on the left and Ideal Radar Patterns are shown on the right. Dashed line represents one to one correlation and red solid line represents the linear least squares fit of the data. The standard deviation value refers to the best fit line. ....	65

Figure 41.	Scatter Plot of Drifter Radial Velocity vs. Radar Radial Velocity for Radar Sites PPIN and NPGS. respectively (First Experiment – 23-27 January 2008). Bottom graph is a combined plot of all Radar Sites in the first experiment. Measured Radar Patterns are shown on the left and Ideal Radar Patterns are shown on the right. Dashed line represents one to one correlation and red solid line represents the linear least squares fit of the data. The standard deviation value refers to the best fit line. ....	66
Figure 42.	Correlation Coefficient and RMS difference plots vs. COMM Radar Look Angle (top) and corresponding Drifter and Radial Standard Deviation plots vs. COMM Radar Look Angle (middle). Bold lines represent measured data and thin lines represent ideal data. The lower plot indicates the number of drifter/radar point matches/observations that occurred vs. COMM Radar Look Angle. The thin blue bar represents the measured pattern and the wide yellow bar represents the ideal pattern. First experiment only. ....	67
Figure 43.	Correlation Coefficient and RMS difference plots vs. FORT Radar Look Angle (top) and corresponding Drifter and Radial Standard Deviation plots vs. FORT Radar Look Angle (middle). Bold lines represent measured data and thin lines represent ideal data. The lower plot indicates the number of drifter/radar point matches/observations that occurred vs. FORT Radar Look Angle. The thin blue bar represents the measured pattern and the wide yellow bar represents the ideal pattern. First experiment only. ....	68
Figure 44.	Correlation Coefficient and RMS difference plots vs. MONT Radar Look Angle (top) and corresponding Drifter and Radial Standard Deviation plots vs. MONT Radar Look Angle (middle). Bold lines represent measured data and thin lines represent ideal data. The lower plot indicates the number of drifter/radar point matches/observations that occurred vs. MONT Radar Look Angle. The thin blue bar represents the measured pattern and the wide yellow bar represents the ideal pattern. First experiment only. ....	69
Figure 45.	Correlation Coefficient and RMS difference plots vs. PESC Radar Look Angle (top) and corresponding Drifter and Radial Standard Deviation plots vs. PESC Radar Look Angle (middle). Thin lines represent ideal data. The lower plot indicates the number of drifter/radar point matches/observations that occurred vs. PESC Radar Look Angle. The wide yellow bar represents the ideal pattern. First experiment only. ....	70
Figure 46.	Correlation Coefficient and RMS difference plots vs. SCRZ Radar Look Angle (top) and corresponding Drifter and Radial Standard Deviation plots vs. SCRZ Radar Look Angle (middle). Bold lines represent measured data and thin lines represent ideal data. The lower plot indicates the number of drifter/radar point matches/observations that occurred vs. SCRZ Radar Look Angle. The thin blue bar represents the measured pattern and the wide yellow bar represents the ideal pattern. First experiment only. ....	71

Figure 47.	Correlation Coefficient and RMS difference plots vs. MLML Radar Look Angle (top) and corresponding Drifter and Radial Standard Deviation plots vs. MLML Radar Look Angle (middle). Bold lines represent measured data and thin lines represent ideal data. The lower plot indicates the number of drifter/radar point matches/observations that occurred vs. MLML Radar Look Angle. The thin blue bar represents the measured pattern and the wide yellow bar represents the ideal pattern. First experiment only. ....	72
Figure 48.	Correlation Coefficient and RMS difference plots vs. PPIN Radar Look Angle (top) and corresponding Drifter and Radial Standard Deviation plots vs. PPIN Radar Look Angle (middle). Bold lines represent measured data and thin lines represent ideal data. The lower plot indicates the number of drifter/radar point matches/observations that occurred vs. PPIN Radar Look Angle. The thin blue bar represents the measured pattern and the wide yellow bar represents the ideal pattern. First experiment only. ....	73
Figure 49.	Correlation Coefficient and RMS difference plots vs. NPGS Radar Look Angle (top) and corresponding Drifter and Radial Standard Deviation plots vs. NPGS Radar Look Angle (middle). Bold lines represent measured data and thin lines represent ideal data. The lower plot indicates the number of drifter/radar point matches/observations that occurred vs. NPGS Radar Look Angle. The thin blue bar represents the measured pattern and the wide yellow bar represents the ideal pattern. First experiment only. ....	74
Figure 50.	Plot of absolute value of (Drifter Radial Velocity minus Radar Radial Velocity) vs. Distance of radial point from radar station for each radar station (North to South). The 3 kilometer spatial range separation of each radar station's data is evident in the vertical groupings of the data. First experiment only. ....	75
Figure 51.	Plot of absolute value of (Drifter Radial Velocity minus Radar Radial Velocity) vs. the # of drifters that matched within 2km of a radial point for each radar station (North to South). Vertical groupings at intervals of 7 are indicative of the predominance of having a full range of drifter data (+/- 30 min) per hourly radar point. First experiment only.....	76
Figure 52.	Plot of absolute value of (Drifter Radial Velocity minus Radar Radial Velocity) vs. the RMS distance of matched drifters within 2km of a radial point. First experiment only.....	77
Figure 53.	Plot of absolute value of (Drifter Radial Velocity minus Radar Radial Velocity) vs. the Standard Deviation of the drifters that matched within 2km of a radial point. Second experiment only. ....	78
Figure 54.	Plot of combined measured radar data for the second experiment vs. various queries. ....	79

THIS PAGE INTENTIONALLY LEFT BLANK

## LIST OF TABLES

Table 1.	Summary of the HF radar stations used for analysis. ....	8
Table 2.	Summary of Instrumentation used for analysis .....	10
Table 3.	Example of portion of Typical Radar Hourly Report generated by CODAR HF Radar System. ....	16
Table 4.	Summary of Each Radar Site Studied including Ideal Radar Patterns. ....	30
Table 5.	Summary of DRAK weighted temporal quality results .....	80
Table 6.	Summary of COMM weighted temporal quality results.....	80
Table 7.	Summary of SLID weighted temporal quality results .....	81
Table 8.	Summary of FORT weighted temporal quality results .....	81
Table 9.	Summary of MONT weighted temporal quality results .....	82
Table 10.	Summary of PILR weighted temporal quality results.....	82
Table 11.	Summary of PESC weighted temporal quality results.....	83
Table 12.	Summary of BIGC weighted temporal quality results.....	83

THIS PAGE INTENTIONALLY LEFT BLANK

## ACKNOWLEDGMENTS

I would like thank Professor Jeff Paduan for his exceptional guidance and mentorship throughout this long journey. In addition, I would like to thank Mike Cook for his patience and assistance with helping me understand MATLAB code generation and insight into the CODAR system. To Professor Mary Batteen for being a second reader and helping me get settled into the graduate school grind. To Fred Bahr for taking his time to help me with various MATLAB programming issues and sharing his office space to do this research. I would also like to thank LT Dave Hudson, LT Sarah Height, LT Adam Thomas, and LT Jason Barrett for helping me through the NPS syllabus and for being lunch pals throughout the week. To my parents, Rachel and Richard, for giving me encouragement and support growing up in order for me to make it into my twenties and ready for the real world. Finally, I would like to thank my wife, Arnheidur, and my two children Embla and Ellert for the support that they have given me during my Navy career and especially these last two years. I spent way too many weekends away from you than I would have liked and appreciate your patience.

THIS PAGE INTENTIONALLY LEFT BLANK

# I. INTRODUCTION

## A. HIGH FREQUENCY RADAR

High Frequency (HF) radar and its application to mapping ocean surface currents is a relatively new field of study in oceanography. Nevertheless, this scientific field produces real, tangible, accurate real-time results readily available to the scientific community as well as many other entities. Measurement of the ocean surface current through high frequency radar dates back to Stewart and Joy (1974) and Barrick et al. (1977), who first discovered its practicable use to the ocean sciences.

The fundamentals of ocean surface current mapping stems from the backscatter of electromagnetic energy in the 3-30 MHz range. This frequency range is significant since Bragg scattering is strong and well characterized here (Crombie, 1955). Bragg scattering is the coherent reflection of the pulsed energy by ocean surface waves, waves which exhibit exactly one-half the wavelength as the transmitted pulse. As each wave that exhibits one-half wavelength presents itself to the radiated energy, the in-phase return contributes to a strong peak in the backscatter spectrum. The primary type of wave that coherently reflects high frequency radar is shown to be surface gravity waves with approximately ten-meter wavelengths (Paduan and Graber, 1997).

The backscatter spectrum that contains the Bragg peaks will show a slight Doppler shift, which is attributed to the underlying ocean current as well as the deep water phase speed of the ocean wave. Since the phase speed of the wave is theoretically known due to the dispersion relation of surface gravity waves, the remaining shift is therefore due only to the current.

Since each HF radar station can only determine the velocity of the current that is directly towards or away from the transmitting station, two or more stations that are offset from each other are needed to determine the true ocean current. The optimum offset is 90 degrees and generally, two radials must have an angle greater than 30 degrees and less than 150 degrees to resolve the current vector (Paduan and Graber, 1997). The addition of both radial vectors from separate radar sites will provide the true current

magnitude and direction for that specific point in the ocean. By combining spatial averaging of about three km in radial length in five-degree increments with temporal averaging of about every hour, a horizontal map of surface current velocities can be obtained.

For angular determination, there are two primary radar configurations that analyze the scattered signal from a given range cell: direction finding and phased array systems (beam forming). The configuration that was used in this study is the direction finding (DF) system and is found on CODAR systems (Coastal Ocean Dynamics Applications Radar). It consists of two crossed loops and a whip for receiving and a single whip for transmitting the HF radio pulses (Paduan and Graber, 1997). A beam forming system, such as the Ocean Surface Current Radar (OSCR), uses a linear array of receive antennae to steer the receive antennae look angle to different directions (Prandle, 1991). Each system has its advantages and disadvantages, but the CODAR system is prevalent on the Central California Coast due to the limited space needed for system deployment and is therefore used in this study.

## **B. EVALUATION OF CODAR SEASONDE HF RADAR ON THE CENTRAL CALIFORNIA COAST**

This study evaluates the statistical correlation between a Pacific Gyre drifting buoy's radial velocities with that of HF radar station (CODAR) radial velocities in order to validate HF radar surface current mapping abilities. There is expected to be a statistical variation right from the start due to the inexact measurement capabilities of both drifter and radar systems and due to the different measurement footprints of the two systems, general errors (i.e., velocity differences) will arise due to the fact that HF radars only measure from the surface down to about 1 meter whereas the drifter buoys have a Drogue centered around 1 meter, which can slip by as much as 1 to 2 cm/s from the ocean water they follow (Niiler et al., 1987). Also, HF radar gives vertically integrated values from the surface where drifters integrate their values over their drag elements (Ohlmann et al., 2006). Furthermore, drifter radial velocities are somewhat of a point measurement of surface velocities. As mentioned above, HF radar measurements are averages of both spatial and temporal scales. These space and time differences in

measurements will account for basic errors and are unavoidable. Determining the magnitude of these errors and whether a consistent pattern emerges from the data is one goal of this study.

Various upgrades to the hourly reports that the Seasonde CODAR suite generates have allowed for further statistical analysis of various other parameters, such as the temporal quality of the HF radar data. Temporal quality is a term used by the CODAR manufacturer and is one of a number of quality factors available in the reports. Quality factors are values that relate to “measurement uncertainties such as noise, a changing surface current pattern, and/or horizontal shear over each measured area. Most temporal uncertainty is due to the current pattern changing with time” (Seasonde, 10). Temporal quality defined is the standard deviation of the velocities at the same range and bearing across the Short-Time radials (10 minute averaged measurements from the radar suite). The effect of temporal quality on HF radar performance is studied, along with other effects such as:

- The distance each radar point is away from the HF radar station
- The number of drifters that matched within a two kilometer filter of each HF radar point
- The Root Mean Square (RMS) distance of matched drifters within a two kilometer filter of each HF radar point
- The standard deviation of drifters that matched within a two kilometer filter of each HF radar point

All of these factors are statistically compared with the absolute value of the difference between the radial velocities of the radar points and the drifters.

The impact of the relative angular measurement from the CODAR station is looked at as well. It has been determined from previous studies that radar accuracy can be affected by the local surrounding environment, i.e., new construction around a radar site (metal fence, building, etc.; Kohut and Glen, 2003). These environmental factors affect the response of the receive antenna element as a function of look angle, which may

imprint sources of error in the DF systems that are, themselves, functions of look angle. To investigate that effect, this study compares the measured antenna pattern velocities with those of the ideal, or theoretical antenna pattern velocities. Since the MUSIC algorithm that is used for direction finding is based upon knowing the angular response pattern of each antenna element, the pattern's accuracy will directly relate to the accuracy of the angular placement of radial current values around a given range cell (Paduan et al., 2006). The effect of accurate calibration of individual radar sites through the use of hand-held transponders to create a measured pattern, is assessed by noting whether or not measured pattern radar data agrees better with the drifter data and whether there are clear angular variations in the radar verses drifter comparisons.

### **1. Use of Drifters in Validation Study**

Modern advancements in navigation and tracking through the use of the Global Positioning System allow drifting buoys to be an excellent choice for validation studies. Drifting buoys have many advantages over other oceanographic sensing equipment in regards to HF radar research. For one, the vertical scales of each system are quite close to each other. Drifting buoys give integrated values over their drag elements (depth down to one meter) whereas HF radar gives velocity values that have been integrated from the surface down to about 0.5 meters. Though not identical, relative to other measurement equipment, such as moored current meters, moored buoys, ship board ADCP equipment, and Underwater Unmanned Vehicles (UUV), the scales are quite close.

While moored current meters and moored buoys have excellent temporal measurement capabilities, they lack in spatial coverage of the ocean. Practically point measurements, they do little to map the needed horizontal scales (up to several hundred km<sup>2</sup>) seen in HF radar measurements. Even though ship board ADCP and UUV systems show improvement in the spatial scale coverage factor, they are still limited by their small numbers. Arrays of drifting buoys, on the other hand, can be dispersed for extended periods of time and cover vast amounts of the ocean surface.

The flexibility to grid the ocean domain of interest is also another excellent advantage of drifting buoys. The proper placement of sensing equipment is paramount in getting the desired data needed for HF radar validation research. Sensors too close, too far away, or at the wrong angular aspect from a radar station will degrade the usefulness of the data obtained. Furthermore, the relative cost of each drifter compared to the other sensor equipment previously mentioned is superior. With little maintenance required in the operation of the buoys, the overall cost of obtaining the data set is a definite advantage.

THIS PAGE INTENTIONALLY LEFT BLANK

## II. DATA COLLECTION

### A. HIGH FREQUENCY RADAR

CODAR type HF radar is predominately deployed along the Central California coast and the type used for this study. Each radar system has transmit and receive antennae and supporting electronics for data storage as shown in Figures 1 and 2. The data from each site is sent to a central computer located at the campus of the University of California at Santa Cruz where it is stored and made available to researchers and the public via the Internet. The website used for data dissemination can be found at <http://www.cencalcurrents.org>. Hourly averaged data from approximately 74 minutes of raw data are taken and tabulated into each report. The most significant data used from the reports were the radial speed (in cm/s) either toward or away from the station. A list of the sites studied can be found in Table 1. The HF radar instrumentation and data used in this study were made available by the State of California's Coastal Ocean Currents Monitoring Program (COCMP; <http://cocmp.org/>).

A majority of the radar sites studied provided data using both a measured beam pattern and an ideal beam pattern. Only the sites BIGC and PESC were limited to having only ideal beam patterns. Numerous studies have shown the measured beam pattern to be more accurate than the ideal (Kohut and Glenn, 2003; Paduan et al., 2006), but the local environment of the site can sometimes make a difference and lead one toward the ideal. Each radar site produces MATLAB-readable tabulated data each hour, each under the measured beam pattern as well as the ideal beam pattern. Measured beam patterns are obtained by taking a survey boat out in the water in the coverage area adjacent to a particular radar site. A semicircular pattern is done by the boat utilizing a constant speed and radius. Equipped with a known transponder that modifies and re-radiates the transmitted signal from the radar site, precise data can be measured and analyzed to get the "real" beam pattern being used by the radar site. It is important to get the correct beam pattern because "errors in the antenna pattern translates into errors in angular placement of radial current values around a given range cell" (Kim, 2004). This

actual (measured) antenna beam pattern, as a function of azimuth angle, is then re-programmed into the Seasonde MUSIC algorithm in order to improve the estimate of the surface currents.

Spatial coverage for HF radars depends upon the frequency of the transmitting station. For a station transmitting in the 25 MHz range, maximum ranges are approximately 42 km, whereas in the 12 MHz range, the range is approximately 83 km. Pattern angular resolution can be set from one to five degrees but all stations in this study were using increments of five degrees. Range resolution for each station was around three km.

A plot of all the locations of the radar stations can be found in Figure 3 along with all of the drifter tracks. Radar station BIGC was inoperable during the first experiment because mechanical failure precluded this station from providing any data. A summary of instrumentation used for analysis can be found in Table 2.

Radar ID	Exp. #	Name	Position	Center Frequency	Beam Pattern Available	
BIGC	2	Big Creek	N 37 05.3670, W 122 16.4502	12.190 MHz	N/A	Ideal
COMM	1&2	Commonweal Center	N 37 54.7062, W 122 43.6908	13.400 MHz	Measured	Ideal
DRAK	2	Drakes Bay	N 38 16.6999, W 122 57.6440	13.400 MHz	Measured	Ideal
FORT	1&2	Fort Funston	N 37 42.7500, W 122 30.0780	13.475 MHz	Measured	Ideal
MLML	1	Moss Landing	N 36 48.1980, W 121 47.2980	25.380 MHz	Measured	Ideal
MONT	1&2	Montara Sanitary District	N 37 32.0232, W 122 31.1532	12.090 MHz	Measured	Ideal
NPGS	1	Naval Postgraduate School	N 36 36.1920, W 121 52.3200	13.470 MHz	Measured	Ideal
PESC	1&2	Pescadero	N 37 15.1500, W 122 24.9672	12.190 MHz	Measured	Ideal
PILR	2	Pillar Point Long Range	N 37 29.8050, W 122 29.9620	4.550 MHz	Measured	Ideal
PPIN	1	Point Pinos	N 36 38.2080, W 121 56.1360	13.390 MHz	Measured	Ideal
SCRZ	1	Santa Cruz	N 36 56.9520, W 122 03.9660	12.150 MHz	Measured	Ideal
SLID	2	Slide Ranch	N 37 52.3500, W 122 35.8548	12.190 MHz	Measured	Ideal

Table 1. Summary of the HF radar stations used for analysis.

## B. DRIFTER

During what is called experiment one, four Pacific Gyre Microstar drifters were released into Monterey Bay on 23 January 2008, and were subsequently picked up on 27 January 2008, near the entrance to the San Francisco Bay. The drifters are current

following Lagrangian surface floats with a drogue centered at approximately 1 meter depth. The surface float contains a telemetry system, antenna, batteries and sensors. The various sensors include GPS (which records the position in 10-minute increments), measurements of sea surface temperature, battery voltage, and submergence. Figure 4 shows a deployed drifter, and Figure 5 shows the 1 meter drogue.

Data from the drifters is transmitted via satellite to the Pacific Gyre website where the data can be retrieved by the end-user in near real time. For experiment one, tracking equipment was brought onboard the research vessel *Point Sur*, shown in Figure 6, out of Moss Landing Marine Laboratory, in order to receive the direct satellite feed and get real time position updates of all drifters. This significantly aided in the retrieval of drifters and led to a 100% recovery rate for Experiment One. Drifter resources and research vessel support during experiment one were provided by the Oceanographer of the Navy and the Naval Postgraduate School.

For Experiment Two, conducted 1-10 April 2008, 32 drifters were deployed from local research vessels, the R/V *John Martin* from Moss Landing Marine Laboratories and the R/V *Mussel Point* (Figure 6) from the Bodega Bay Marine Laboratory. The boats deployed a majority of the drifters on 1 April 2008 within a grid in the Gulf of Farallones, just west of San Francisco bay. Both vessels repositioned several drifters three days later in order to keep them within the HF radar footprint. Near real time tracking equipment was once again brought onboard, this time on the R/V *John Martin*, which aided situational awareness and recovery operations. At the end of the experiment, most of the drifters were recovered without incident, even though a few drifters were lost due to poor GPS reception and/or battery failure. For the larger experiment two, drifter and research vessel support was provided by COCMP and by a grant from NOAA's Coastal Response Research Center, grant number NA04NOS4190063, Project Number 07-061.

<b>Instrument</b>	<b>Period 2008</b>	<b>Measured depth</b>	<b>Measured Period</b>	<b>Data Interval</b>
<b>HF Radar</b>	<b>22 Jan 17:00 - 27 Jan 23:00 (GMT)</b>	<b>~ 1 m</b>	<b>1 hour</b>	<b>1 hour</b>
	<b>01 Apr 05:00 - 10 Apr 18:00 (GMT)</b>	<b>~ 1 m</b>	<b>1 hour</b>	<b>1 hour</b>
<b>Drifters</b>	<b>23 Jan 20:30 - 27 Jan 18:00 (GMT)</b>	<b>~ 1 m</b>	<b>10 minutes</b>	<b>10 minutes</b>
	<b>01 Apr 05:00 - 10 Apr 18:00 (GMT)</b>	<b>~ 1 m</b>	<b>10 minutes</b>	<b>10 minutes</b>

Table 2. Summary of Instrumentation used for analysis

### III. DATA ANALYSIS AND RESULTS

#### A. HIGH FREQUENCY RADAR COMPARED TO DRIFTER DATA

For each drifter track, two velocity components were determined at 10-minute intervals, one in the North direction  $V_D$ , and one in the East direction  $U_D$ . These velocity components were then rotated in the direction of each subsequent HF radar location to produce each radial velocity

$$U'_D = U_D \times \cos(\alpha) + V_D \times \sin(\alpha) \quad (1)$$

where  $\alpha$  is the angle of the drifter to a particular radar site and  $U'_D$  is the radial speed of the drifter toward the HF radar site (Kim, 2004).

After the radial velocities were determined from the drifting buoys, these values were statistically compared to the radar radial velocities. For each hourly radar report, there are tens if not hundreds of radar measurement points generated. For each of these points, all drifter tracks that fell within two kilometers spatially and plus or minus 30 minutes temporally were captured for comparison purposes. A two-kilometer filter was used because it is comparable to the HF radar grid size and it is large enough to avoid gaps in coverage of the ocean surface as shown in Figure 7. This ties the closest surface current measurements from the drifters to their representative radar point. Figure 8 visually depicts a typical calculation made during the analysis. A portion of the radar points from FORT is shown along with all of the drifter tracks in closest proximity to these points. For the time of 0200Z on 04 April 2008, all ten minute drifter positions within two kilometers of the radar point in question are highlighted in magenta. For each ten minute drifter position a radial velocity was computed using center differencing. Each drifter endpoint position was assigned a velocity using forward or backward differencing as appropriate. All of these velocity values, up to seven per drifter for a given radar match, also has an associated radial velocity according to (1). Figure 8 includes 7 points from one drifter and 7 points from a second drifter, for a total of 14 points/matches. The mean radial velocity of these 14 matches was then compared to the

radar radial velocity of the subject radar point. This process was done for each radar measurement point, for each radar, for each hourly report.

Various statistical results were then computed from the resulting data, from correlation coefficient, coefficient of determination ( $r^2$ ), root mean squared (RMS) differences, and slope intercept values of the regression analysis. The correlation coefficient was computed as follows:

$$r_{.xy} = \frac{\sum_{i=1}^n (x_i - \bar{x})(y_i - \bar{y})}{\sqrt{\sum (x_i - \bar{x})^2} \sqrt{\sum (y_i - \bar{y})^2}}, \quad (2)$$

where  $\bar{x}$  and  $\bar{y}$  are the sample means of  $X$  and  $Y$ , and  $n$  = the number of pairs  $(x_1, y_1) \dots (x_n, y_n)$ .

The square of the sample correlation coefficient, which is also known as the coefficient of determination, is the fraction of the variance in  $y_i$  that is accounted for by a linear fit of  $x_i$  to  $y_i$ :

$$r^2_{.xy} = 1 - \frac{s^2_{y|x}}{s^2_y} \quad (3)$$

where  $s^2_{y|x}$  is the square of the error of a linear regression of  $x_i$  on  $y_i$  by the equation

$$y = a + bx :$$

$$s^2_{y|x} = \frac{1}{n-1} \sum_{i=1}^n (y_i - a - bx_i)^2 \quad (4)$$

and  $s^2_y$  is just the variance of  $y$ :

$$s^2_y = \frac{1}{n-1} \sum_{i=1}^n (y_i - \bar{y})^2 \quad (5)$$

(Devore,2004)

Scatter plots were produced comparing the mean of all drifter radial data matches (30 minutes prior to and 30 minutes after the top of the hour) and the hourly HF radial data. Least squares fitting was done for regression analysis to obtain the slope and intercept of the scatter plots.

## **B. EXPERIMENT NUMBER TWO RESULTS**

At the heart of the experiment was the validation of HF radar's ability to effectively map the horizontal surface currents of the littoral ocean. Experiment Two contained unique characteristics in its drifter trajectories which aided in the radar analysis. Shown in Figure 10, Experiment Two exhibited excellent spatial coverage within a limited area of the Gulf of Farallones. Also, the speed regime of the drifters stayed on the lower side of the spectrum. This spatial coverage resulted in saturation of a specified area and allowed for a thorough analysis of a number of radar sites, primarily DRAK, SLID and FORT, as shown in Figure 11. Figure 12 contains the coverage factor (i.e., radar radial sampling grid) of the remaining radars used in Experiment Two.

### **1. Scatter Plot of Radial Data**

Scatter plots comparing the drifter radial velocities vs. radar radial velocities were computed for specific radar sites that contained the drifters within its coverage factor. Shown in Figures 13 through 15, the data is presented starting from the Northern most radar site, DRAK, and ends with the Southern most site, BIGC. Measured pattern data is displayed in the left hand column and ideal pattern data is displayed in the right hand column. Numerous studies have already shown the measured beam pattern to be more accurate than the ideal in most situations (Kohut and Glenn, 2003), and this study continues to document this fact. Each and every measured pattern during the second experiment showed an improvement in the  $r^2$  value over the ideal pattern, signifying an increased correlation of the data. DRAK radar site had the best correlation, with an  $r^2$  value of 59.9% for the measured pattern. The slope of the linear regression of each measured data set went from 0.83 for DRAK down to 0.36 for PESC. It is peculiar to note that as the radar sites progressed from the North to the South, the  $r^2$  value decreased as well. This could be due to the overall angular aspect of the radar pattern to the drifter

field or to some other environmental or instrumental factor. The data sets obtained from the CODAR hourly reports did not provide any further insight into this phenomenon due to the independent nature of each radar sites' data. Nevertheless, there is excellent overall correlation between the data, especially the measured pattern data, signifying that HF radar is an adequate tool for operators wishing to obtain near real-time insight into local ocean surface currents. The RMS differences of the measured pattern data ranged from 8.2 cm/s at COMM down to 15.9 cm/s for the lower resolution 5 MHz PILR site. The lower end of this range is close to the theoretical precision of the radar measurement.

## **2. Effect of Radar Angular Aspect**

Being able to plot the relative positions of the radar points allows one to look at the effects that angular aspect has on the correlation. Figures 16-23 plot the above results of each radar station (North to South) in five degree bins. The RMS difference in (cm/s) is computed for each radar / drifter match within the respective angular bin. In addition, its corresponding correlation coefficient is plotted as well (top graphs). The bottom graphs note the number of observations / comparisons done per bin to give an adequate representation as to the relative influence each bin has to the overall RMS difference value. As can be seen from most of the data, if there are fewer observations per bin, a general trend is observed in that there are more fluctuations in RMS difference relative to adjacent bins.

Two examples that are indicative of a solid radar coverage factor are seen in Figures 16 and 18 with radars DRAK and SLID, respectfully. DRAK's corresponding angular aspect graph, Figure 16, and SLID's corresponding angular aspect graph, Figure 18, both are representative of increasing RMS differences toward the limits of coverage. In other words, the further away one angularly gets from the center of the radar coverage, there tends to be less correlation. This "U" shaped trend, or upside down bell curve, is typical of the radar's accuracy relative to angular coverage factor. DRAK results also indicate that between 170-175 degrees clockwise from North, there is a strong increase in the RMS difference. This could reflect environmental factors from that specific angle that degrade the accuracy of the pulsed radar returns due, possibly, to local distortions of

the instrument's antenna patterns. Other peaks worth mentioning that document this observation are shown in Figure 22 (PESC), in the angular bin range of between 300 and 305 degrees clockwise from North. Nevertheless, throughout most of the angular coverage factor of any typical radar, there seems to be a relative steady RMS difference associated with a radar, indicating that a typical radar (and the MUSIC algorithm) produces quite stable returns, regardless of angular aspect.

### **3. Effect of Drifter and Radar Standard Deviation**

Figures 16-23 plot the effect of drifter standard deviation and radar standard deviation in relation to the angular aspect of each radar station (North to South) in five degree bin increments (middle of the page(s)). The solid lines represent drifter standard deviation and the dashed line represents the radar standard deviation. Also, the thicker lines represent the measured patterns and the thinner lines represent the ideal patterns. The bottom graphs notes the number of observations / comparisons done per bin to give an adequate representation as to the relative influence each bin has to the overall standard deviation values.

Each graph shows the general trend as to when the drifter standard deviation increases, the radar standard deviation increases as well. The same can be said for when both values decrease. This correlation is expected since we expect the radar to exhibit fluctuating values when the ocean surface current is fluctuating as well. Significant examples of when the correlation is strong can be seen in a majority of the radar sites. In addition, when there is a peak in the standard deviation of the drifters, an associated peak in the radar standard deviation can be seen as well. This phenomenon can be seen in examples such as DRAK from 165-175 degrees clockwise from North in Figure 16, FORT from 230 to 235 degrees clockwise from North in Figure 19 and PILR from 230 to 235 degrees clockwise from North in Figure 21 to name a few.

It can also be noted that when there is an associated increase in the standard deviation of either drifter or radar values, a similar increase in RMS difference can be seen. The more variation in ocean current direction that one observes per given unit of time, there is greater error, or RMS difference, associated with the radar's accuracy.

Noted examples of this can be seen in DRAK from 165-175 degrees clockwise from North in Figure 16, FORT from 230 to 235 degrees clockwise from North in Figure 19, MONT from 290 to 335 degrees clockwise from North in Figure 20, and PESC from 295 to 310 degrees clockwise from North in Figure 22.

#### 4. Effect of Temporal Quality

Various upgrades to the hourly reports that the Seasonde CODAR suite generates have allowed for further statistical analysis of various other parameters. Specifically, the temporal quality of the HF radar data that is generated is now able to be studied. Table 3 is an example of a portion of a generated report from COMM on 03 April 2008 at 0100Z. Temporal quality values are values that relate to “measurement uncertainties such as noise, a changing surface current pattern, and/or horizontal shear over each measured area. Most temporal uncertainty is due to the current pattern changing with time” (CODAR, 10). Temporal quality is defined as the standard deviation of the velocities at the same range and bearing across the Short-Time radials (10 minute averaged measurements). Sample temporal quality values can be seen in Table 3 in column number six.

Longitude (deg)	Latitude (deg)	U comp (cm/s)	V comp (cm/s)	Spatial Quality	Temporal Quality	Velocity Maximum	Velocity Minimum	Quality DVCount	Quality RTCount
-122.760	37.918	-18.636	4.640	3.098	4.625	-15.765	-22.287	2	6
-122.761	37.916	-18.792	2.970	2.174	1.411	-17.939	-20.113	1	4
-122.761	37.914	-16.809	1.169	999	11.151	-16.848	-16.848	1	7
-122.761	37.911	-15.578	-0.277	6.893	3.267	-10.871	-19.022	2	4
-122.761	37.909	-4.863	-0.513	999	11.099	-4.894	-4.894	1	3
-122.761	37.907	-12.800	-2.493	2.717	3.875	-9.242	-16.848	4	7
-122.760	37.905	-11.496	-3.301	2.174	2.241	-10.871	-13.045	1	4
-122.759	37.902	-7.608	-2.923	999	5.220	-8.151	-8.151	1	5
-122.758	37.900	-5.369	-2.621	999	3.674	-5.977	-5.977	1	4
-122.757	37.898	-1.864	-1.121	999	1.625	-2.174	-2.174	1	2

Table 3. Example of portion of Typical Radar Hourly Report generated by CODAR HF Radar System.

In addition to these temporal quality values, an associated Quality RTCount value is generated, as seen in Table 3, column number 10. This temporal count is the number of velocities that went into the temporal calculation. Therefore, the higher the number of

Quality RTCount, the more representative the temporal quality value is to the real ocean environment. One basically has more values to average from, giving a better statistical result for the temporal quality value. Therefore, in this study, we calculated a weighted temporal quality based upon the number of Quality RTCount values.

$$TQ_{wgt} = \frac{TQ}{\sqrt{QRTC}} \quad (6)$$

$TQ_{wgt}$  = the weighted temporal quality,  $TQ$  = un-weighted temporal quality, and  $QRTC$  = the Quality RTCount number.

The highest value of Quality RTCount that is expected for a specific radar point in an hourly report is seven, since this would indicate a valid ten minute interval return for every possible measurement cycle in a report. QRTC values greater than seven are possible in theory because radial velocity determinations are made, independently, from both the positive and negative Bragg peaks in the backscatter spectra. In reality, each report timeframe is between 74-75 minutes long to allow for a slight overlap in the seven (ten minute intervals), to ensure data capture. This can be seen in the third and sixth entry in Table 3 where every 10 minute interval had a valid temporal quality return.

Figures 24-31 plots the absolute value of difference between drifter and radar radial velocities vs. the weighted temporal quality (top graphs). As a general trend, as the weighted temporal quality increases in value, there are less and less difference values that fall close to zero. If a difference value is closer to zero, that would indicate better correlation between drifter and radar, i.e. a more accurate radar reading.

The middle graphs in Figures 24-31 are the cumulative effects of increasing weighted temporal values in relation to RMS differences and  $r^2$  values. For example, Figure 24 shows the weighted temporal quality effects on radar site DRAK. For all drifter / radar matches that had an associated weighted temporal quality between zero and one, the cumulative RMS value was 8.763 cm/s and an associated  $r^2$  value of 0.7234. If you then includes the weighted temporal quality values from zero to two, the RMS difference value decreases to 8.5862 and the associated  $r^2$  value increases to 0.7289. As you can see, if you take all temporal quality values between 0 and 2 and disregard all

other values, you get the optimum lowest RMS difference and maximum  $r^2$  value. This has its consequences though since, as seen in the bottom of Figure 24, only 32.78% of the data is used. This is not realistic in a practical sense, because too much data is thrown away. Nevertheless, there is a definite trade-off between the weighted temporal quality value chosen as a filter (to increase reliability in radar data output) and the percent data discarded.

One interesting radar site, MONT, shown in Figure 28, has an excellent choice of a weighted temporal quality value to use as a filter. A slight dip in RMS difference is noticed if a temporal quality value of five is used (which would in effect include all values from zero to five). This would result in 64% of the data being used with a net decrease of 0.7977 cm/s in RMS difference and a net increase of 0.0622 in  $r^2$ . Another viable candidate would be the radar site PILR, shown in Figure 29. A temporal quality filter of 9 would be adequate here since there is a noticeable increase in RMS difference after this value. Here, 79% of the data is used, netting a decrease in 2.047 cm/s in RMS difference and a gain of 0.1235 in  $r^2$ . Absent of a significant dip occurring in the RMS difference line, and containing a large portion of the data set, one would then have to consider how much of a trade-off to use in choosing an appropriate temporal quality value. Nevertheless, it is shown that there is an advantage to discard some of the values toward the high end of the scale in order to increase the effectiveness of HF radar output.

## **5. Effect of Radar Point Distance to the Radar Site**

The effect of radar point distance to the radar site was looked at as well. By looking at Figure 32, it can be concluded that initially, there is good correlation in the three kilometer range. But, there is a significant decrease in correlation from about six to 18 kilometers away before again improving at about 45 kilometers. The best range, from about 40-45 kilometers away, is pretty much the midpoint of a radar's field of view. After 45 kilometers, very few points fall in the low range, signifying poorer correlation. Radar sites DRAK, COMM, SLID, and MONT, are typical examples of these trends.

## **6. Effect of the Number of Drifters that Matched within the Two-Kilometer Filter**

Figure 33 shows the effect that the number of drifters matched within the two-kilometer filter has on correlation. An encouraging trend is shown within each radar site. As the number of drifters that matched increases, the difference between the average drifter radial current and the radar radial current decreases. This signifies that there is better spatial and/or temporal sampling being represented in the drifter averages, which correlates better with the radar results. Therefore, if many more drifters were used in the experiment throughout a larger spatial area, one could conclude that better correlation of the results would occur. This also implies that the radar is possibly doing a better job at mapping the ocean currents than the data exhibit.

In the graphs, the significant peaks at intervals of seven can be contributed to the inclusion of a vast majority of drifters that had a full range of data. As previously discussed, there is a maximum of seven, ten minute intervals per drifter associated with a specific radar point if the entire drifter trajectory is captured within the two kilometer filter.

Geographically, the further south that a radar site is located, then the less predictable and less correlated the data becomes. This can be contributed to the fact that a majority of the drifter data was confined to the Northern most radar positions. The effect of radar point distance becomes a contributing factor to this lack of correlation. Radar sites DRAK, COMM, SLID and FORT most represent this phenomenon, that the closer a drifter field is to the optimal range of a radar site (40-45 km, frequency dependant though), the better the correlation tends to be.

## **7. Effect of RMS Distance of Matched Drifters within the Two-Kilometer Filter**

In Figure 34, the effect of RMS distance of the matched drifters within the two kilometer filter, relative to the radar point, was analyzed. It is interesting to note that as the RMS distance of the matched drifters decreases, there tends to be better correlation in the data. This is not intuitively an expected result, since the Seasonde HF radar suite's

MUSIC algorithm doesn't put any statistical weight as to where an energy return comes from within a radar point's ocean coverage. This coverage, again, is approximately three kilometers in the radial direction and contains five degrees in horizontal azimuth. Evidently, there seems to be a better correlation with drifters that have a smaller RMS distances from the centroid of the radar grid point in question.

## **8. Effect of Drifter Standard Deviation**

The effects of drifter standard deviation on correlation were analyzed too as shown in Figure 35. The results of this section are the most counter-intuitive of all the data studied. Contradictory to the previous conclusions discussed in the angular aspect section and the results of Ohlmann et al. (2006), these data suggest that as the velocity standard deviation of the drifters that matched within the two-kilometer filter increases, there is better correlation within the radar data. The reasons behind this phenomenon are not quite understood at this juncture. One would expect the opposite result, assuming that the cause of the drifter versus radar mismatch is true environmental velocity variation within the footprint of the radar grid point.

## **9. Overall Summary of Combined Radar Site Data**

Figures 36 and 37 show a summary of each parameter studied that includes all the radar sites' combined measured data. Specific trends already discussed are more prominent in these graphs. Of particular note is the RMS distance of matched drifters within two kilometers of a radar point shown in Figure 37 (top). A general decrease in correlation is observed the higher the RMS distance becomes, but with this increase in RMS distance, there is an associated increase in the number of values observed. Because of this non-uniformity of sample data points across the full spectrum of RMS distance values, it is difficult to determine whether the decrease in correlation is attributed to the RMS distance or due to the number of samples. Further experiments that contain equal amounts of data points with varying RMS distances would resolve this..

## C. EXPERIMENT NUMBER ONE RESULTS

At the heart of the experiment was the validation of HF radar's ability to effectively map the horizontal surface currents of the littoral ocean. Experiment One contained unique characteristics in its drifter trajectories which aided in the radar analysis. Shown in Figures 12 and 38, Experiment One exhibited excellent angular aspects with regards to specific radar sites, primarily SCRZ, PESC, and MONT. Additionally, there was variety of speed regimes of the drifters to look at in the study. This experiment was a nice compliment to the second experiment because of the different nature of the data. The only drawback to this experiment was the relatively few drifters that were deployed, which were four. Nevertheless, general conclusions can be made from the resulting data.

### 1. Scatter Plot of Radial Data

Scatter plots comparing the drifter radial velocities vs. radar radial velocities were computed for specific radar sites that contained the drifters within its coverage factor. Shown in Figures 39 through 41, the data are presented starting from the Northern most radar site, COMM, and ending with the Southern most site, NPGS. Measured pattern data are displayed in the left hand column and ideal pattern data are displayed in the right hand column. With the exception of SCRZ data, each and every measured pattern during the first experiment showed an improvement in the  $r^2$  value over the ideal pattern, signifying an increased correlation of the data. FORT radar site had the best correlation, with an  $r^2$  value of 81.1% for the measured pattern. The slope of the linear regression of each measured data set went from 0.92 for FORT down to -0.1 for COMM. The data in the first experiment was much more correlated overall compared to the second experiment. This could be due to the fact that there was less variation in the drifters' trajectories in comparison to the second experiment's drifter trajectories. In addition, the speed range covered in experiment one was significantly larger than in Experiment Two.

As shown in Figure 39, MONT measured data showed strong correlation. An interesting observation in the data set is the fact that MONT contained a section of data that had extremely high ocean surface currents as well as low ocean currents. Within its

scatter plot, there are definitely two data regimes that are discernable. After the radial velocity of the drifters was over 15 cm/s positive (toward the radar station), there was a drastic shift in correlation for the worse. Unfortunately, this was the only radar site that had such high velocities associated with it for research purposes. Future experiments with high velocities need to be done in order to try to repeat these results. Only then, can the effectiveness of HF radar be documented in the high velocity ocean current environment. Nevertheless, there is excellent overall correlation between the data, especially the measured pattern data, signifying that HF radar is an adequate tool for operators wishing to obtain near real-time insight into local ocean surface currents. With the exception of COMM data, RMS difference values for the measured pattern data ranged from 9.0 cm/s to 19.1 cm/s.

## **2. Effect of Radar Angular Aspect**

Being able to plot the relative positions of the radar points allows one to look at the effects that angular aspect has on the correlation. Figures 42-49 plot the above results of each radar station (North to South) in five degree bins. The RMS difference in (cm/s) is computed for each radar / drifter match within the respective angular bin. In addition, its corresponding correlation coefficient is plotted as well (top graphs). The bottom graphs notes the number of observations / comparisons done per bin to give an adequate representation as to the relative influence each bin has to the overall RMS difference value. As can be seen from most of the data, if there are fewer observations per bin, a general trend is observed in that there are more fluctuations in RMS difference relative to adjacent bins.

Two examples that are indicative of a solid radar coverage factor are seen in Figure 12 with radars MONT and PESC. MONT's corresponding angular aspect graph, Figure 44, and PESC's corresponding angular aspect graph, Figure 45, both are representative of increasing RMS differences toward the limits of coverage. In other words, the further away one angularly gets from the center of the radar coverage, there tends to be less correlation. This "U" shaped trend, or upside down bell curve, is typical of the radar's accuracy relative to angular coverage factor. PESC' data between 325-335

degrees clockwise from North is an excellent example of this trend. This could reflect environmental factors from that specific angle that degrade the accuracy of the pulsed radar returns. Nevertheless, throughout most of the angular coverage factor of any typical radar, there seems to be a relative steady RMS difference associated with a radar, indicating that a typical radar (and the MUSIC algorithm) produces quite stable returns, regardless of angular aspect.

### **3. Effect of Drifter and Radar Standard Deviation**

Figures 42-49 plot the effect of drifter standard deviation and radar standard deviation in relation to the angular aspect of each radar station (North to South) in five degree bin increments (middle of the page(s)). The solid lines represent drifter standard deviation and the dashed line represents the radar standard deviation. Also, the thicker lines represent the measured patterns and the thinner lines represent the ideal patterns. The bottom graphs notes the number of observations / comparisons done per bin to give an adequate representation as to the relative influence each bin has to the overall standard deviation values.

Each graph shows the general trend as to when the drifter standard deviation increases, the radar standard deviation increases as well. The same can be said for when both values decrease. This correlation is expected since we expect the radar to exhibit fluctuating values when the ocean surface current is fluctuating as well. Significant examples of when the correlation is strong can be seen in a majority of the radar sites. In addition, when there is a spike in the standard deviation of the drifters (up or down), an associated spike in the radar standard deviation can be seen as well. This phenomenon can be seen in examples such as PESC from 315 to 335 degrees clockwise from North in Figure 45, PPIN from 315 to 345 degrees clockwise from North in Figure 48 and NPGS from 320 to 335 degrees clockwise from North in Figure 49 to name a few.

It can also be noted that when there is an associated increase in the standard deviation of either drifter or radar values, a similar increase in RMS difference can be seen. The more variation in ocean current direction that one observes per given unit of time, there is greater error, or RMS difference, associated with the radar's accuracy.

Noted examples of this can be seen in PESC from 315-335 degrees clockwise from North in Figure 45, MLML from 245 to 295 degrees clockwise from North in Figure 47 and NPGS from 310 to 335 degrees clockwise from North in Figure 49.

#### **4. Effect of Radar Point Distance to the Radar Site**

The effect of radar point distance to the radar site was looked at as well. By looking at Figure 50, it can be concluded that there is initially adequate correlation which gradually gets better up to about 20 kilometers in distance. This data set also indicates that after about 22-25 kilometers away, correlation becomes far worse. With the limited data set though, these conclusions would have to be further studied with multiple similar experiments in order to replicate these findings.

#### **5. Effect of the Number of Drifters that Matched within the Two Kilometer Filter**

Figure 51 shows the effect of the number of drifters matched within the two kilometer filter has on correlation. An encouraging trend is shown within each radar site. As the number of drifters that matched increases, the better the overall correlation. This was evident in experiment number two as well. This signifies that there is better spatial coverage being represented in the drifter averages, which correlates better with the radar results. Therefore, if many more drifters were used in the experiment throughout a larger spatial area, one could conclude that better correlation of the results would occur. This also implies that the radar is possibly doing a better job at mapping the ocean currents than the data exhibit.

In the graphs, the significant peaks at intervals of seven can be contributed to the inclusion of a vast majority of drifters that had a full range of data. As previously discussed, there is a maximum of seven, ten minute intervals per drifter associated with a specific radar point if the entire drifter trajectory is captured within the two kilometer filter.

## **6. Effect of RMS Distance of Matched Drifters within the Two Kilometer Filter**

In Figure 52, the effect of RMS distance of the matched drifters within the two kilometer filter, relative to the radar point, is analyzed. It is interesting to note that as the RMS distance of the matched drifter decreases, there tends to be better correlation in the data. This data trend is less obvious here in experiment one than it is in experiment number two. This is due to the limited number of data points from only four drifters being used. Again, this is not intuitively an expected result, since the Seasonde HF radar suite's MUSIC algorithm doesn't put any statistical weight as to where an energy return comes from within a radar point's ocean coverage. This coverage, again, is approximately three kilometers in the radial direction and contains five degrees in horizontal azimuth. Evidently, there seems to be a better correlation with drifters that have a smaller RMS distances from the centroid of the radar grid point in question.

## **7. Effect of Drifter Standard Deviation**

The effects of drifter velocity standard deviation on correlation were analyzed too, as shown in Figure 53. The results of this section are the most counter-intuitive of all the data studied, similar to Experiment Two's results. Contradictory to the previous conclusions discussed in the angular aspect section, these data suggest that as the velocity standard deviation of the drifters that matched within the two kilometer filter increases, there is better correlation within the data. The reasons behind this phenomenon are not quite understood at this juncture. One would expect the opposite result, assuming that the cause of the drifter verses radar mismatch is true environmental velocity variation within the footprint of the radar grid point.

## **8. Overall Summary of Combined Radar Site Data**

Figure 54 shows a summary of each parameter studied that includes all the radar sites' combined measured data. Specific trends already discussed are more prominent in these graphs.

THIS PAGE INTENTIONALLY LEFT BLANK

## IV. SUMMARY

### A. STATISTICAL SUMMARY

CODAR type HF radar validated through the use of Lagrangian drifters is documented throughout this study. Specific results are shown in Table 4 and document a robust correlation between in-situ measurements and surface current velocity vectors produced via the CODAR system suite. Previous validation studies have been conducted in the past, specifically with moored current meters and profiler data. Holbrook and Frisch (1991) and Schott et al. (1996) studied the correlation between HF radar and current meters and found the RMS differences ranged between 10-15 cm/s. Paduan and Rosenfeld (1996) compared both ADCP and drifter data to show RMS differences between 10-20 cm/s. Chapman et al. (1997) compared shipborne current meter data and HF radar data and showed the upper bound of HF radar accuracy to be around 7-8 cm/s. Recent point measurement studies by Kohut and Glenn (2003), Emery et al. (2004), Paduan et al. (2006), Ohlmann et al. (2006) and Kaplan et al. (2005) showed RMS differences between 7 and 19 cm/s.

This study's results fall in line with the previous studies mentioned above. With the exception of COMM data in the first experiment, the RMS differences of the measured patterns had a reasonable spread of between 9.0 cm/s to upwards of 19.1 cm/s. In the second experiment, RMS differences ranged from 9.8 cm/s to 15.9 cm/s. Due to the inherent nature of data discrepancies mentioned previously, such as temporal and spatial scale miss-matches, comparing two quantities that have not come from the same testing environment tends to lead to slight biased differences, differences that can amount to roughly 5 cm/s (Ohlmann, 2006). Nevertheless, even with these inherent differences, correlation between drifter derived radial velocity vectors and HF radar-derived radial velocity vectors is quite good, as shown by the results in Table 4.

This study also further documents that measured radar patterns, for the most part, are far superior to that of ideal radar patterns. Having recent, calibrated radar patterns via the use transmitters on range boats leads to better radar predictions of ocean surface

currents. Though not the main focus of this study, these results are nonetheless evident in the data analysis and are provided to further bolster measured pattern effectiveness.

One conclusion gathered from the analysis is that, through the use of a user defined filter in the temporal quality from the data generated in a Seasonde CODAR hourly radar report, one can improve the accuracy of radar surface current mapping. Even though a certain percentage of data on the high end of the temporal scale is discarded, a majority of this data tends not to be correlated with drifter radial velocity values, and therefore slight improvements in  $r^2$  values and decreases in RMS differences can be obtained. The numerical results of varying the temporal quality cut off value are shown by radar site in Table 5 through Table 12.

Another conclusion can be made from the fact that as more drifter tracks were captured within a two kilometer filter of a radar measurement point, drifter and radar radial velocity correlations showed significant improvements. With more drifter tracks being captured, a better coverage factor of the horizontal ocean surface is obtained, leading to a better, more representative mean ocean current flow. As a result, it can be hypothesized that HF radar capabilities might be better than previously advertised in past studies. As more and more in-situ data becomes available to the researcher, this trend can hopefully be further documented.

Finally, it was shown that as the RMS distance of drifter tracks to a radar point decreased, there tended to be a better correlation between the radial values. This result is not intuitively obvious or expected, since the MUSIC algorithm is documented to not put any statistical weight on where a specific pulsed return is measured within its given horizontal coverage factor. Again, a general decrease in correlation is observed the higher the RMS distance becomes, but with this increase in RMS distance, there is an associated increase in the number of values observed. Because of this non-uniformity of sample data points across the full spectrum of RMS distance values, it is difficult to determine whether the decrease in correlation is attributed to the RMS distance or due to the number of samples. Further experiments that contain equal amounts of data points with varying RMS distances would solve this inconclusive result.

Future studies should address and document the effect that spatial averaging has on the HF derived surface current vectors. Possible improvements in radar resolution to further increase the 5 degree bin resolution to 1 to 2 degrees could aid in making more precise measurements. Additionally, with the combination of more deployed drifters, moored current meters and ship-board VMADCP data working in conjunction with each other could help quantify the errors exhibited by HF radar measurements. Multiple experiments over the same swath of the ocean surface, ones which contain a variety of ocean trajectories and current velocities, would help in complimenting the conclusions made in this study.

**First Experiment 23-27 January 2008**

<b>Radar Site</b>	<b>Type</b>	<b>Correlation Coefficient</b>	<b>R<sup>2</sup> (%)</b>	<b>RMS Difference (cm/s)</b>	<b>Slope</b>	<b>Intercept</b>	<b>Total # of Radial points with match</b>	<b>Total # of 10 min drifter positions that matched</b>
<b>COMM</b>	Measured	-0.177	3.1	72.943	-0.10	33.80	44	249
	Ideal	0.046	0.2	32.939	0.03	29.62	71	478
<b>FORT</b>	Measured	0.901	81.1	9.310	0.92	4.44	270	1701
	Ideal	0.069	0.5	17.764	0.05	1.34	154	997
<b>MONT</b>	Measured	0.899	80.9	19.124	1.06	7.75	423	2589
	Ideal	0.824	67.8	25.312	1.12	12.00	506	3080
<b>PESC</b>	Measured	N/a	N/a	N/a	N/a	N/a	N/a	N/a
	Ideal	0.834	69.6	24.083	0.83	-12.59	295	1566
<b>SCRZ</b>	Measured	0.735	54.0	9.001	0.66	3.40	388	2218
	Ideal	0.799	63.8	12.139	1.07	-3.00	514	2798
<b>MLML</b>	Measured	0.817	66.8	8.954	0.87	3.87	366	2283
	Ideal	0.539	29.1	16.035	0.62	-9.55	531	3250
<b>PPIN</b>	Measured	0.730	53.3	14.157	0.85	-10.74	342	1904
	Ideal	0.622	38.7	15.718	0.71	-13.30	334	1882
<b>NPGS</b>	Measured	0.628	39.5	14.949	0.63	-13.60	252	1386
	Ideal	0.153	2.3	21.173	0.20	-17.89	69	415
<b>All Sites</b>	Measured	0.785	61.6	16.933	0.94	1.73	2085	12330
	Ideal	0.755	57.0	19.561	0.94	-3.58	2474	14466

**Second Experiment 1-10 April 2008**

<b>Radar Site</b>	<b>Type</b>	<b>Correlation Coefficient</b>	<b>R<sup>2</sup> (%)</b>	<b>RMS Difference (cm/s)</b>	<b>Slope</b>	<b>Intercept</b>	<b>Total # of Radial points with match</b>	<b>Total # of 10 min drifter positions that matched</b>
<b>DRAK</b>	Measured	0.774	59.9	10.597	0.83	1.48	2309	19844
	Ideal	0.469	22.0	17.876	0.44	-3.90	2164	18401
<b>COMM</b>	Measured	0.759	57.6	8.164	0.75	-1.71	3288	28047
	Ideal	0.552	30.5	11.770	0.54	-1.26	2567	22963
<b>SLID</b>	Measured	0.669	44.7	9.830	0.67	-0.40	3146	31323
	Ideal	0.507	25.7	14.824	0.51	-5.35	1493	14697
<b>FORT</b>	Measured	0.504	25.4	11.938	0.48	1.43	1910	17544
	Ideal	0.488	23.8	11.602	0.54	1.10	2143	20004
<b>MONT</b>	Measured	0.465	21.6	15.812	0.39	3.12	1395	12614
	Ideal	0.420	17.6	15.535	0.44	1.57	1743	15576
<b>PILR</b>	Measured	0.536	28.7	15.935	0.49	-0.47	345	2724
	Ideal	0.605	36.6	13.497	0.66	-0.08	353	2782
<b>PESC</b>	Measured	0.353	12.4	15.191	0.39	-1.24	750	6396
	Ideal	0.431	18.6	14.222	0.46	0.24	761	6016
<b>BIGC</b>	Measured	N/a	N/a	N/a	N/a	N/a	N/a	N/a
	Ideal	0.497	24.7	19.687	0.77	5.92	137	672
<b>All Sites</b>	Measured	0.631	39.8	11.252	0.62	0.21	13143	118492
	Ideal	0.457	20.9	14.400	0.44	-1.21	11361	101111

Table 4. Summary of Each Radar Site Studied including Ideal Radar Patterns.

## V. APPENDIX



Figure 1. The SeaSonde measurement system includes a transmit chassis and receive chassis. The MUSIC algorithm processes the radar returns to provide hourly radial velocity reports.



Figure 2. The HF radar antenna suite for the SeaSonde system off the California Coast, consisting of a crossed loop and monopole receive antenna (left) and a monopole transmit antenna (right).

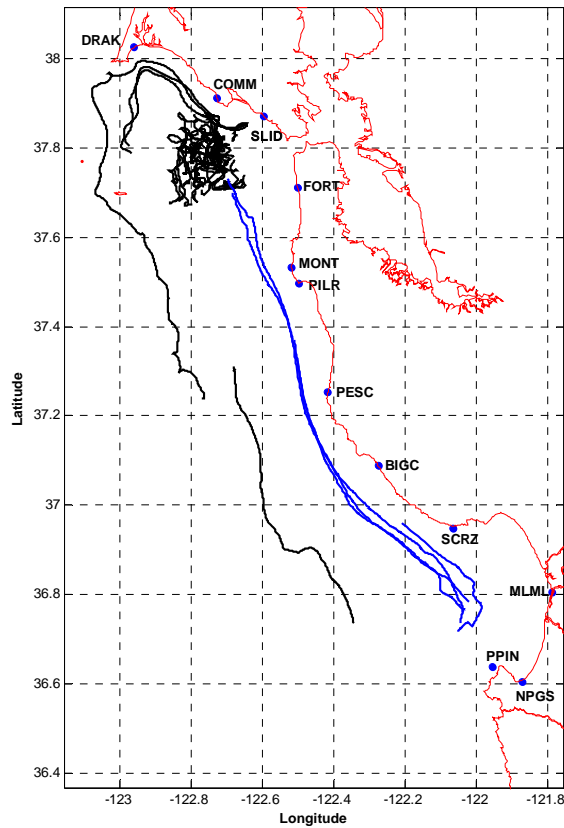


Figure 3. Plot of drifter tracks obtained during both experiments. The first experiment was conducted from 23-27 January 2008 using four drifters and is shown in blue. A second experiment was conducted from 1-10 April 2008 using 32 drifters and is shown in black. HF radar station locations and their 4 letter identifiers are shown as well.



Figure 4. Deployment of the Pacific Gyre Microstar drifter. The surface float contains the telemetry system, antenna, batteries and sensors. Drifter positions are calculated by an onboard Global Positioning System (GPS) receiver that records and transmits a position every 10 minutes.

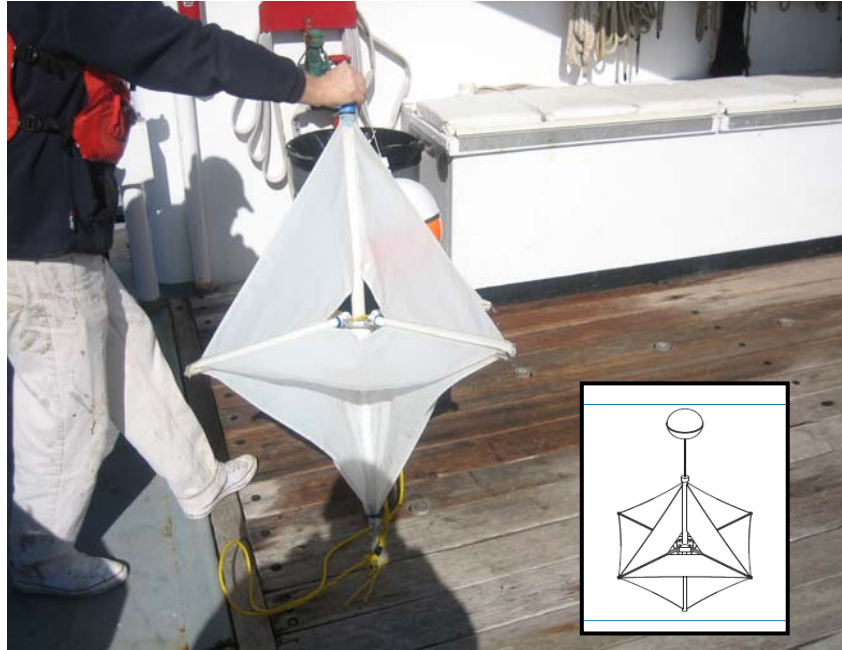


Figure 5. Collapsible Nylon drogue shown with depth centered at approximately one meter.

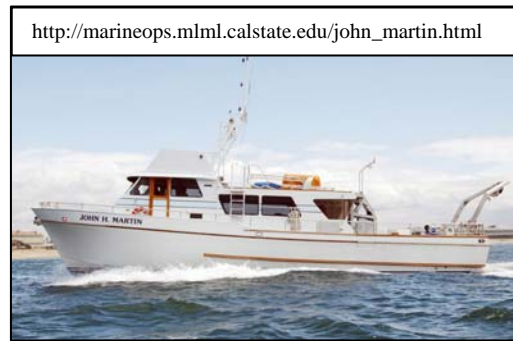


Figure 6. Research vessel *Point Sur* (top left) was used in Experiment One. Research vessels *John H. Martin* (top right) and *Mussel Point* (bottom) were used during Experiment Two. All were used to deploy and retrieve the drifters.

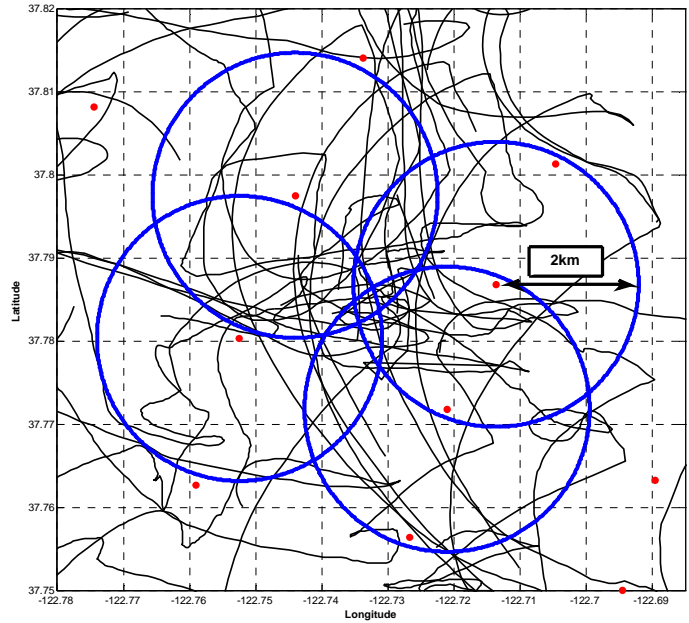


Figure 7. Representation of the spatial scale used in drifter/radial calculations. Section of FORT radial pattern shown in area of a majority of Experiment Two drifter tracks. A two kilometer filter (blue circle(s)) limits the closest drifter tracks to each respective radar point (red dot) used in velocity comparisons. Only four circular filters shown here to exhibit no gaps in coverage.

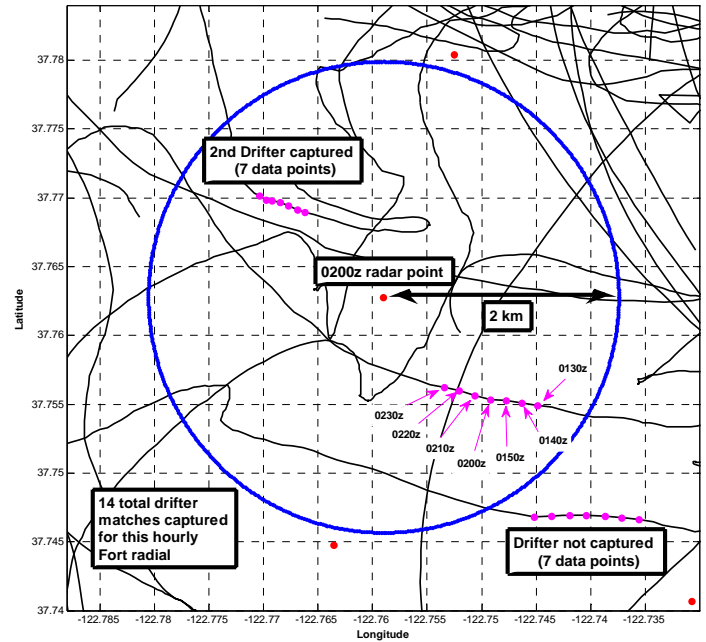


Figure 8. Example of how a representative radar / drifter calculation was made. For each hourly radar point (only one 0200Z radar point highlighted/described here), drifter tracks corresponding to plus or minus 30 minutes and less that 2km away are captured (magenta points inside blue circle). This example has 14 total drifter matches. This process is done for each of the radar points in each hourly report, for each station.

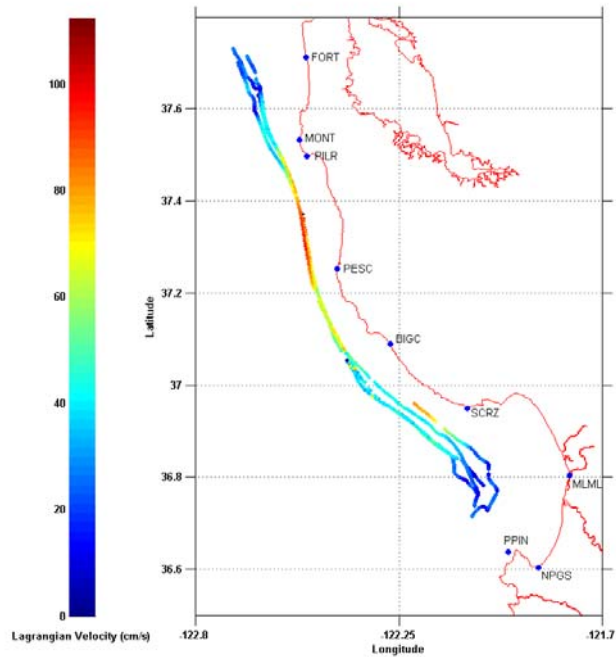


Figure 9. Representation of the drifter speeds shown during Experiment One. This experiment exhibited excellent angular aspects with a wide variety of speed regimes. Spatial coverage around a specific radar point was deficient here.

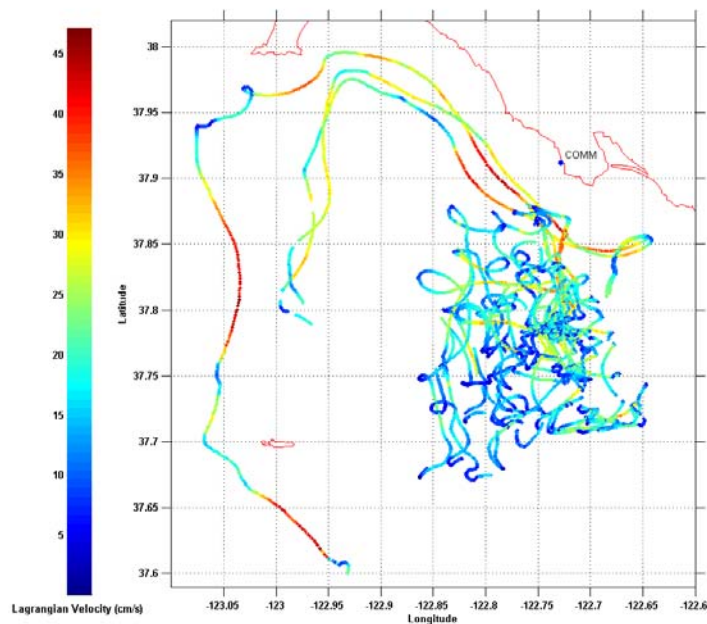


Figure 10. Representation of the drifter speeds shown during Experiment Two. This experiment exhibited excellent spatial coverage within a limited area with moderate speed regimes.

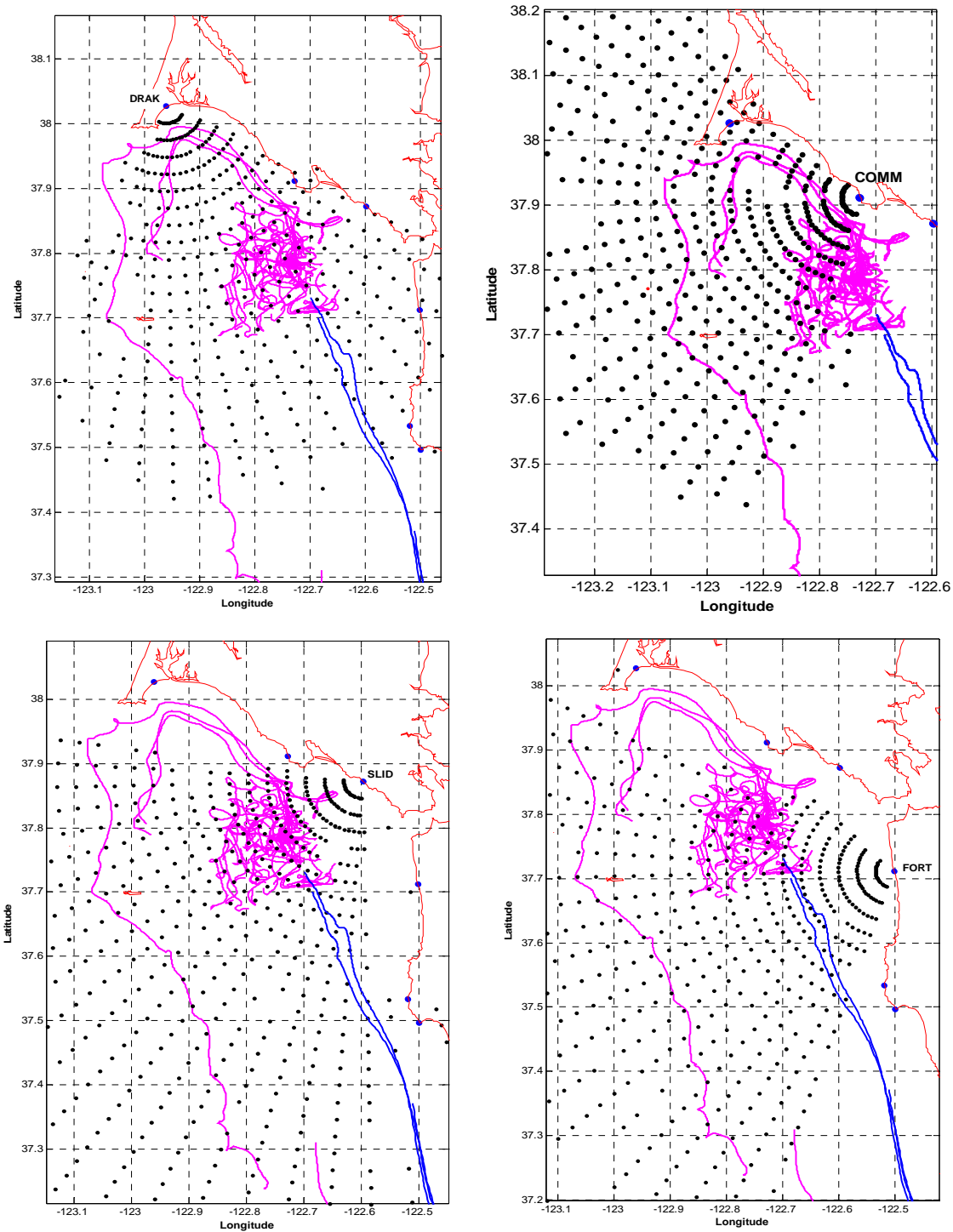


Figure 11. Typical measured radar patterns showing ocean coverage for DRAK, COMM, SLID and FORT, respectively. First experiment drifter tracks are shown in blue and second experiment drifter tracks are shown in magenta.

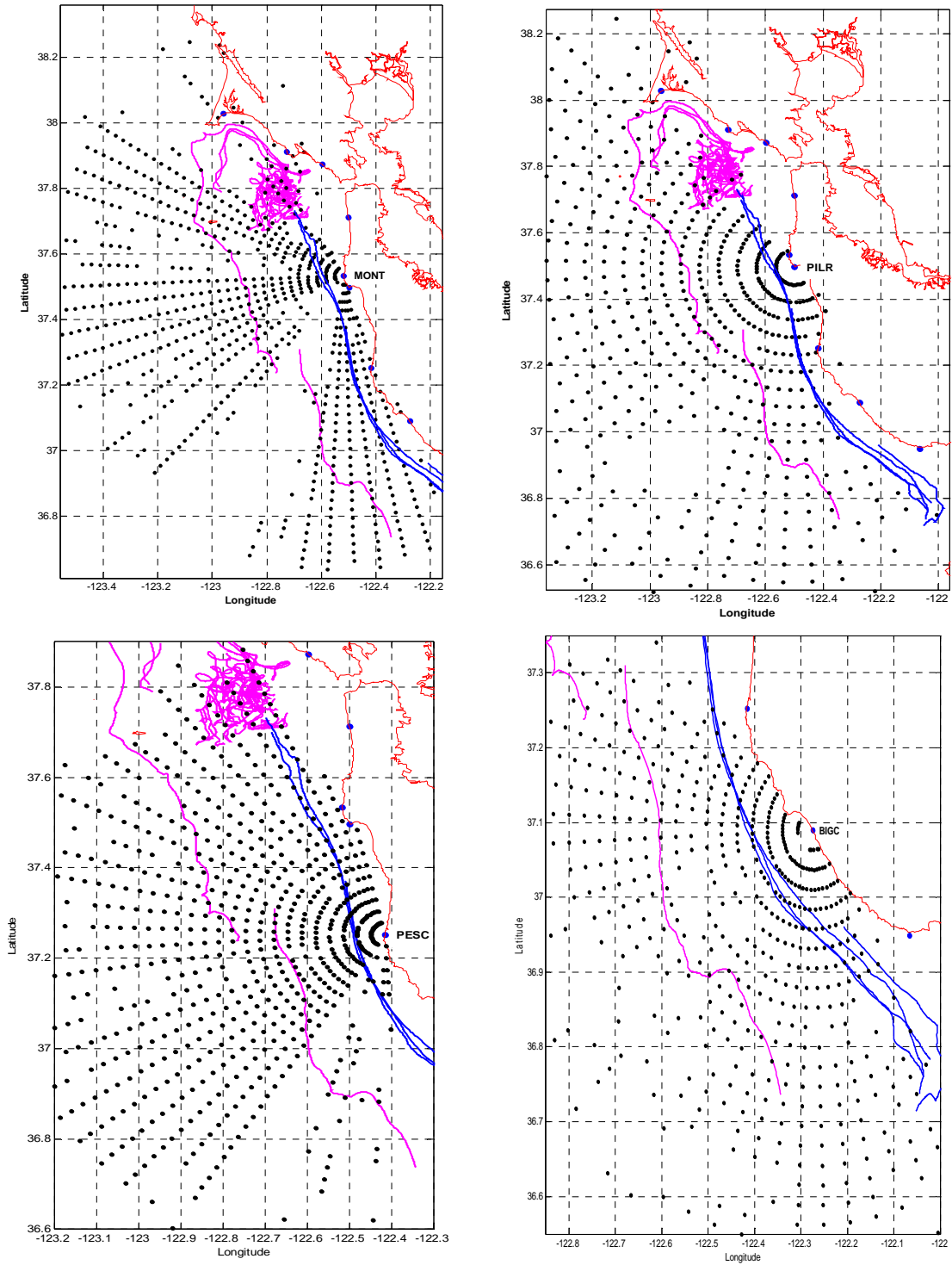


Figure 12. Typical measured radar patterns showing ocean coverage for MONT, PILR, PESC and BIGC (ideal pattern), respectively. First experiment drifter tracks are shown in blue and second experiment drifter tracks are shown in magenta.

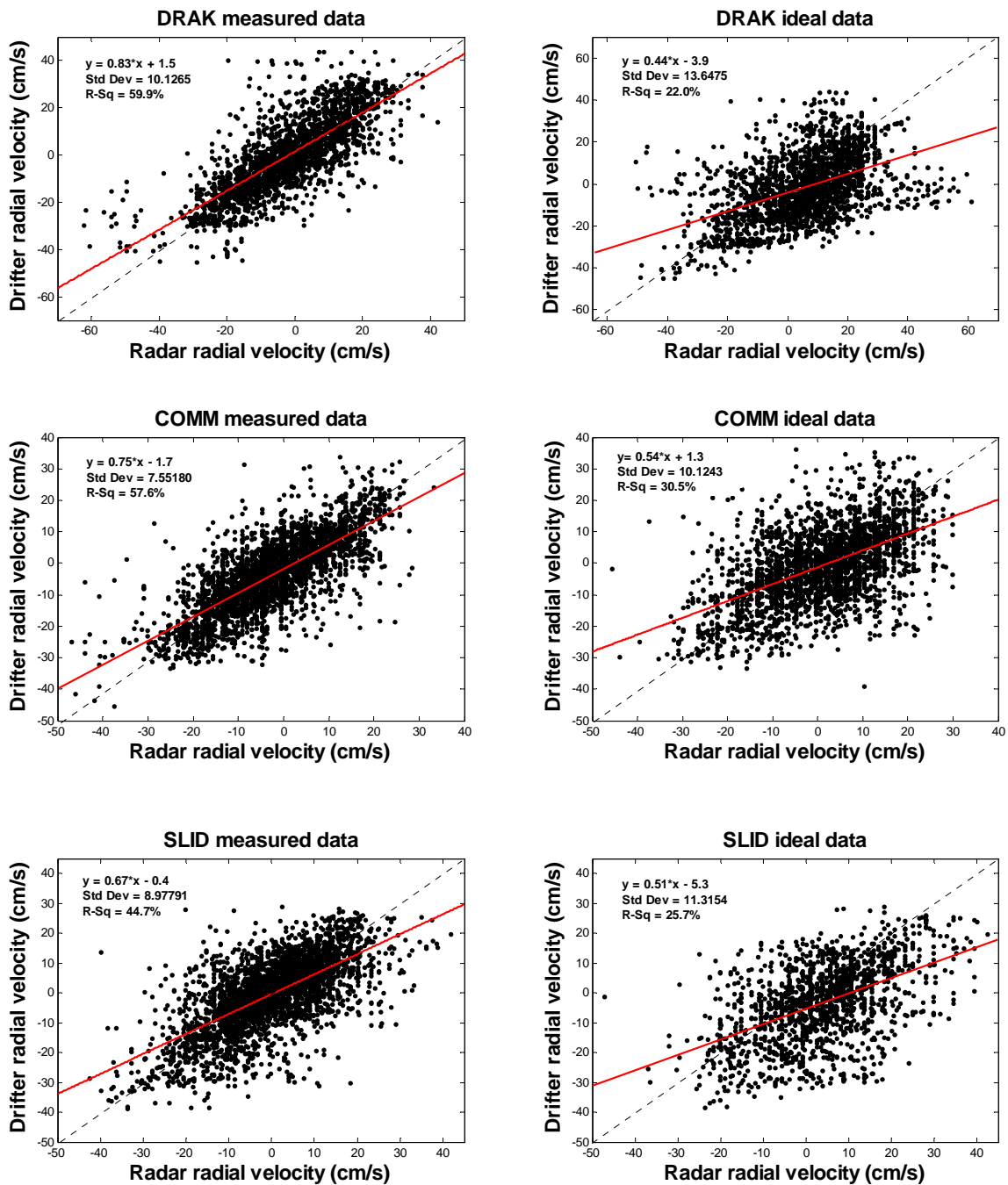


Figure 13. Scatter Plot of Drifter Radial Velocity vs. Radar Radial Velocity for Radar Sites DRAK, COMM and SLID respectively (Second Experiment). Measured Radar Patterns are shown on the left and Ideal Radar Patterns are shown on the right. Dashed line represents one to one correlation and red solid line represents the linear least squares fit of the data. The standard deviation value refers to the best fit line.

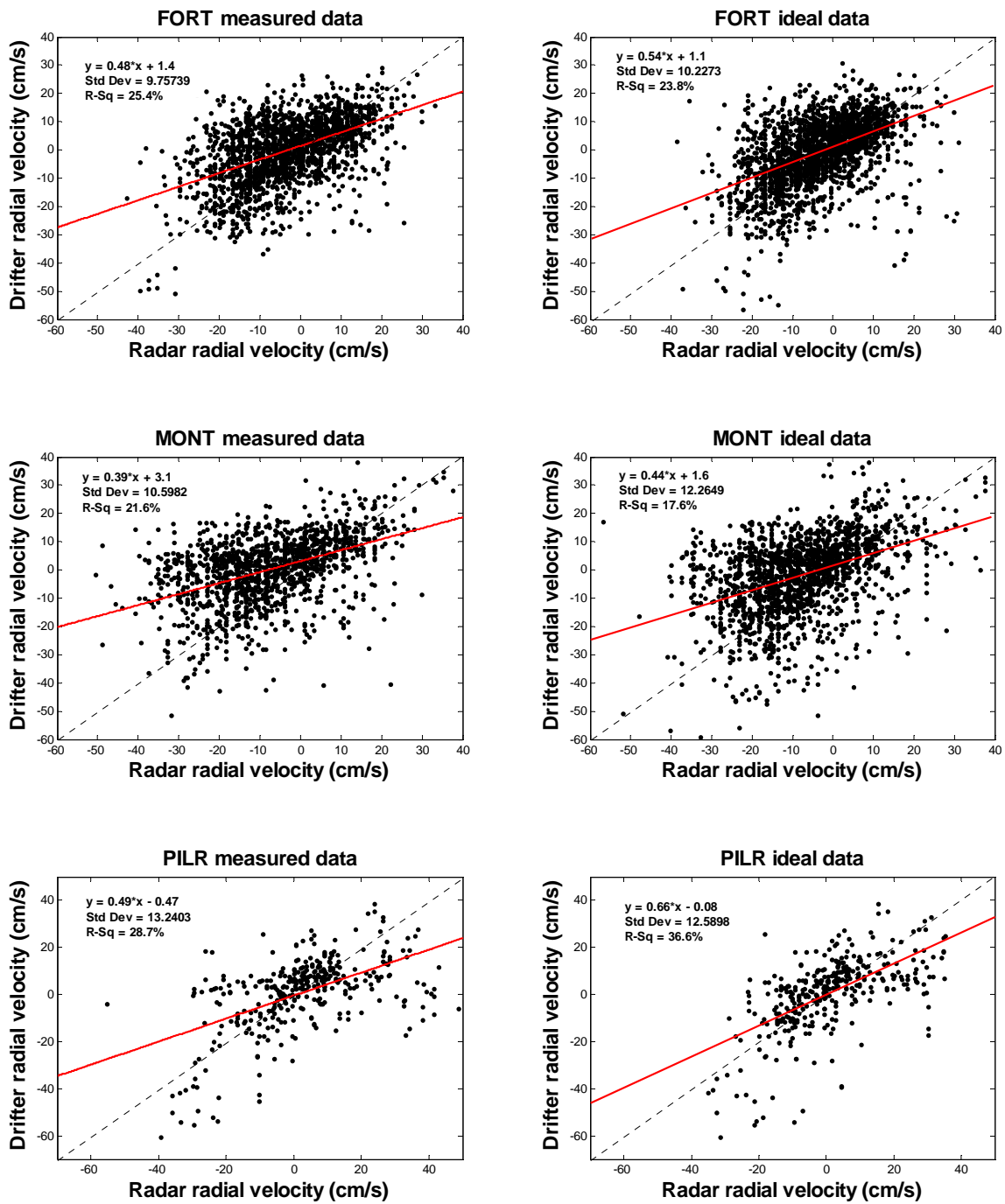
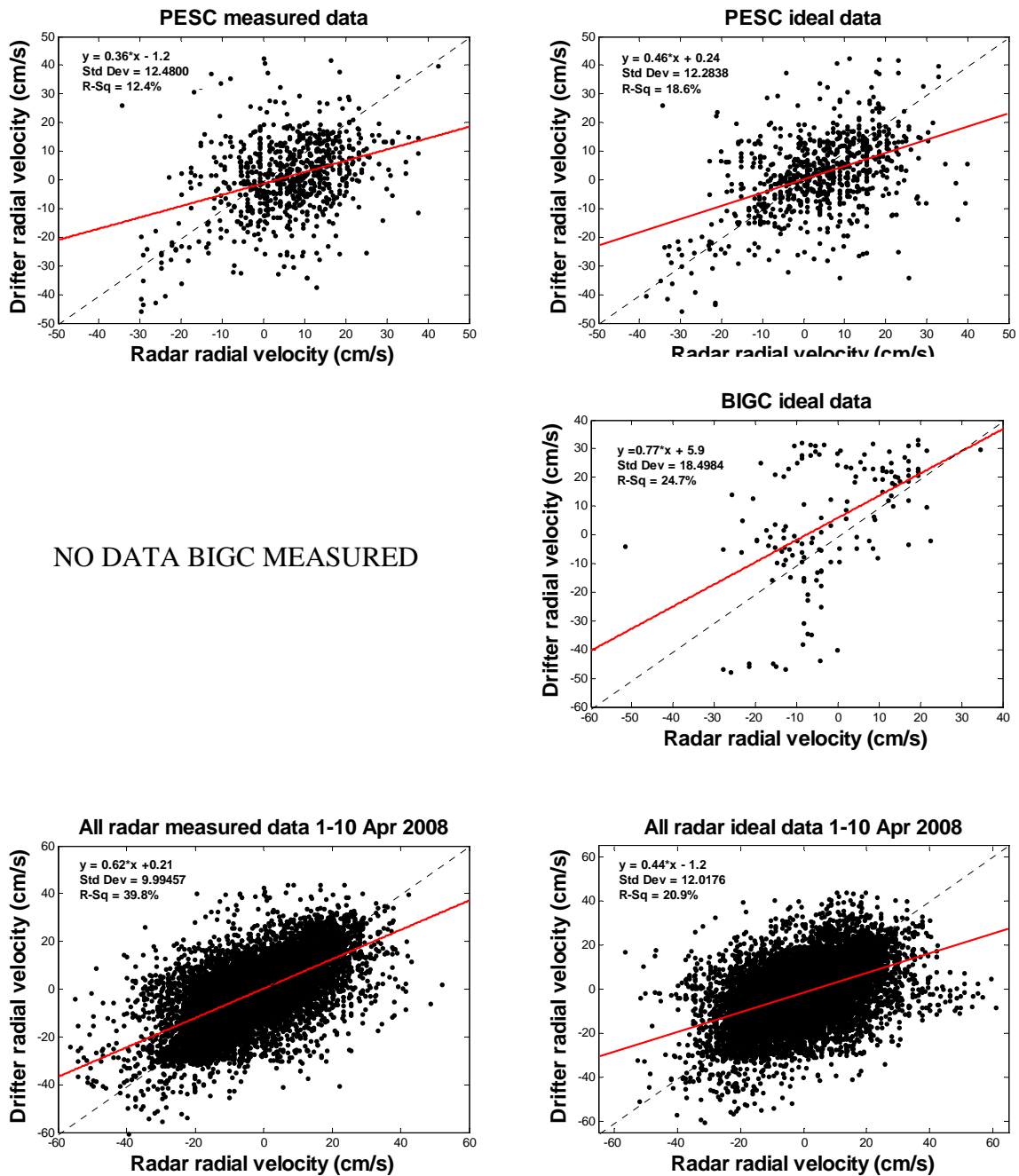


Figure 14. Scatter Plot of Drifter Radial Velocity vs. Radar Radial Velocity for Radar Sites FORT, MONT and PILR, respectively (Second Experiment). Measured Radar Patterns are shown on the left and Ideal Radar Patterns are shown on the right. Dashed line represents one to one correlation and red solid line represents the linear least squares fit of the data. The standard deviation value refers to the best fit line.



NO DATA BIGC MEASURED

Figure 15. Scatter Plot of Drifter Radial Velocity vs. Radar Radial Velocity for Radar Sites PESC and BIGC, respectively (Second Experiment). Bottom graph is a combined plot of all Radar Sites. Measured Radar Patterns are shown on the left and Ideal Radar Patterns are shown on the right. Dashed line represents one to one correlation and red solid line represents the linear least squares fit of the data. The standard deviation value refers to the best fit line.

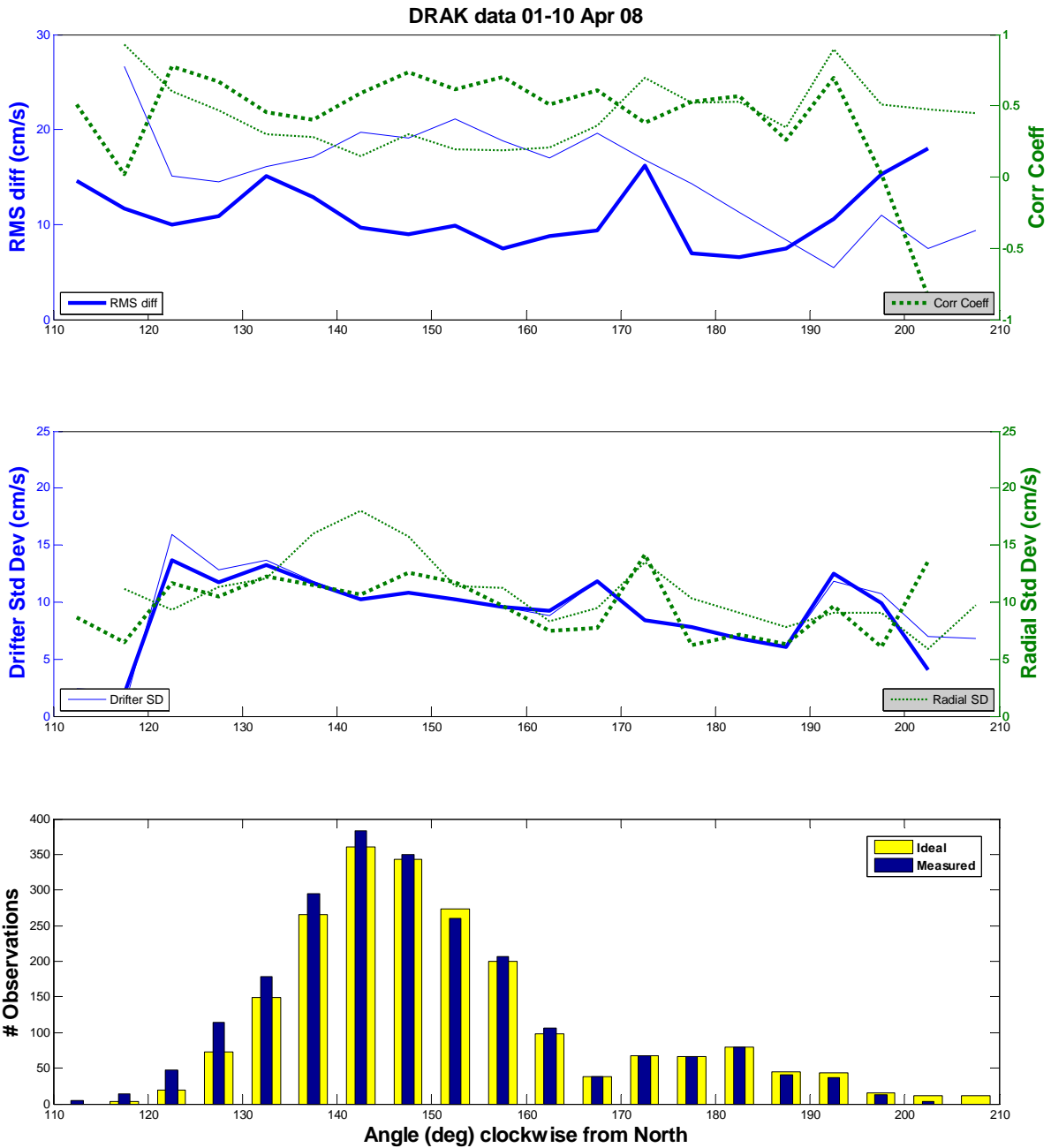


Figure 16. Correlation Coefficient and RMS difference plots vs. DRAK Radar Look Angle (top) and corresponding Drifter and Radial Standard Deviation plots vs. DRAK Radar Look Angle (middle). Bold lines represent measured data and thin lines represent ideal data. The lower plot indicates the number of drifter/radar point matches/observations that occurred vs. DRAK Radar Look Angle. The thin blue bar represents the measured pattern and the wide yellow bar represents the ideal pattern. Second experiment only.

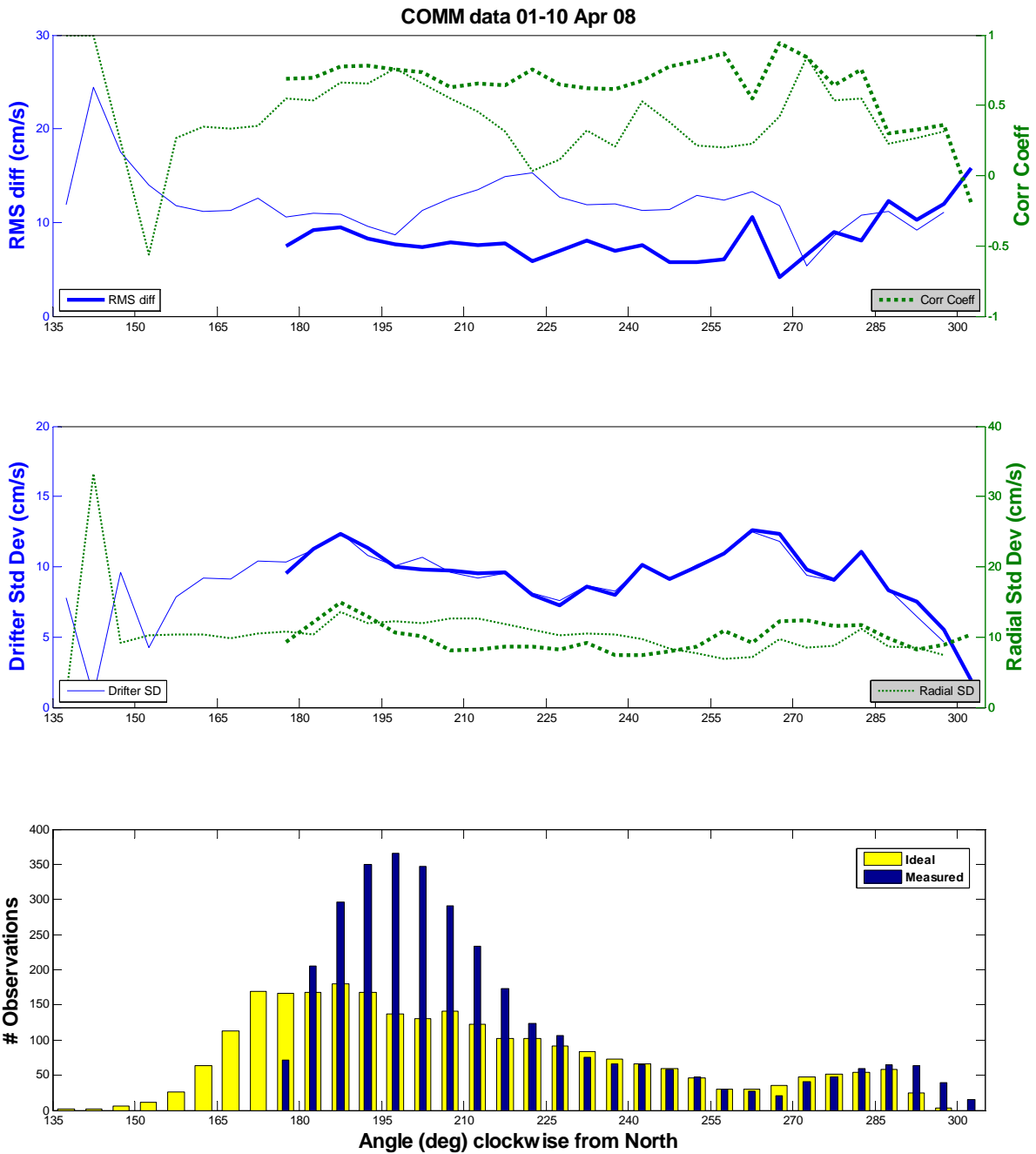


Figure 17. Correlation Coefficient and RMS difference plots vs. COMM Radar Look Angle (top) and corresponding Drifter and Radial Standard Deviation plots vs. COMM Radar Look Angle (middle). Bold lines represent measured data and thin lines represent ideal data. The lower plot indicates the number of drifter/radar point matches/observations that occurred vs. COMM Radar Look Angle. The thin blue bar represents the measured pattern and the wide yellow bar represents the ideal pattern. Second experiment only.

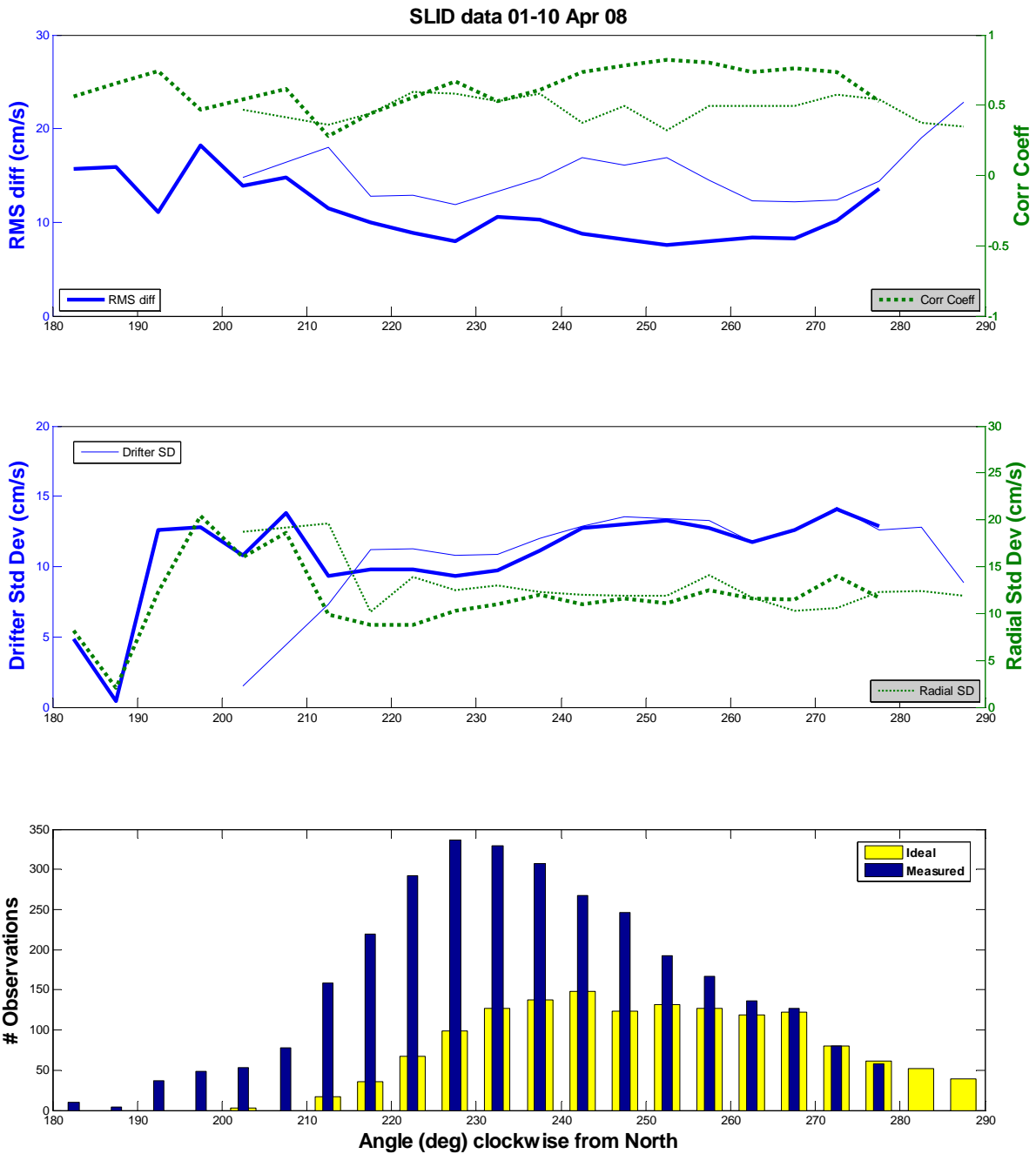


Figure 18. Correlation Coefficient and RMS difference plots vs. SLID Radar Look Angle (top) and corresponding Drifter and Radial Standard Deviation plots vs. SLID Radar Look Angle (middle). Bold lines represent measured data and thin lines represent ideal data. The lower plot indicates the number of drifter/radar point matches/observations that occurred vs. SLID Radar Look Angle. The thin blue bar represents the measured pattern and the wide yellow bar represents the ideal pattern. Second experiment only.

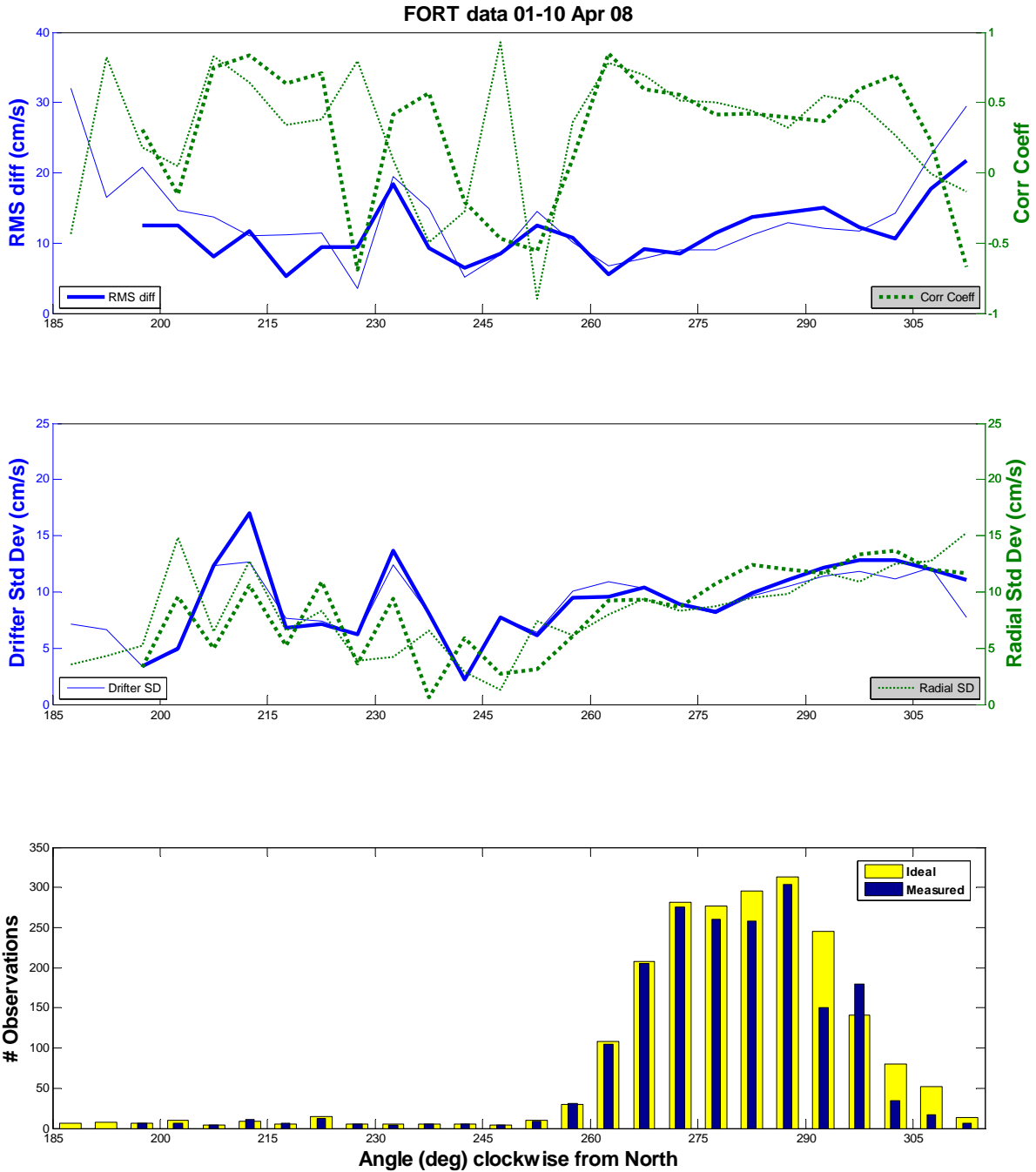


Figure 19. Correlation Coefficient and RMS difference plots vs. FORT Radar Look Angle (top) and corresponding Drifter and Radial Standard Deviation plots vs. FORT Radar Look Angle (middle). Bold lines represent measured data and thin lines represent ideal data. The lower plot indicates the number of drifter/radar point matches/observations that occurred vs. FORT Radar Look Angle. The thin blue bar represents the measured pattern and the wide yellow bar represents the ideal pattern. Second experiment only.

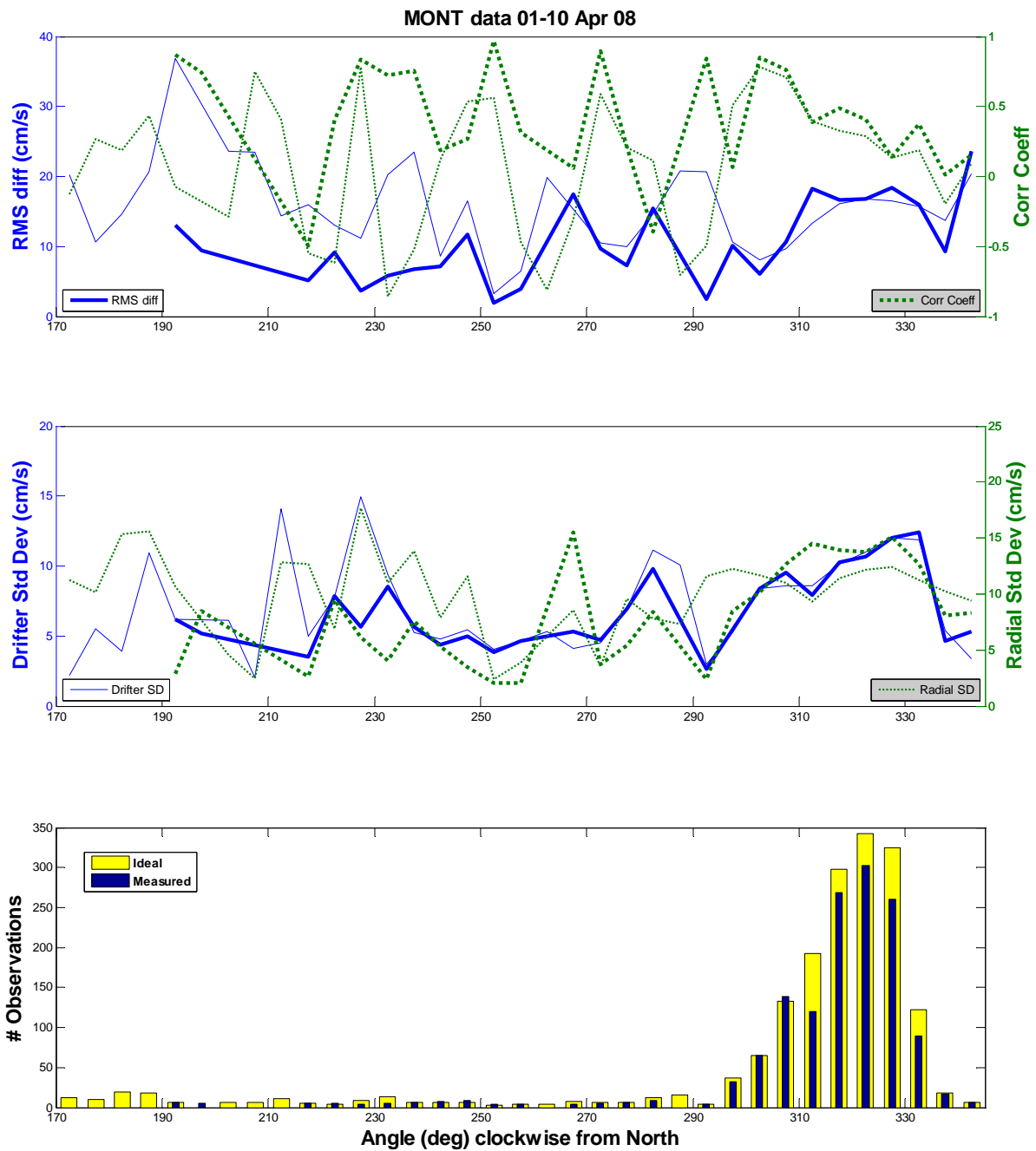


Figure 20. Correlation Coefficient and RMS difference plots vs. MONT Radar Look Angle (top) and corresponding Drifter and Radial Standard Deviation plots vs. MONT Radar Look Angle (middle). Bold lines represent measured data and thin lines represent ideal data. The lower plot indicates the number of drifter/radar point matches/observations that occurred vs. MONT Radar Look Angle. The thin blue bar represents the measured pattern and the wide yellow bar represents the ideal pattern. Second experiment only.

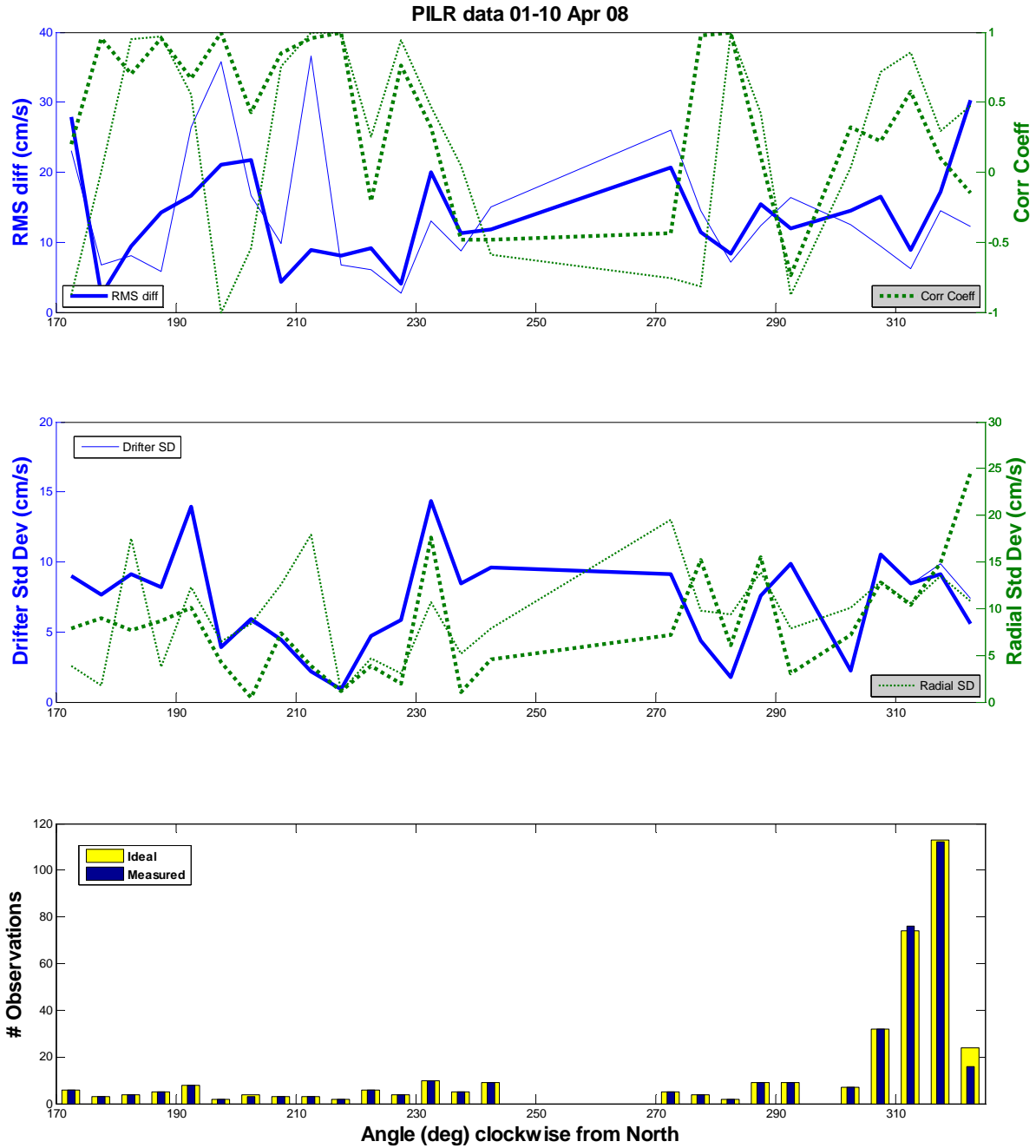


Figure 21. Correlation Coefficient and RMS difference plots vs. PILR Radar Look Angle (top) and corresponding Drifter and Radial Standard Deviation plots vs. PILR Radar Look Angle (middle). Bold lines represent measured data and thin lines represent ideal data. The lower plot indicates the number of drifter/radar point matches/observations that occurred vs. PILR Radar Look Angle. The thin blue bar represents the measured pattern and the wide yellow bar represents the ideal pattern. Second experiment only.

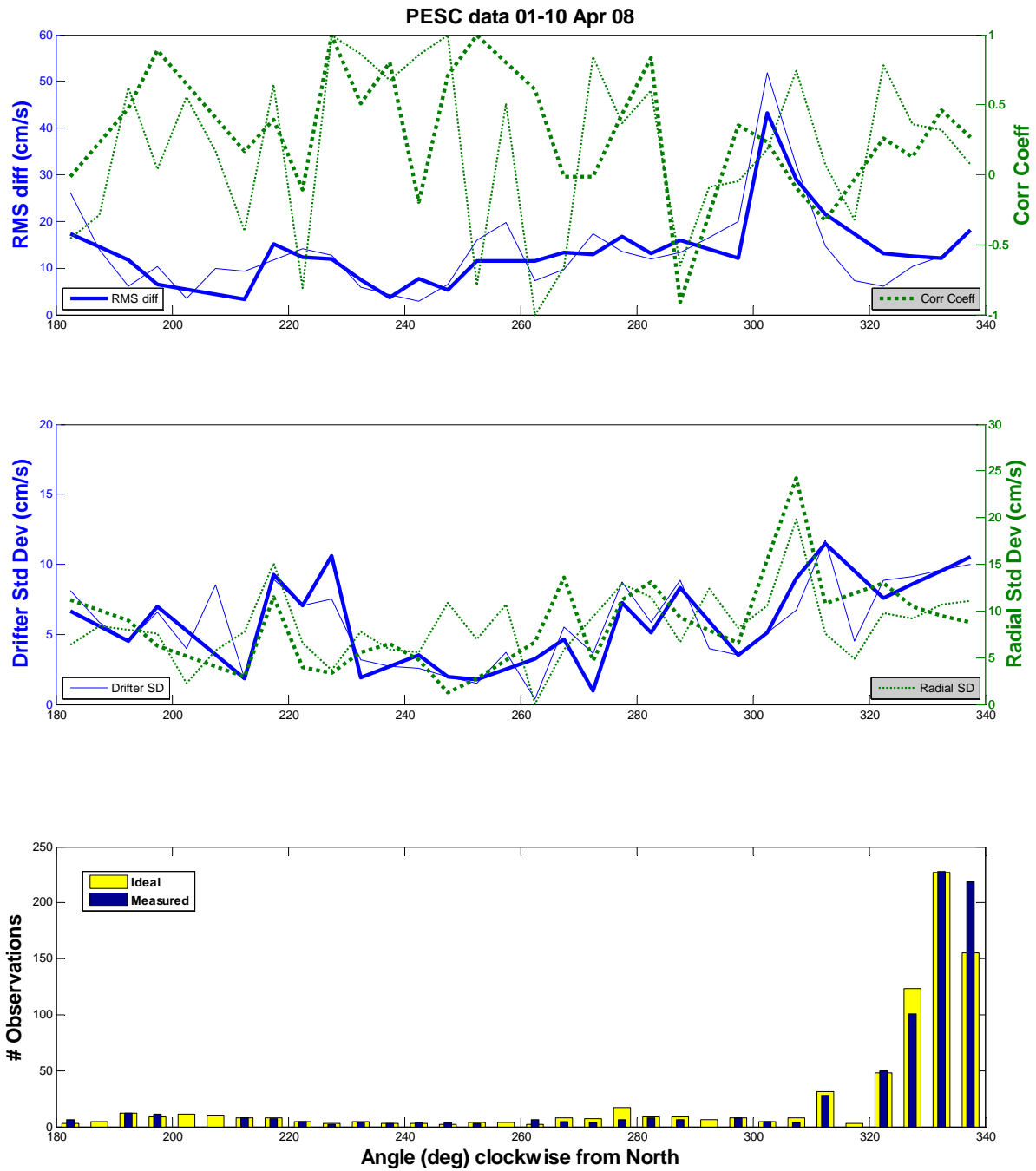


Figure 22. Correlation Coefficient and RMS difference plots vs. PESC Radar Look Angle (top) and corresponding Drifter and Radial Standard Deviation plots vs. PESC Radar Look Angle (middle). Bold lines represent measured data and thin lines represent Ideal data. The lower plot indicates the number of drifter/radar point matches/observations that occurred vs. PESC Radar Look Angle. The thin blue bar represents the measured pattern and the wide yellow bar represents the ideal pattern. Second experiment only.

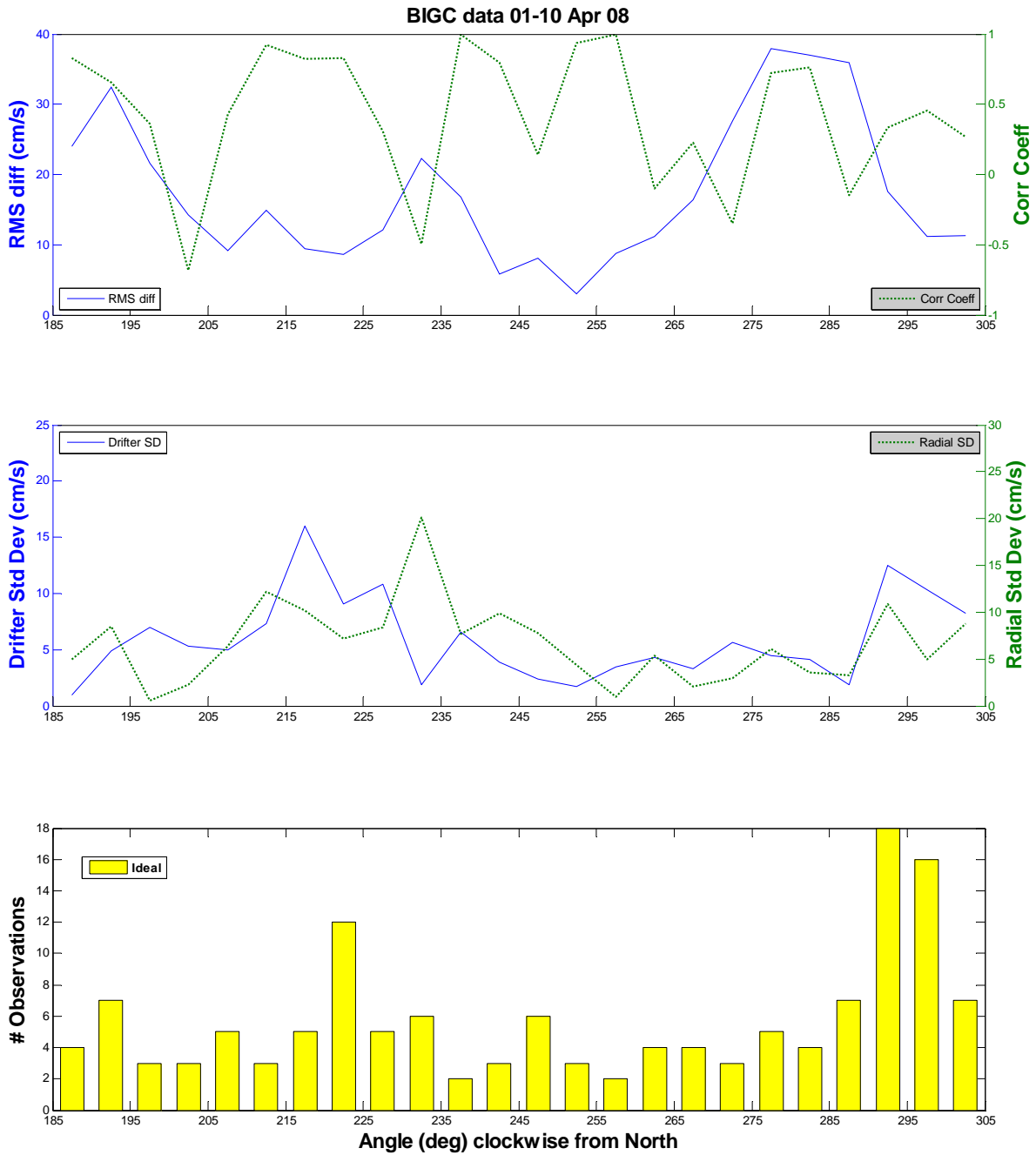


Figure 23. Correlation Coefficient and RMS difference plots vs. BIGC Radar Look Angle (top) and corresponding Drifter and Radial Standard Deviation plots vs. BIGC Radar Look Angle (middle). Thin lines represent ideal data. The lower plot indicates the number of drifter/radar point matches/observations that occurred vs. BIGC Radar Look Angle. The wide yellow bar represents the ideal pattern. Second experiment only.

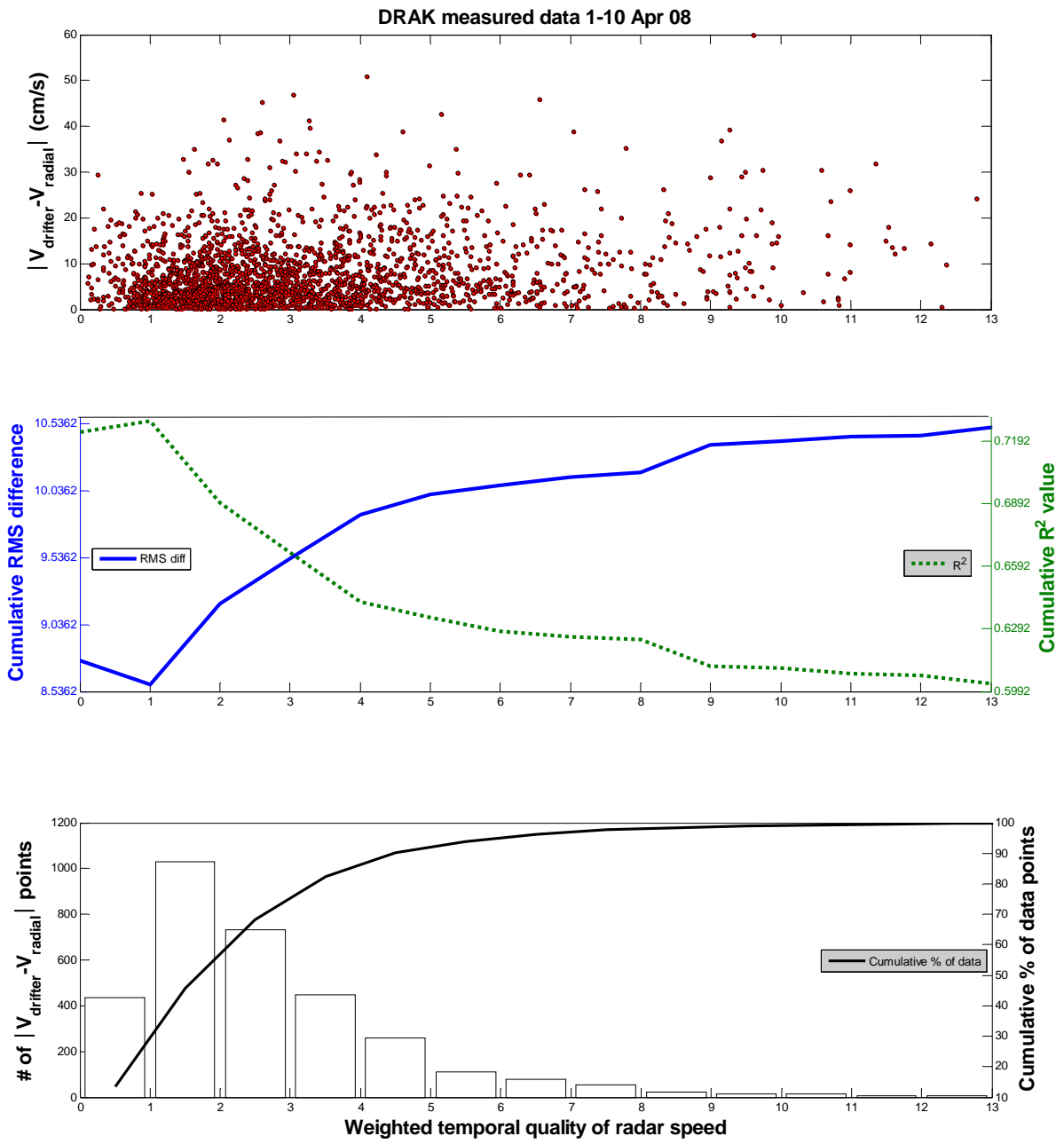


Figure 24. Plot of absolute value of (Drifter Radial Velocity minus Radar Radial Velocity) vs. weighted temporal quality of the DRAK Radar Data (top). The middle plot represents the cumulative RMS difference and cumulative R<sup>2</sup> value vs. weighted temporal quality as you increase temporal values from left to right. The bottom plot includes the number of data points contained in each temporal increment and its associated cumulative percent of data. Second experiment only.

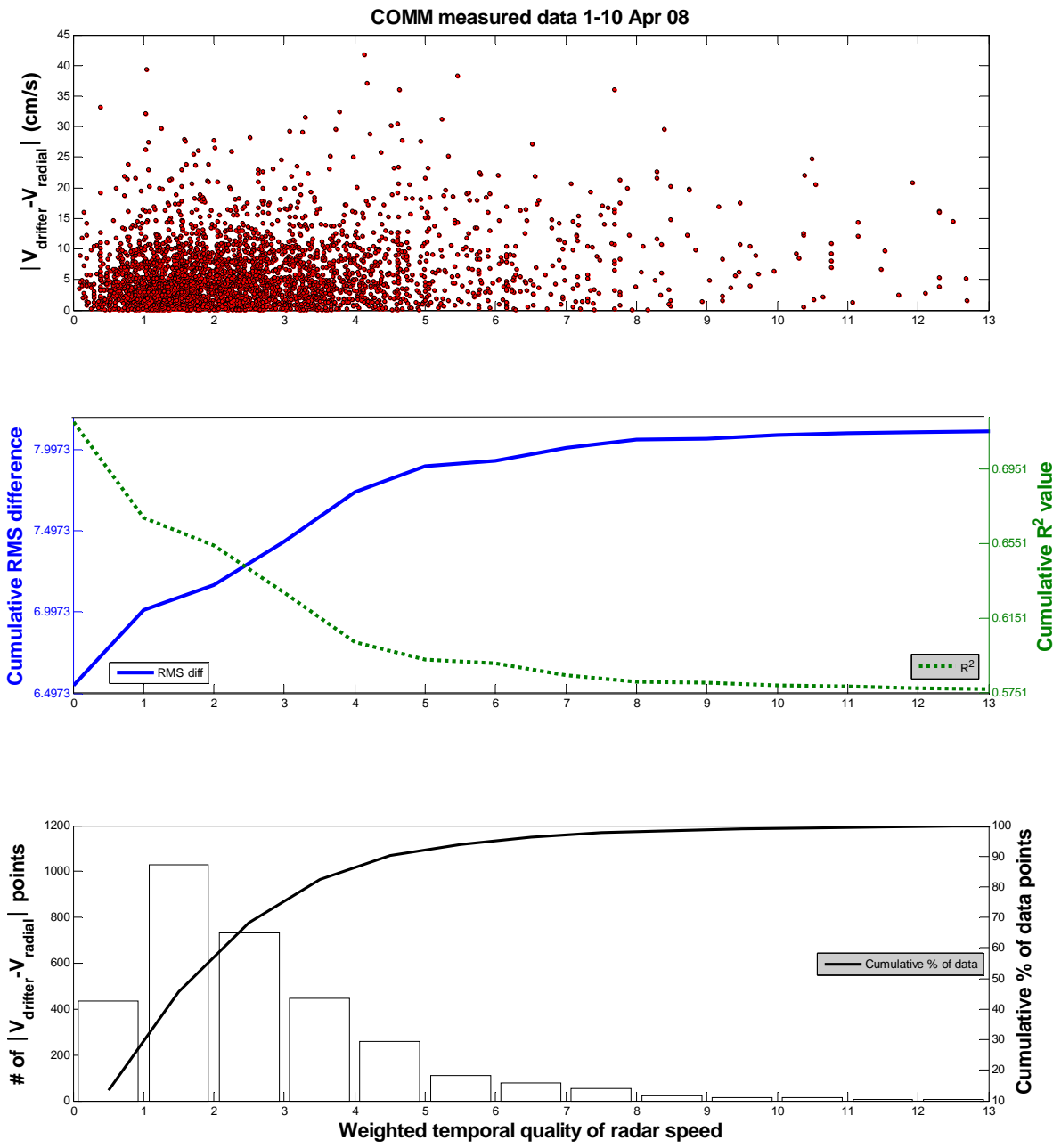


Figure 25. Plot of absolute value of (Drifter Radial Velocity minus Radar Radial Velocity) vs. weighted temporal quality of the COMM Radar Data (top). The middle plot represents the cumulative RMS difference and cumulative  $R^2$  value vs. weighted temporal quality as you increase temporal values from left to right. The bottom plot includes the number of data points contained in each temporal increment and its associated cumulative percent of data. Second experiment only.

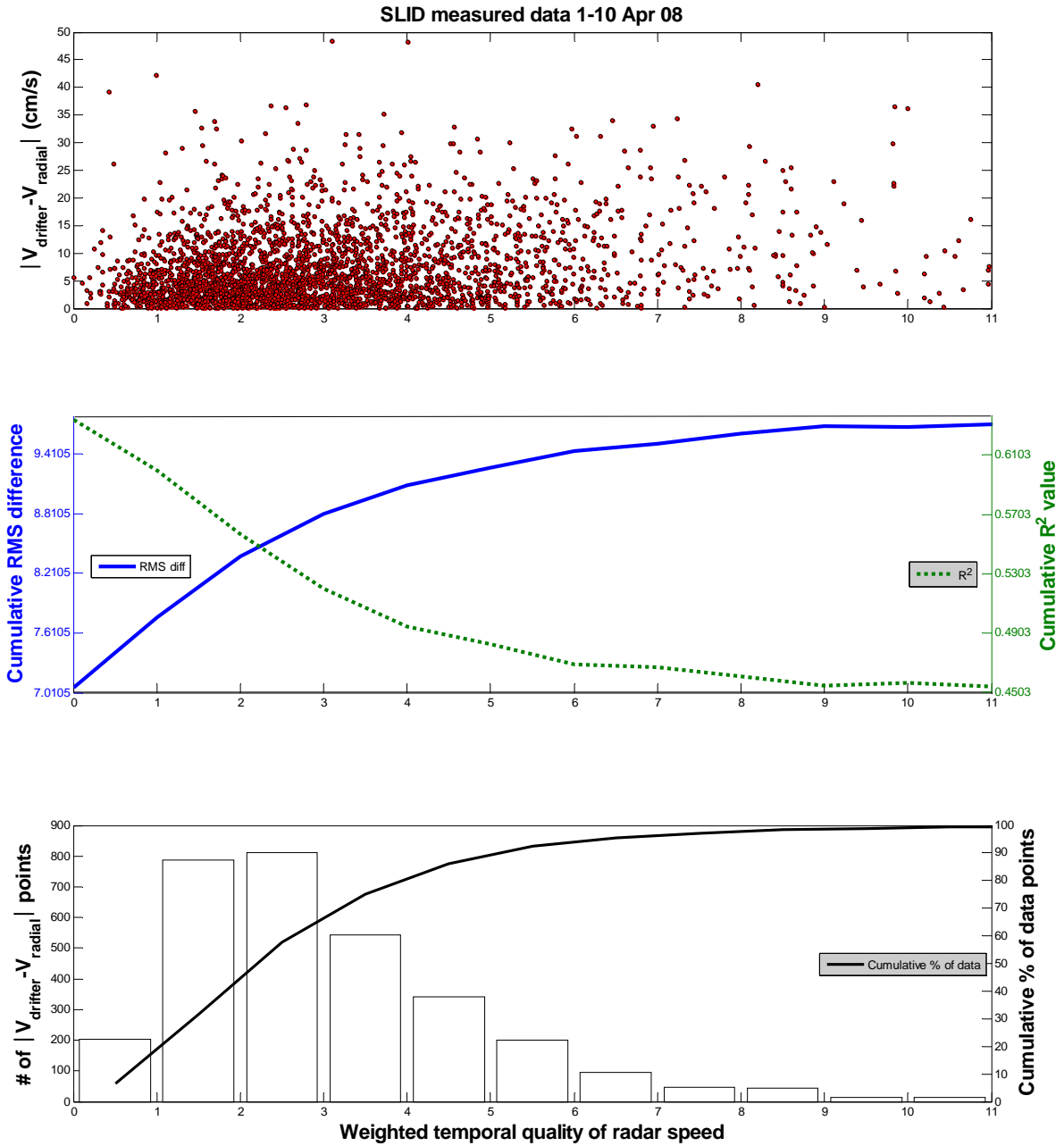


Figure 26. Plot of absolute value of (Drifter Radial Velocity minus Radar Radial Velocity) vs. weighted temporal quality of the SLID Radar Data (top). The middle plot represents the cumulative RMS difference and cumulative R<sup>2</sup> value vs. weighted temporal quality as you increase temporal values from left to right. The bottom plot includes the number of data points contained in each temporal increment and its associated cumulative percent of data. Second experiment only.

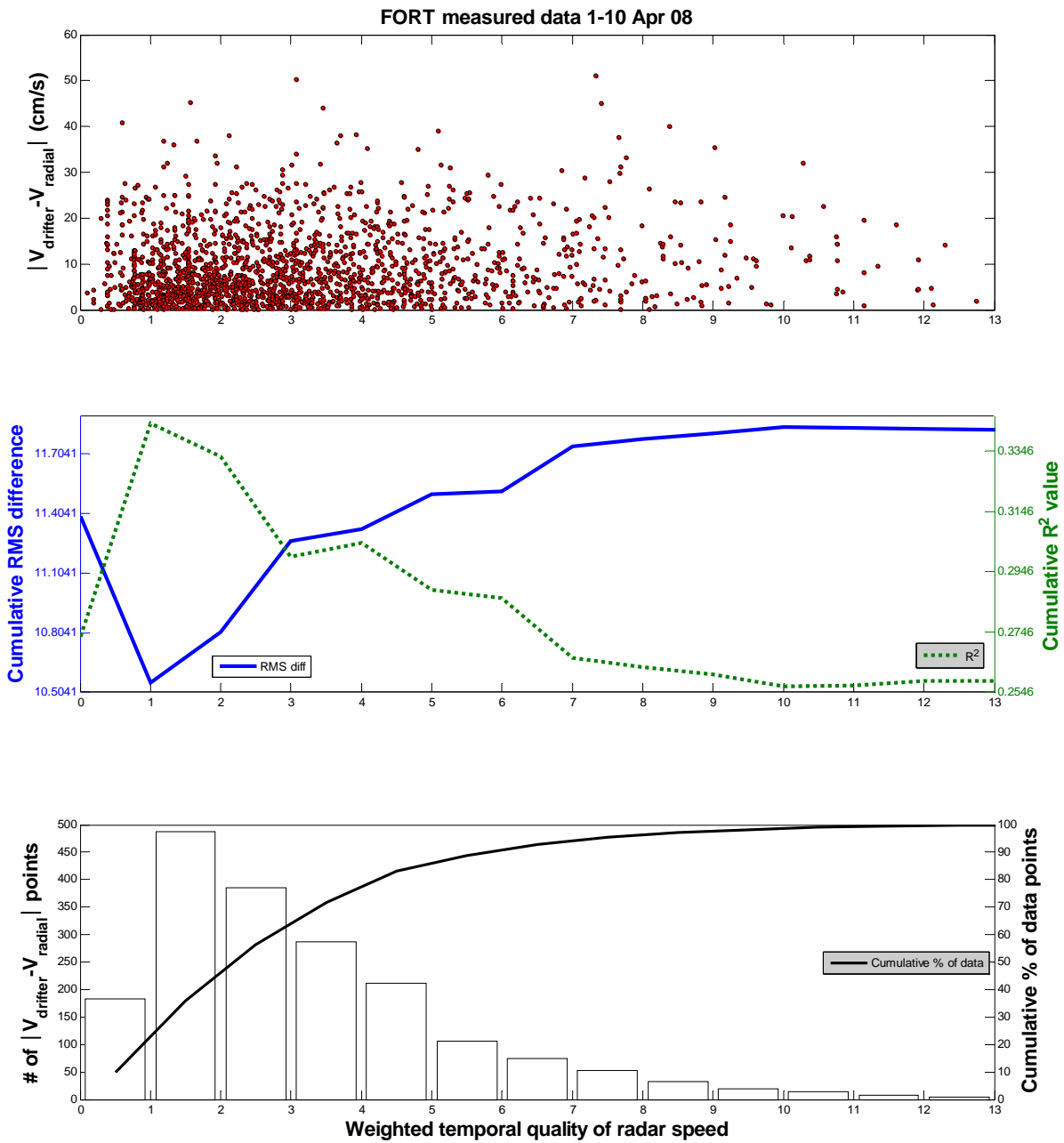


Figure 27. Plot of absolute value of (Drifter Radial Velocity minus Radar Radial Velocity) vs. weighted temporal quality of the FORT Radar Data (top). The middle plot represents the cumulative RMS difference and cumulative  $R^2$  value vs. weighted temporal quality as you increase temporal values from left to right. The bottom plot includes the number of data points contained in each temporal increment and its associated cumulative percent of data. Second experiment only.

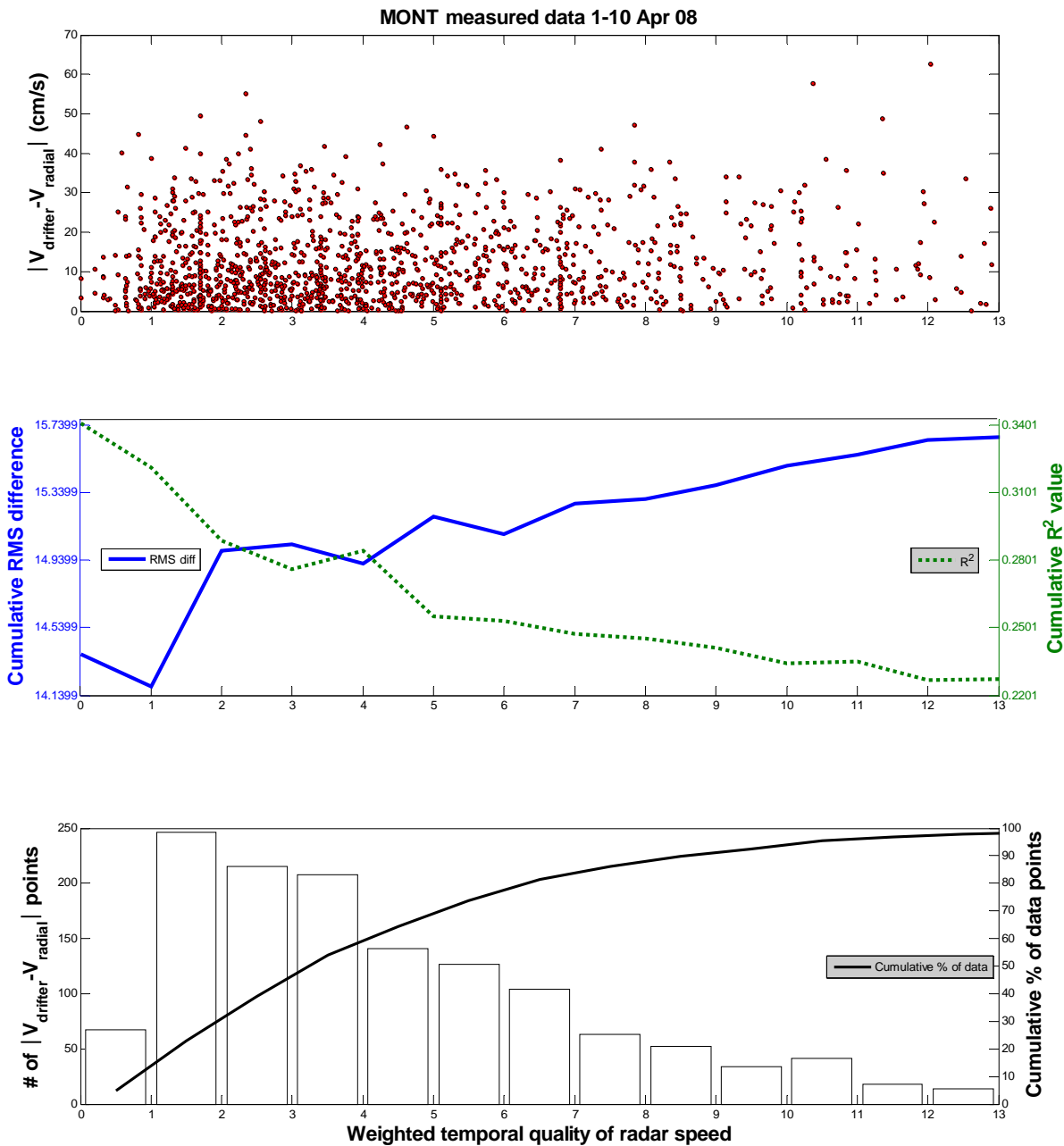


Figure 28. Plot of absolute value of (Drifter Radial Velocity minus Radar Radial Velocity) vs. weighted temporal quality of the MONT Radar Data (top). The middle plot represents the cumulative RMS difference and cumulative  $R^2$  value vs. weighted temporal quality as you increase temporal values from left to right. The bottom plot includes the number of data points contained in each temporal increment and its associated cumulative percent of data. Second experiment only.

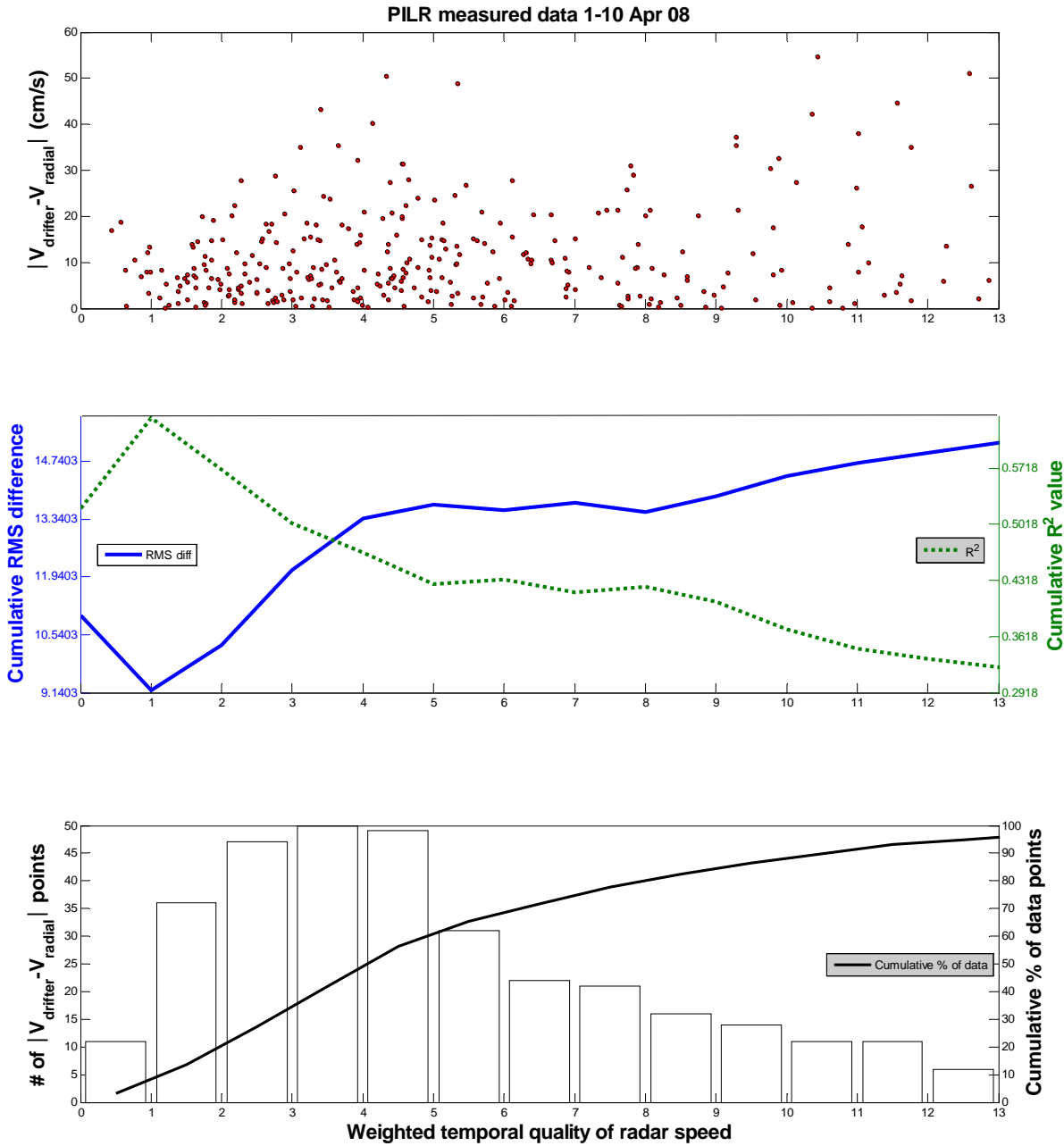


Figure 29. Plot of absolute value of (Drifter Radial Velocity minus Radar Radial Velocity) vs. weighted temporal quality of the PILR Radar Data (top). The middle plot represents the cumulative RMS difference and cumulative R<sup>2</sup> value vs. weighted temporal quality as you increase temporal values from left to right. The bottom plot includes the number of data points contained in each temporal increment and its associated cumulative percent of data. Second experiment only.

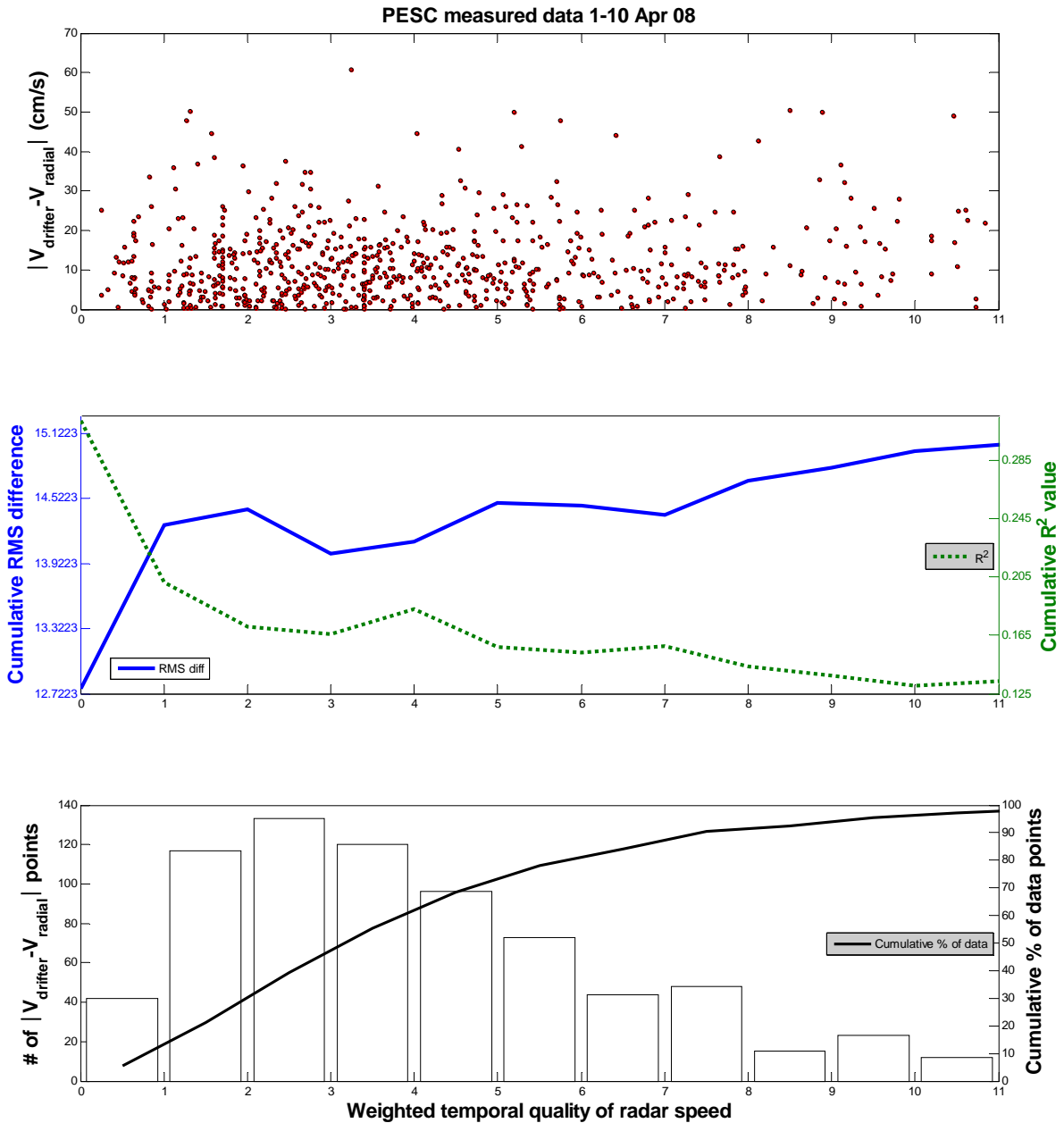


Figure 30. Plot of absolute value of (Drifter Radial Velocity minus Radar Radial Velocity) vs. weighted temporal quality of the PESC Radar Data (top). The middle plot represents the cumulative RMS difference and cumulative  $R^2$  value vs. weighted temporal quality as you increase temporal values from left to right. The bottom plot includes the number of data points contained in each temporal increment and its associated cumulative percent of data. Second experiment only.

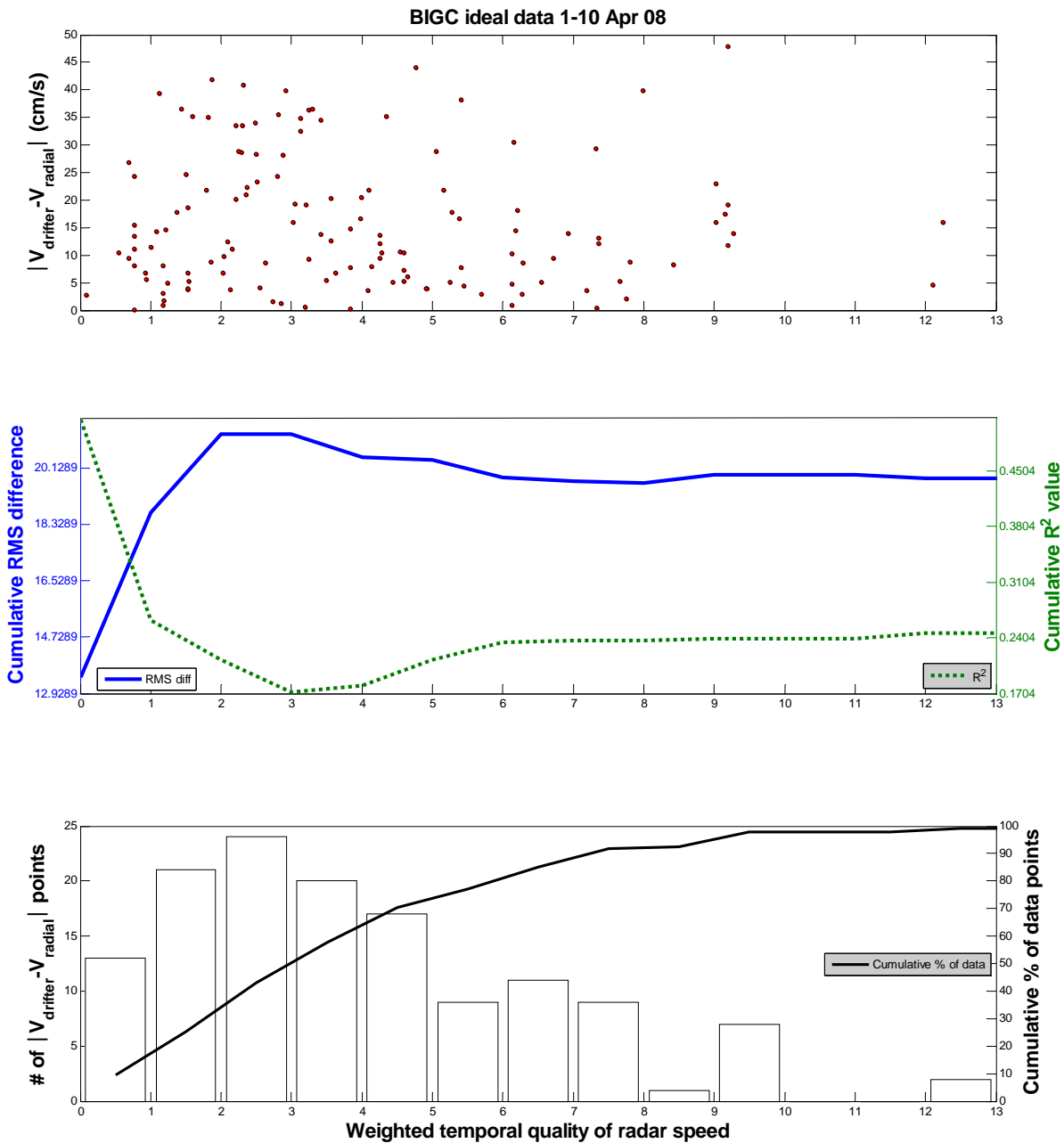


Figure 31. Plot of absolute value of (Drifter Radial Velocity minus Radar Radial Velocity) vs. weighted temporal quality of the BIGC Radar Data (top). The middle plot represents the cumulative RMS difference and cumulative  $R^2$  value vs. weighted temporal quality as you increase temporal values from left to right. The bottom plot includes the number of data points contained in each temporal increment and its associated cumulative percent of data. Second experiment only.

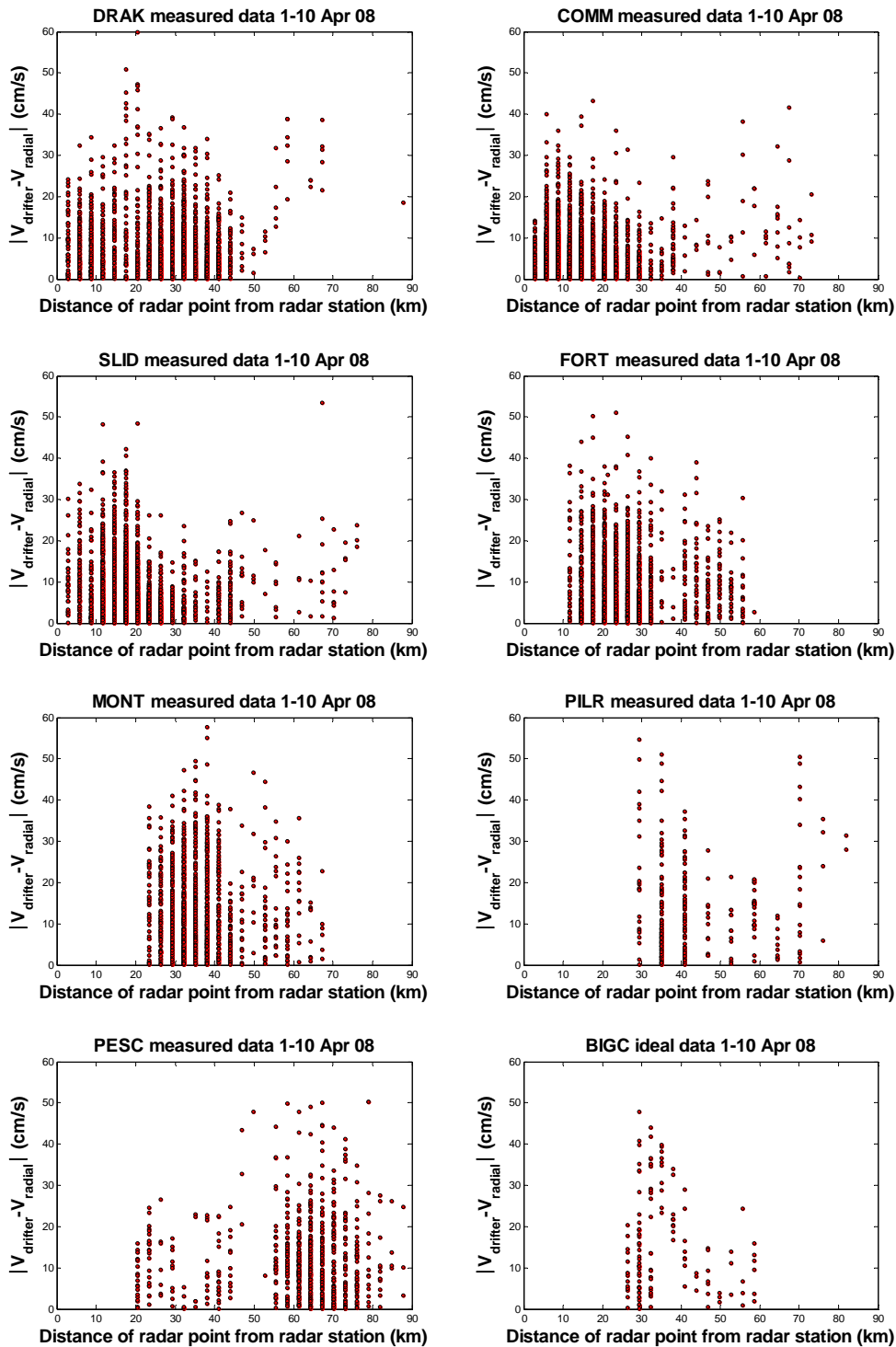


Figure 32. Plot of absolute value of (Drifter Radial Velocity minus Radar Radial Velocity) vs. distance of radar point from radar station for each radar station (North to South). The three kilometer spatial range separation of each radar station's data is evident in the vertical groupings of the data. Second experiment only.

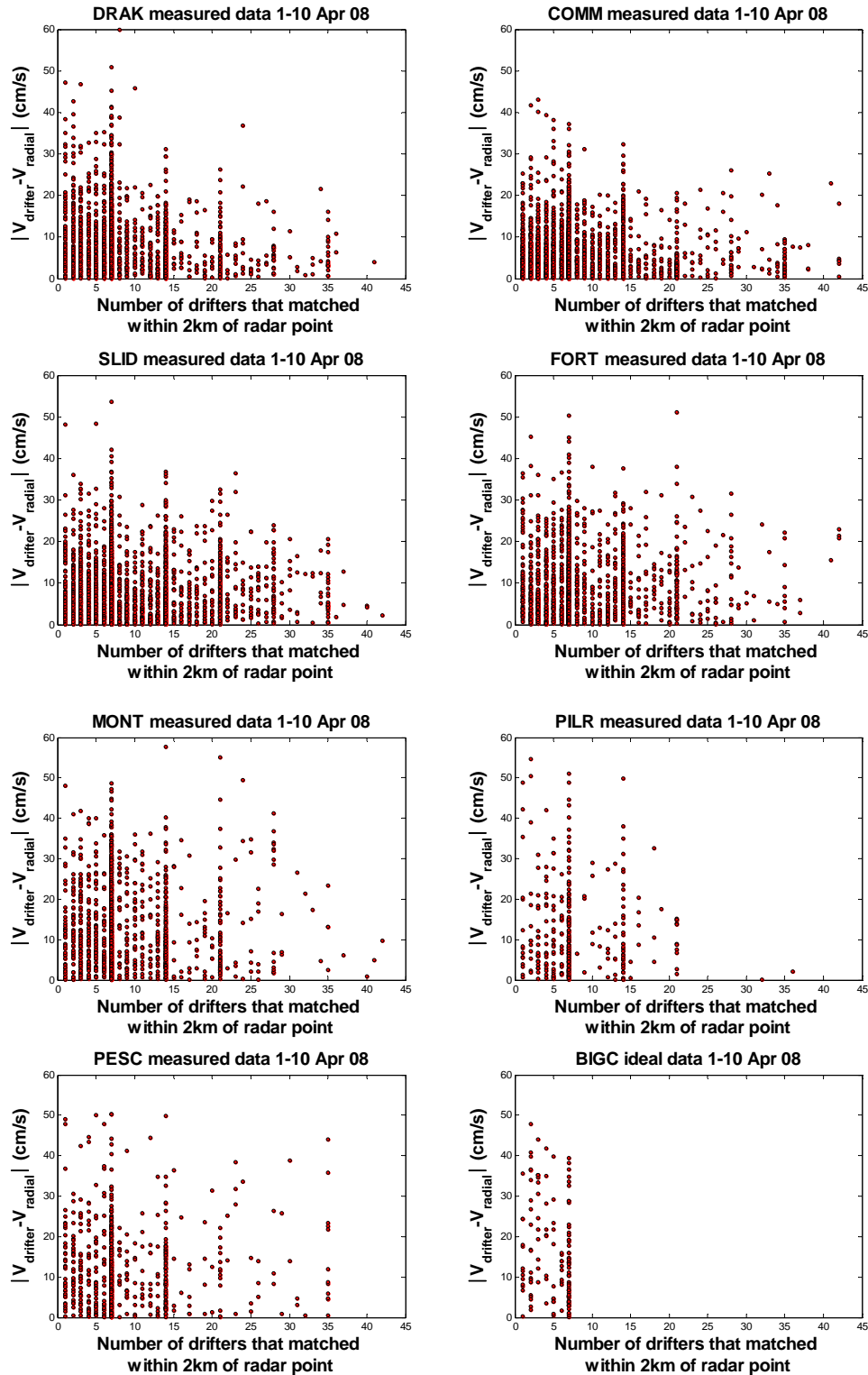


Figure 33. Plot of absolute value of (Drifter Radial Velocity minus Radar Radial Velocity) vs. the # of drifters that matched within 2km of a radar point for each radar station (North to South). Vertical groupings at intervals of 7 are indicative of the predominance of having a full range of drifter data (+/- 30 min) per hourly radar point. Second experiment only.

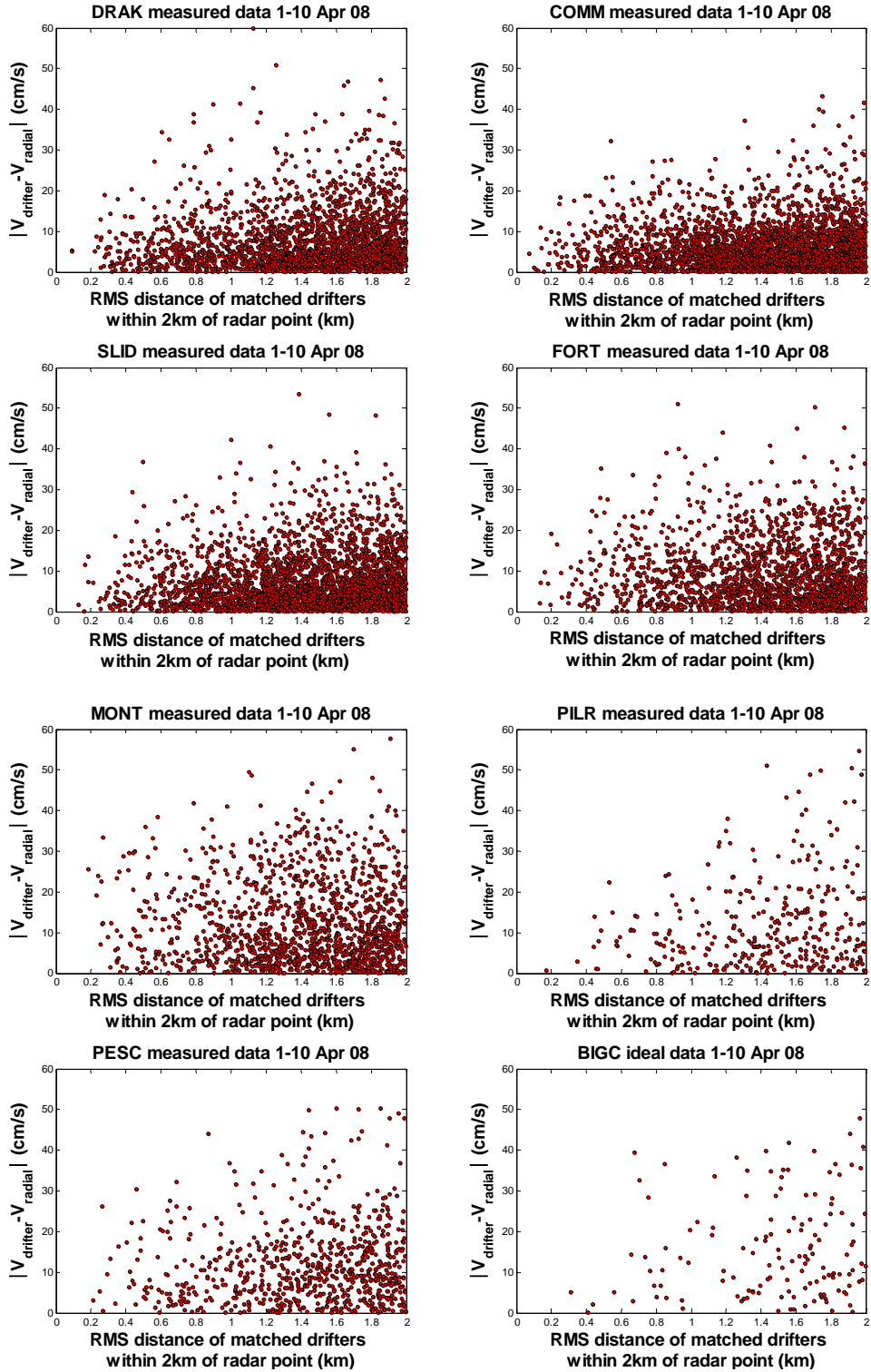


Figure 34. Plot of absolute value of (Drifter Radial Velocity minus Radar Radial Velocity) vs. the RMS distance of matched drifters within 2km of a radial point. Second experiment only.

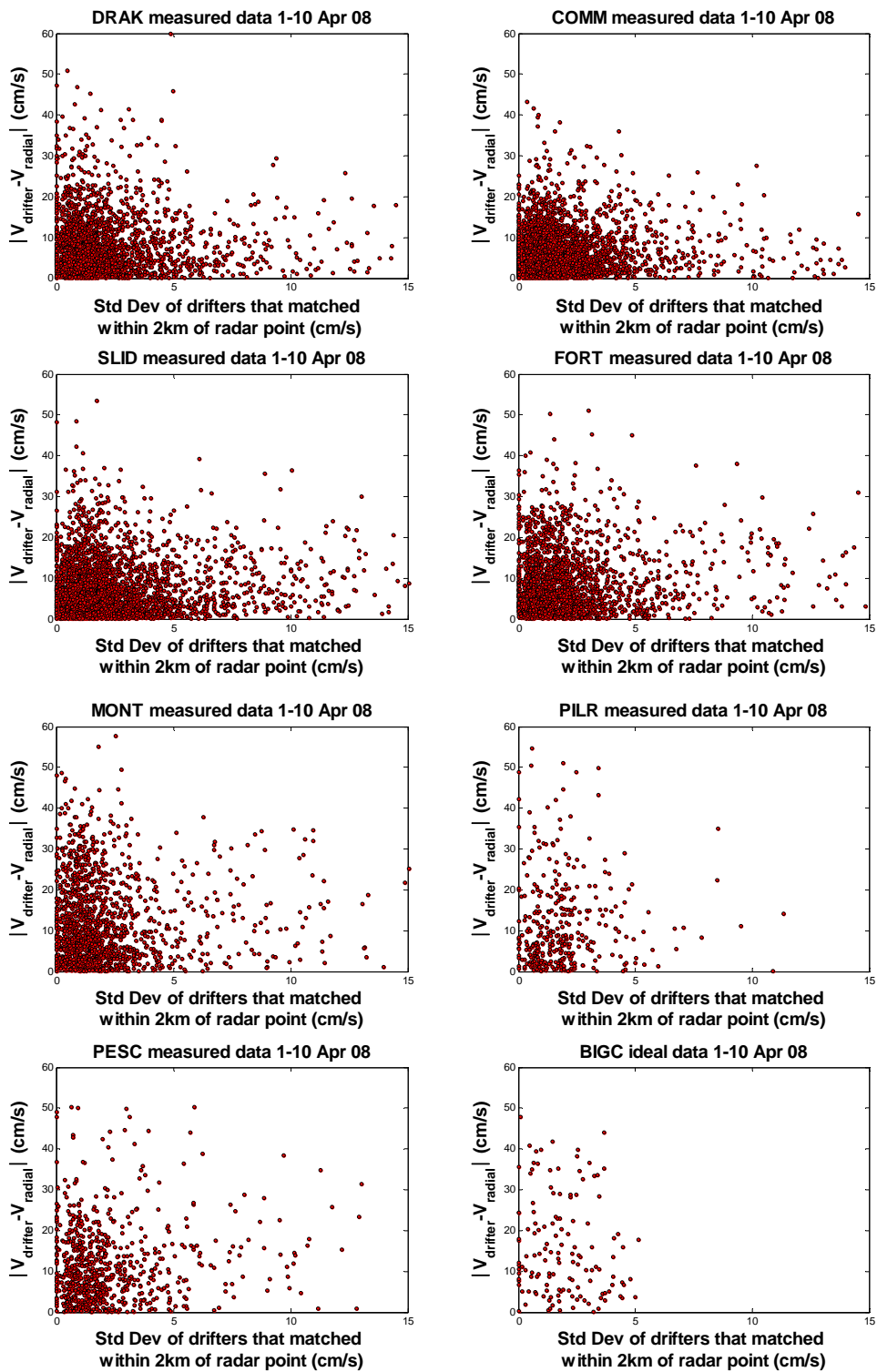
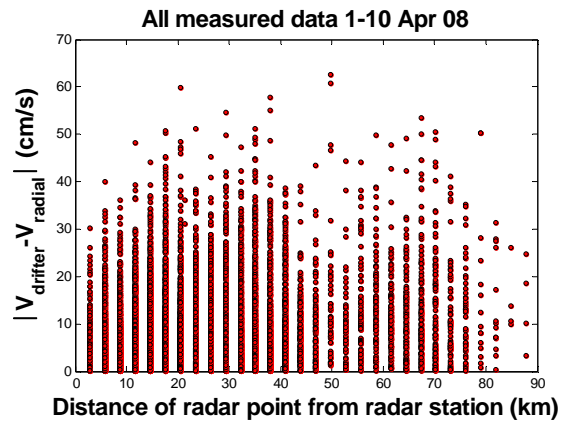
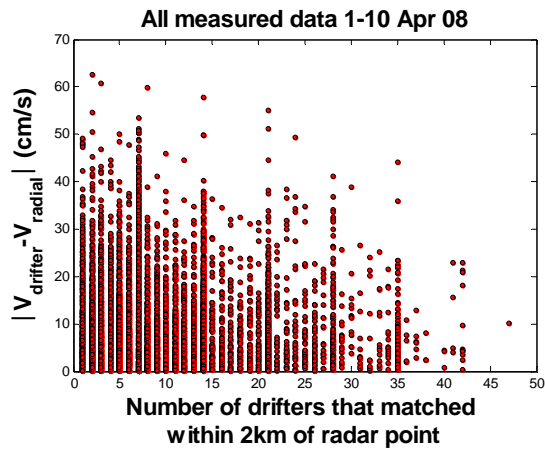
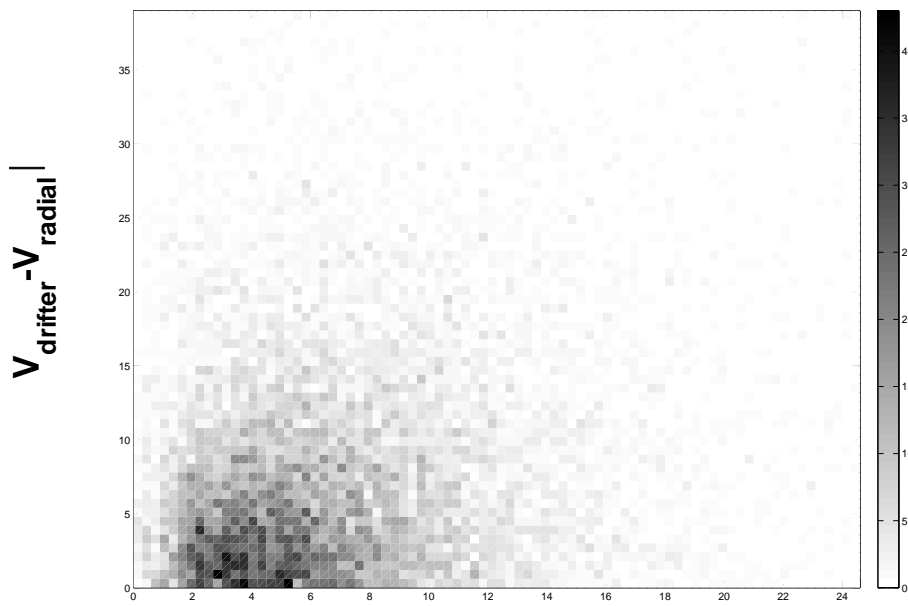


Figure 35. Plot of absolute value of (Drifter Radial Velocity minus Radar Radial Velocity) vs. the Standard Deviation of the radial velocities of the drifters that matched within 2km of a radar point. Second experiment only.



All measured data 1-10 Apr 08



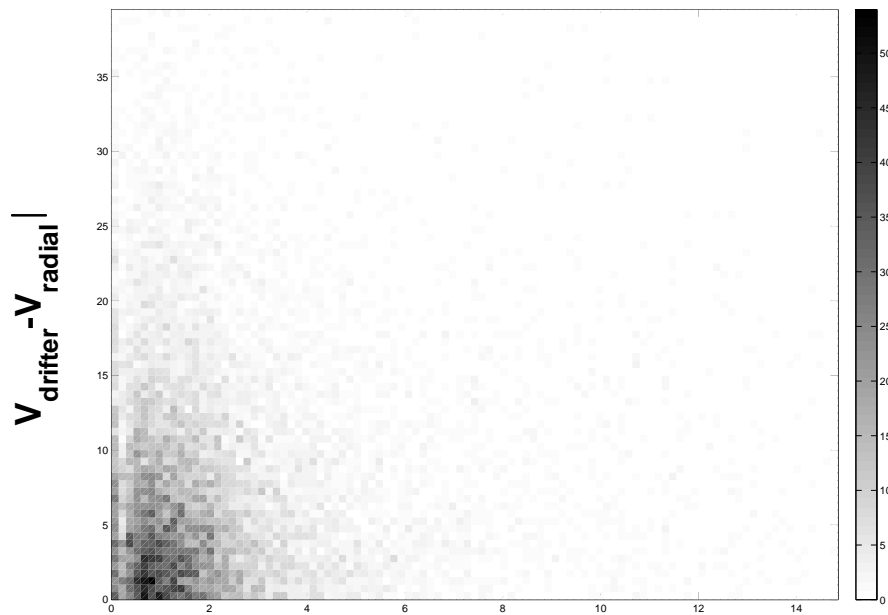
Weighted temporal quality of radar radial speed

Figure 36. Scatter Plot of combined measured radar data for the second experiment vs. various queries. Bottom chart includes density of points via use of a colorbar.

All measured data 1-10 Apr 08

$V_{drifter} - V_{radial}$

RMS distance of matched drifters  
within 2km of radar point



Std Dev of drifters that matched  
within 2km of radar point

Figure 37. Scatter Plot (with relative density of points) of combined measured radar data for the second experiment vs. various queries.

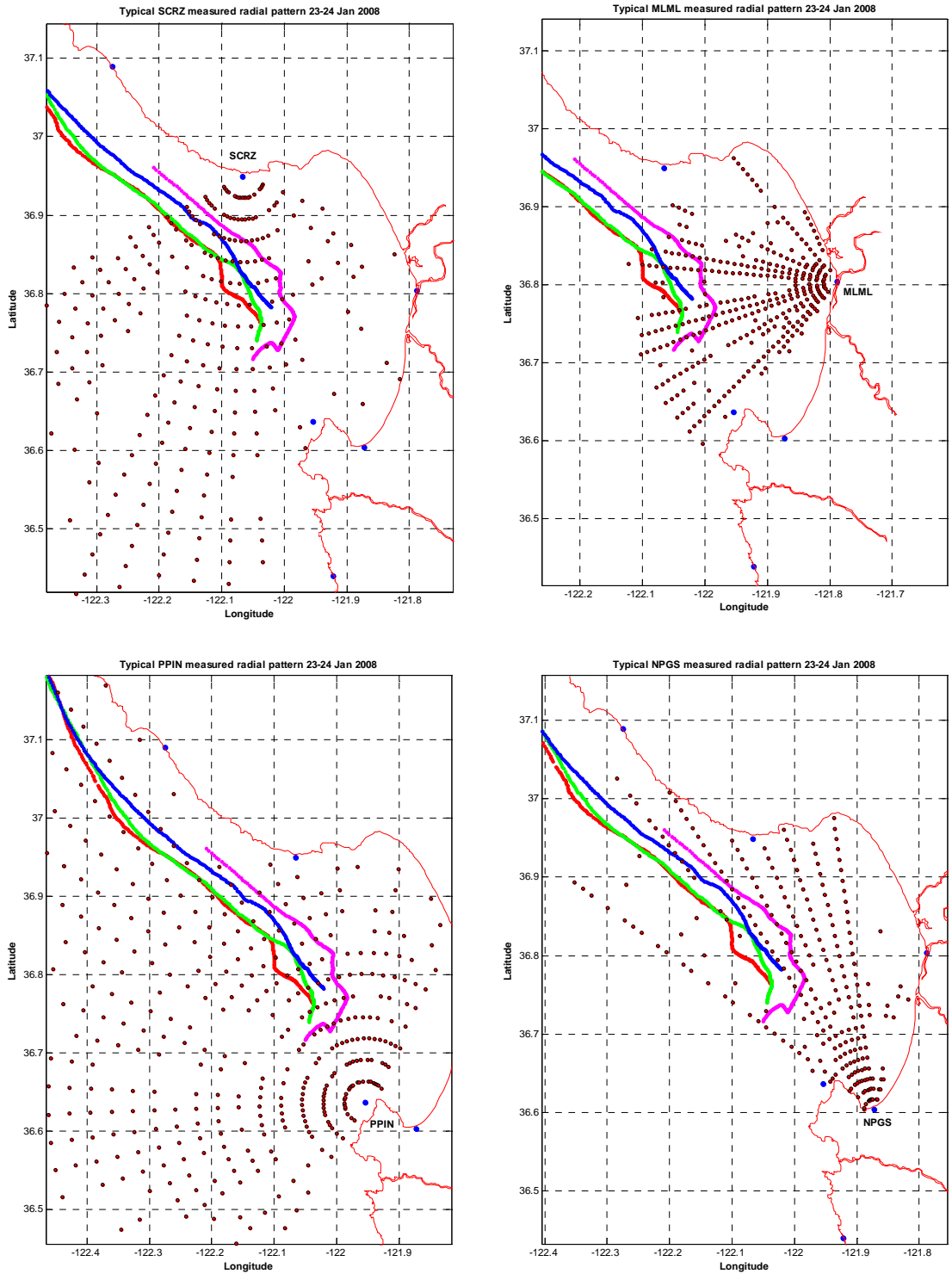


Figure 38. Typical measured radar patterns showing ocean coverage for SCRZ, MLML, PPIN and NPGS, respectively. First experiment drifter tracks are shown red, green, blue and magenta.

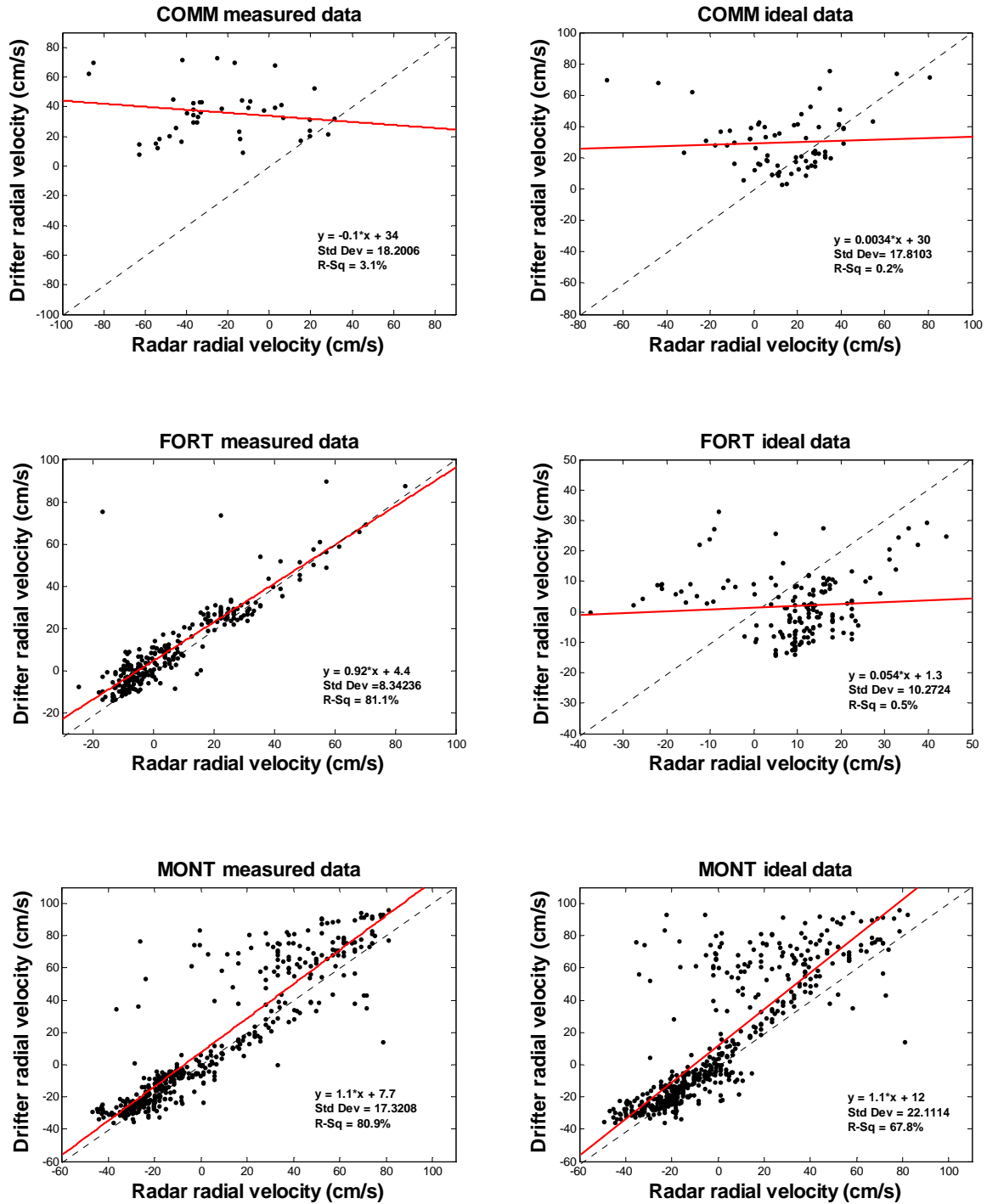


Figure 39. Scatter Plot of Drifter Radial Velocity vs. Radar Radial Velocity for Radar Sites COMM, FORT and MONT, respectively (First Experiment – 23-27 January 2008). Measured Radar Patterns are shown on the left and Ideal Radar Patterns are shown on the right. Dashed line represents one to one correlation and red solid line represents the linear least squares fit of the data. The standard deviation value refers to the best fit line.

NO DATA PESC MEASURED

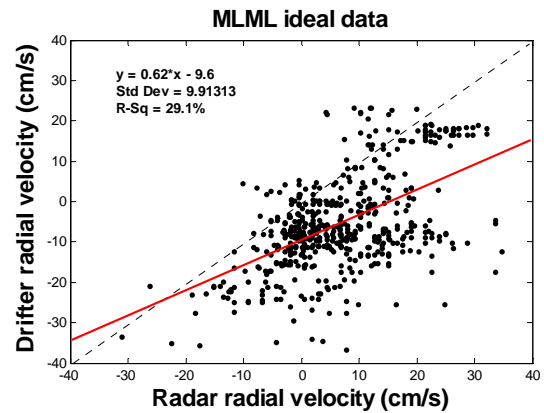
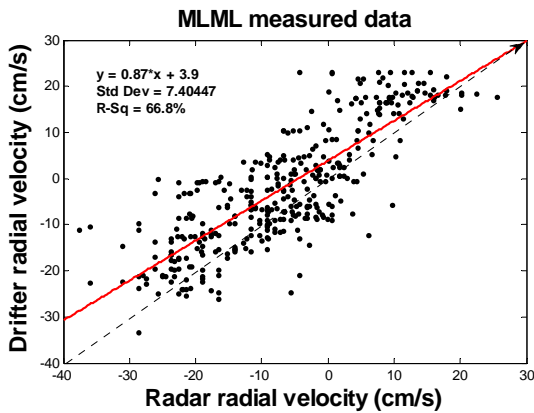
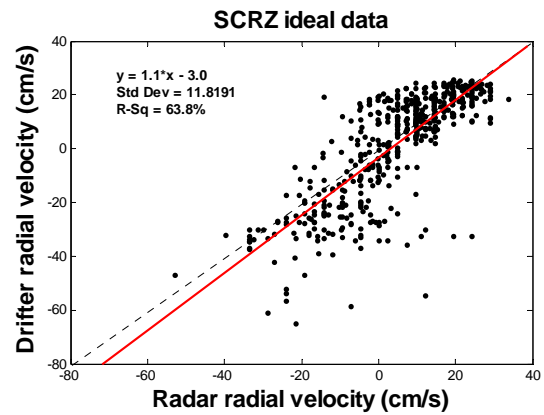
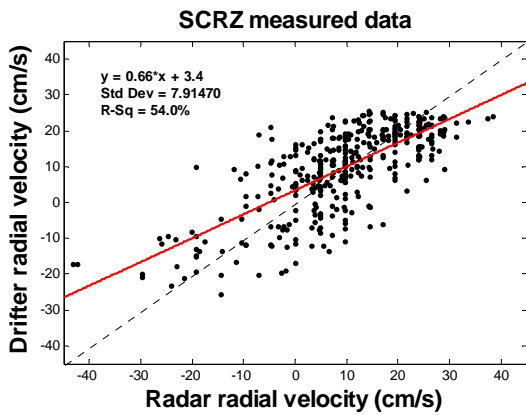
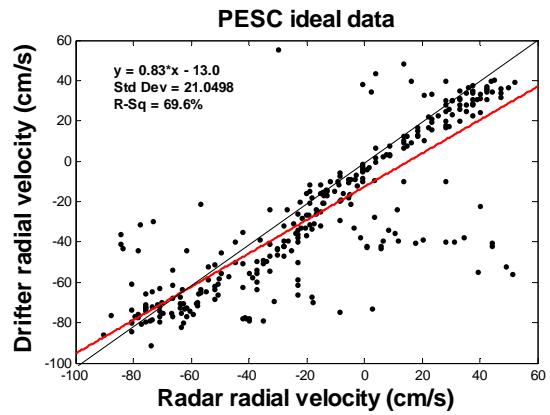


Figure 40. Scatter Plot of Drifter Radial Velocity vs. Radar Radial Velocity for Radar Sites PESC, SCRZ and MLML, respectively (First Experiment – 23-27 January 2008). Measured Radar Patterns are shown on the left and Ideal Radar Patterns are shown on the right. Dashed line represents one to one correlation and red solid line represents the linear least squares fit of the data. The standard deviation value refers to the best fit line.

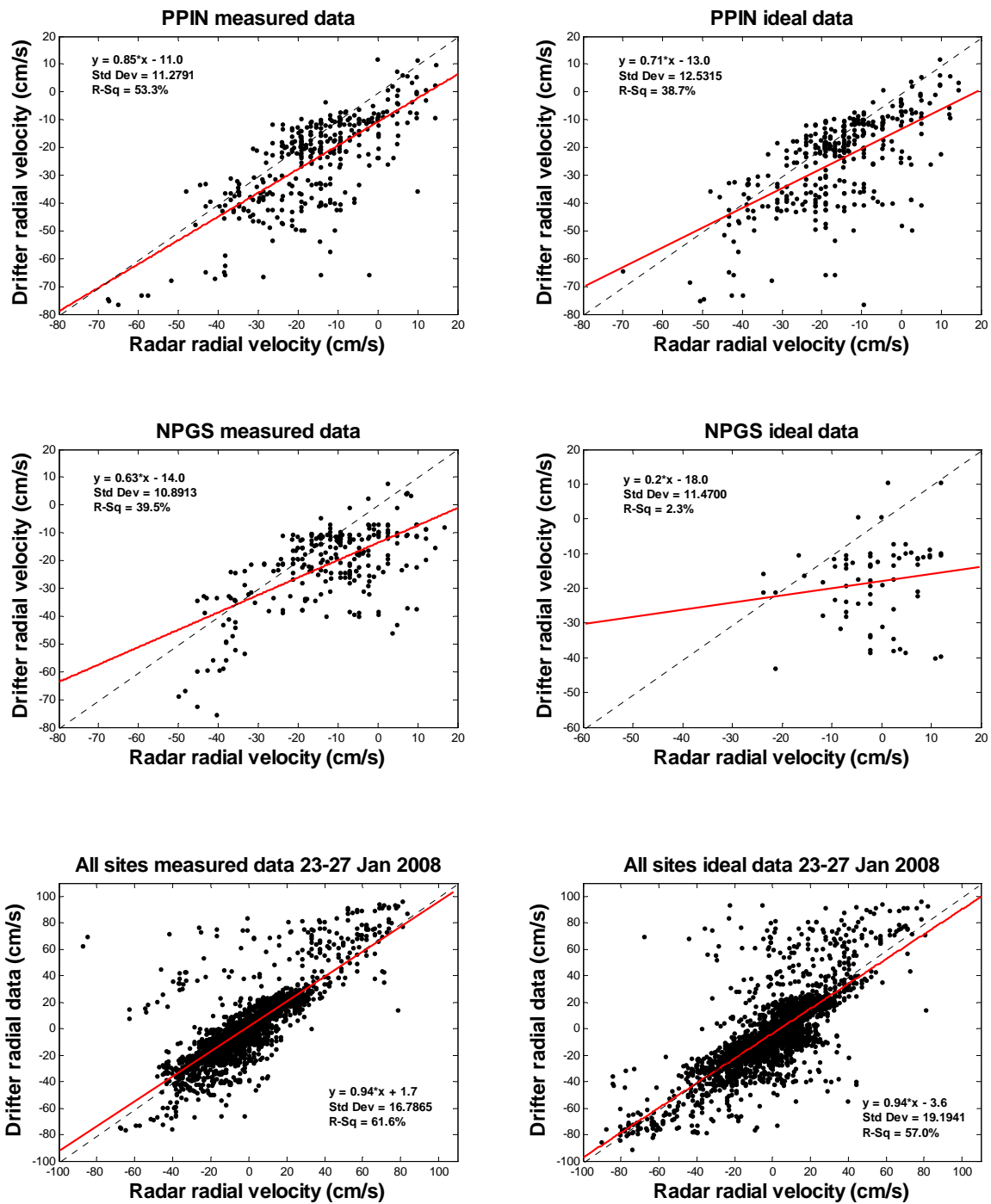


Figure 41. Scatter Plot of Drifter Radial Velocity vs. Radar Radial Velocity for Radar Sites PPIN and NPGS, respectively (First Experiment – 23-27 January 2008). Bottom graph is a combined plot of all Radar Sites in the first experiment. Measured Radar Patterns are shown on the left and Ideal Radar Patterns are shown on the right. Dashed line represents one to one correlation and red solid line represents the linear least squares fit of the data. The standard deviation value refers to the best fit line.

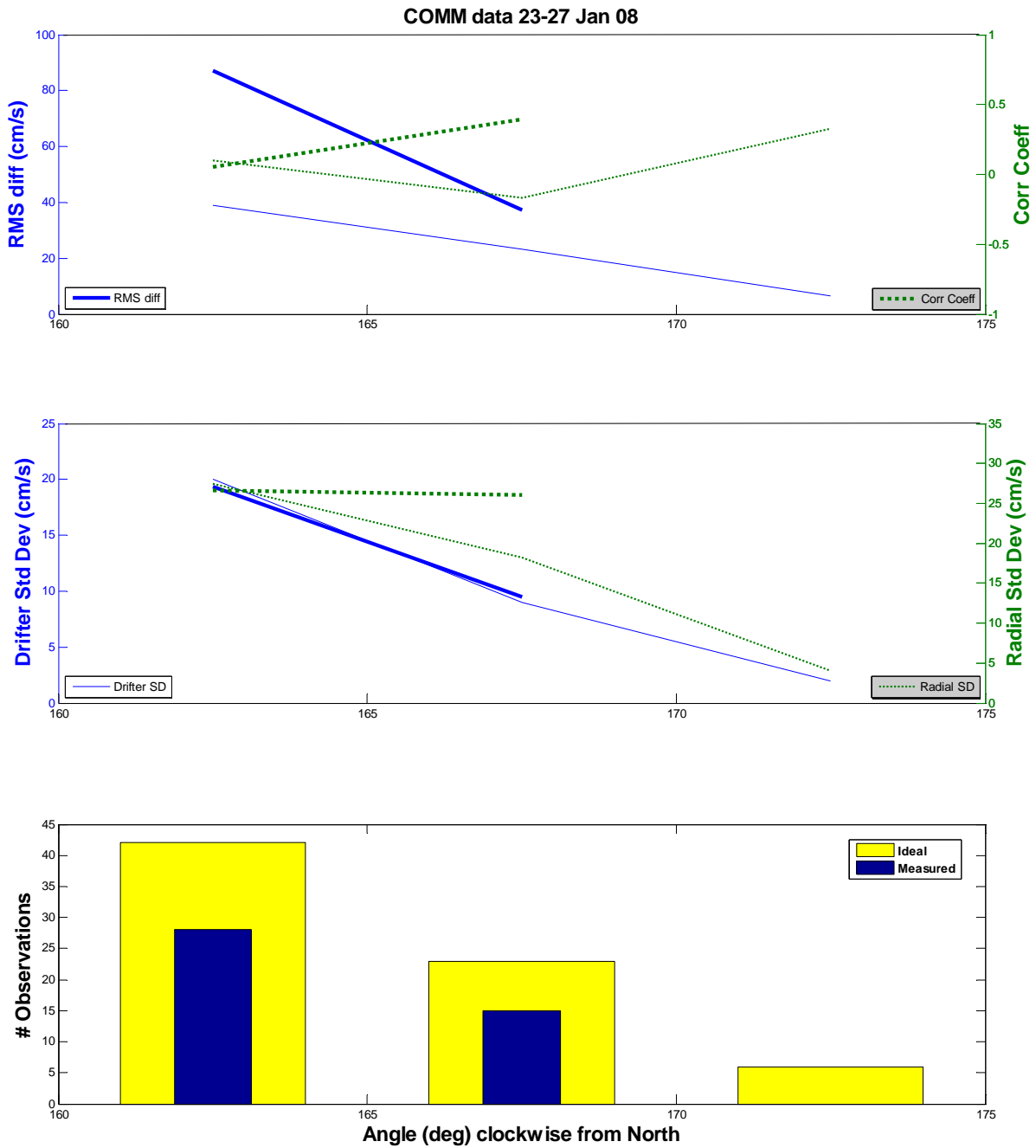


Figure 42. Correlation Coefficient and RMS difference plots vs. COMM Radar Look Angle (top) and corresponding Drifter and Radial Standard Deviation plots vs. COMM Radar Look Angle (middle). Bold lines represent measured data and thin lines represent ideal data. The lower plot indicates the number of drifter/radar point matches/observations that occurred vs. COMM Radar Look Angle. The thin blue bar represents the measured pattern and the wide yellow bar represents the ideal pattern. First experiment only.

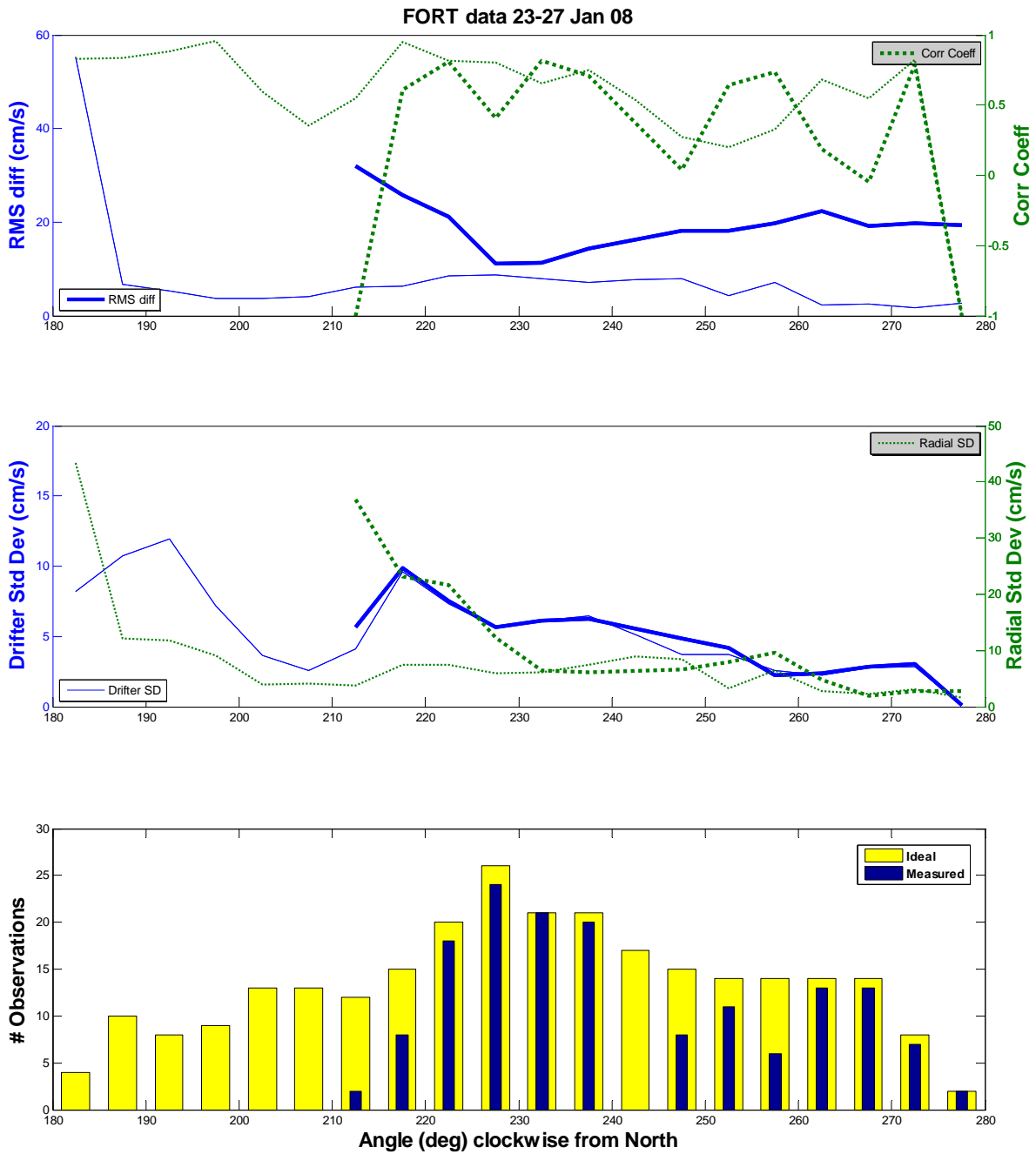


Figure 43. Correlation Coefficient and RMS difference plots vs. FORT Radar Look Angle (top) and corresponding Drifter and Radial Standard Deviation plots vs. FORT Radar Look Angle (middle). Bold lines represent measured data and thin lines represent ideal data. The lower plot indicates the number of drifter/radar point matches/observations that occurred vs. FORT Radar Look Angle. The thin blue bar represents the measured pattern and the wide yellow bar represents the ideal pattern. First experiment only.

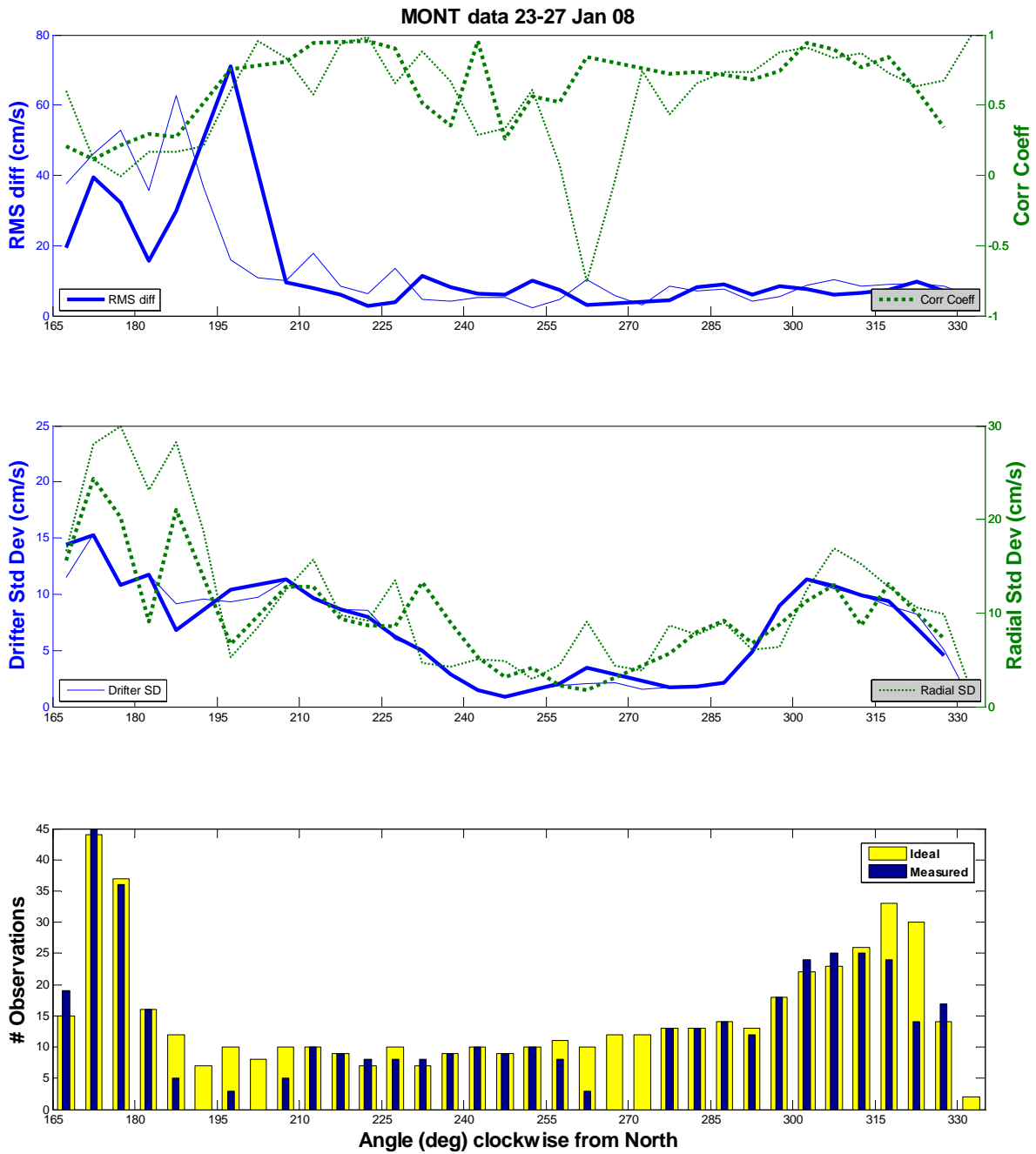


Figure 44. Correlation Coefficient and RMS difference plots vs. MONT Radar Look Angle (top) and corresponding Drifter and Radial Standard Deviation plots vs. MONT Radar Look Angle (middle). Bold lines represent measured data and thin lines represent ideal data. The lower plot indicates the number of drifter/radar point matches/observations that occurred vs. MONT Radar Look Angle. The thin blue bar represents the measured pattern and the wide yellow bar represents the ideal pattern. First experiment only.

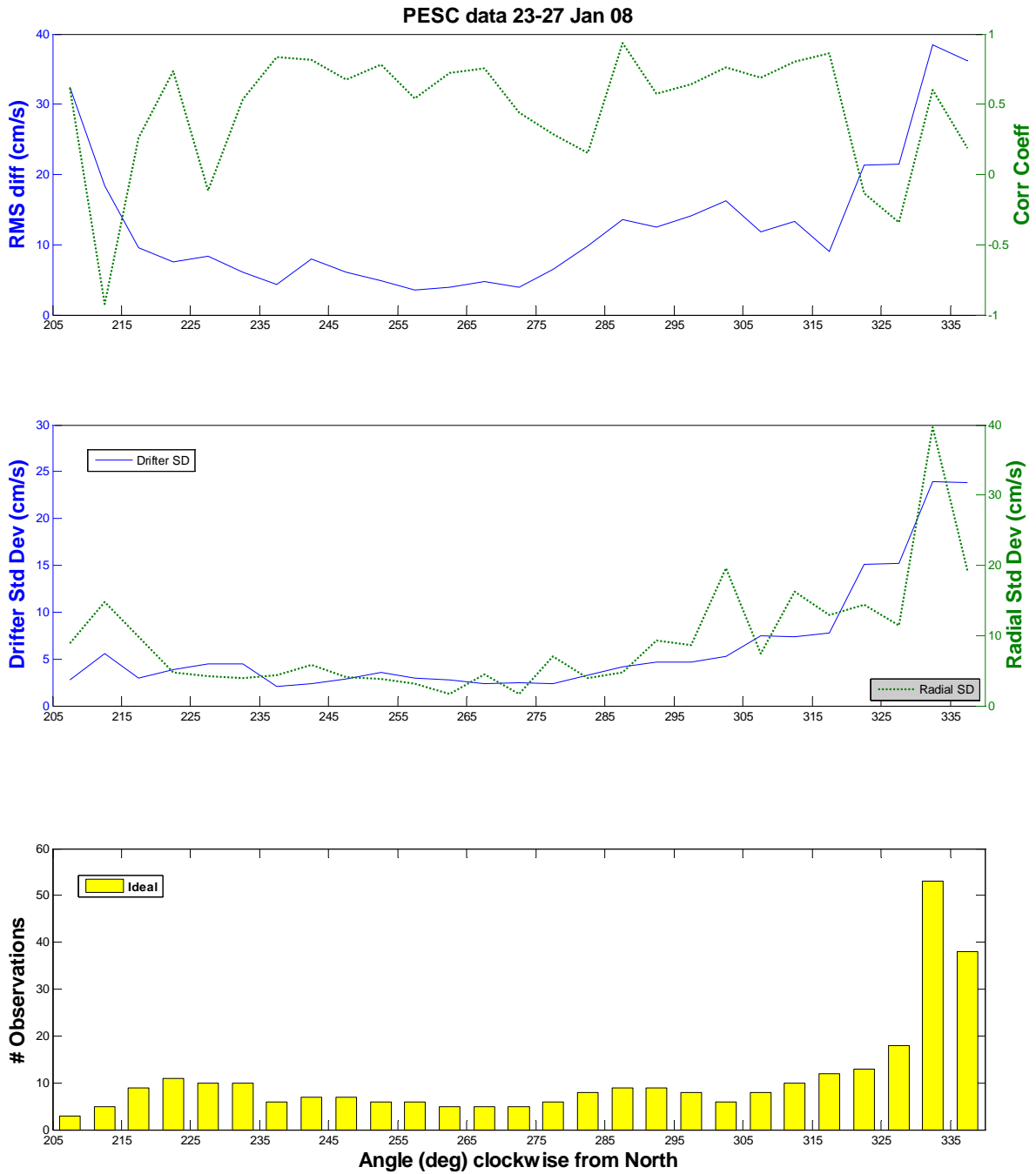


Figure 45. Correlation Coefficient and RMS difference plots vs. PESC Radar Look Angle (top) and corresponding Drifter and Radial Standard Deviation plots vs. PESC Radar Look Angle (middle). Thin lines represent ideal data. The lower plot indicates the number of drifter/radar point matches/observations that occurred vs. PESC Radar Look Angle. The wide yellow bar represents the ideal pattern. First experiment only.

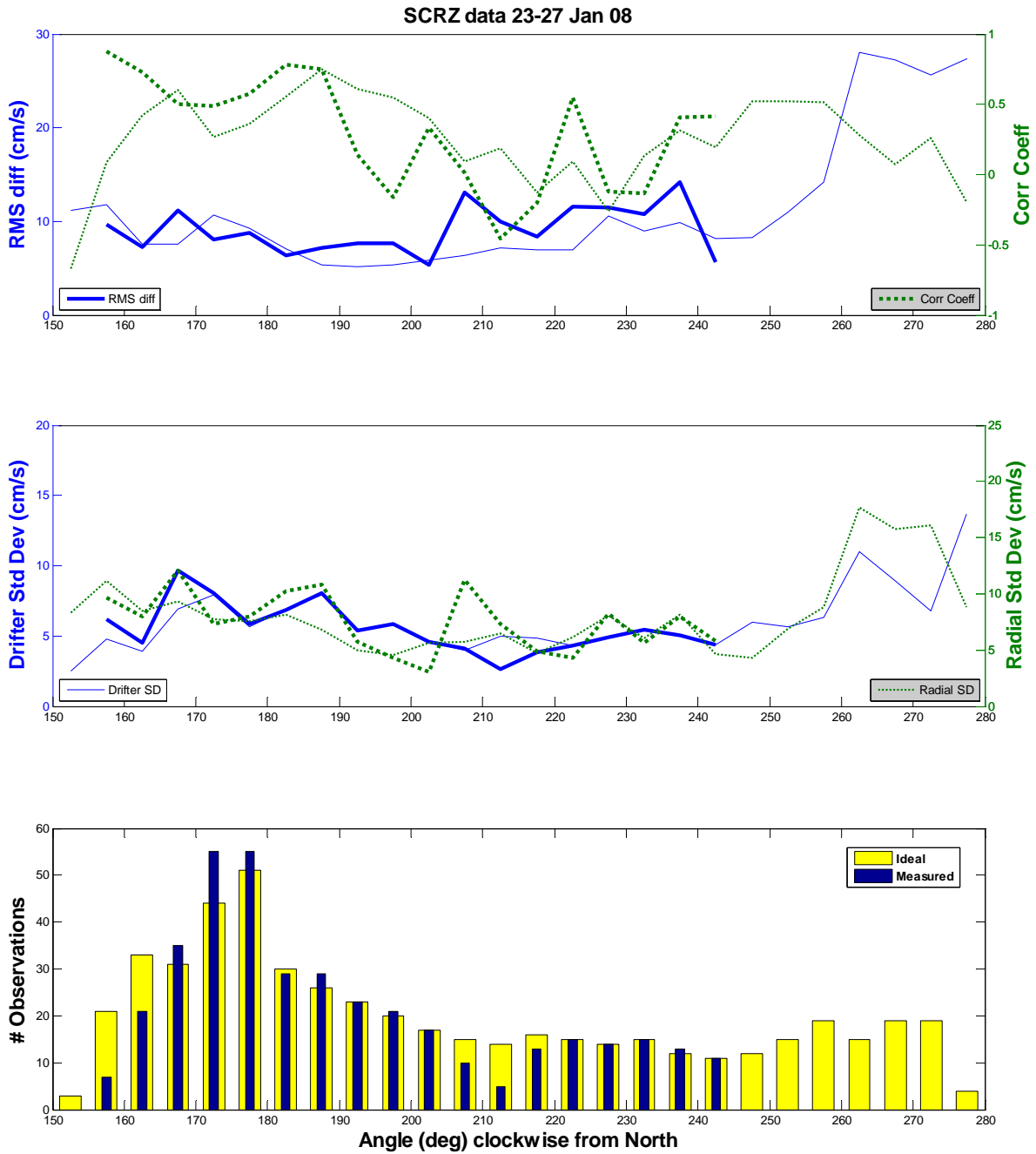


Figure 46. Correlation Coefficient and RMS difference plots vs. SCRZ Radar Look Angle (top) and corresponding Drifter and Radial Standard Deviation plots vs. SCRZ Radar Look Angle (middle). Bold lines represent measured data and thin lines represent ideal data. The lower plot indicates the number of drifter/radar point matches/observations that occurred vs. SCRZ Radar Look Angle. The thin blue bar represents the measured pattern and the wide yellow bar represents the ideal pattern. First experiment only.

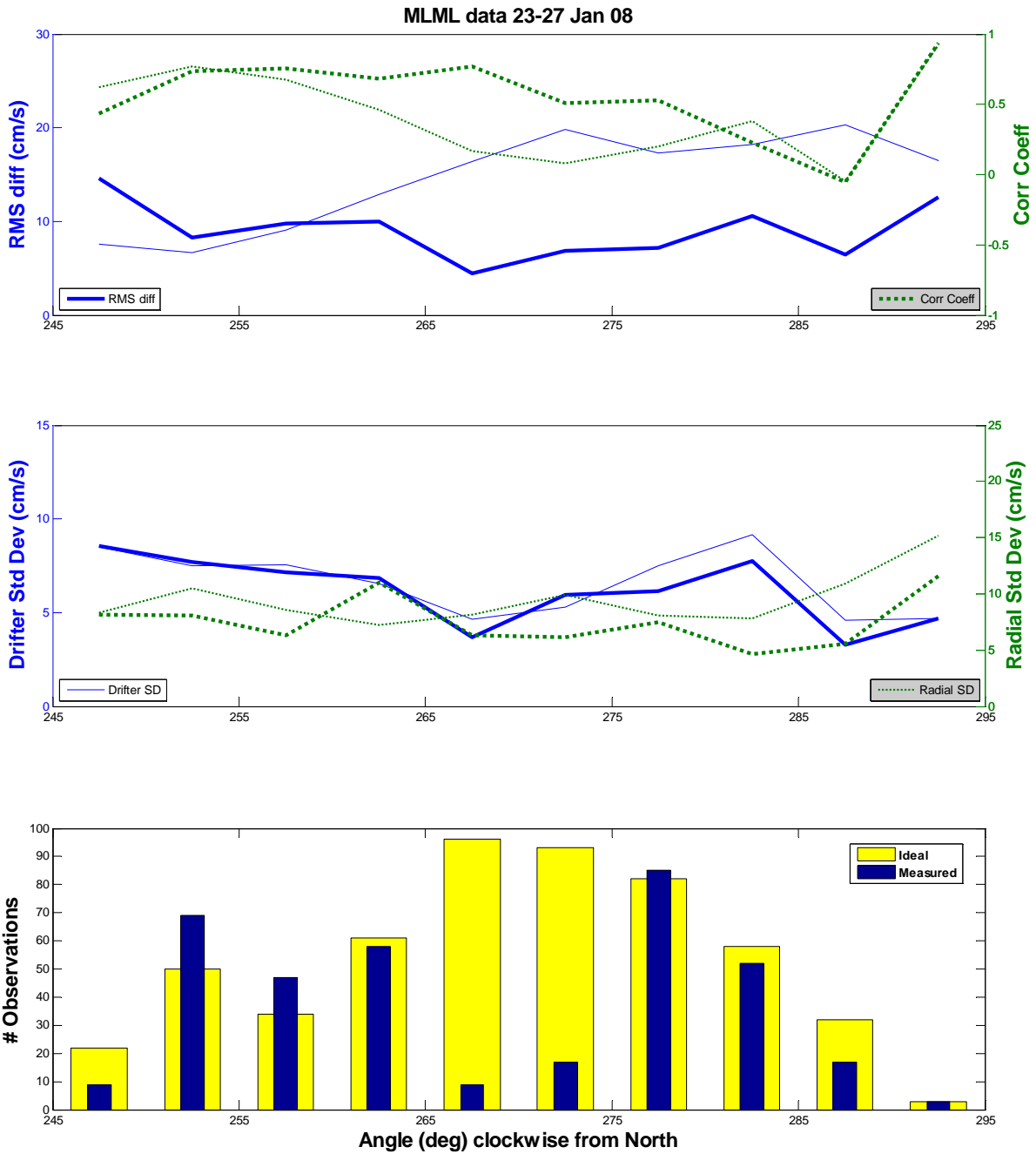


Figure 47. Correlation Coefficient and RMS difference plots vs. MLML Radar Look Angle (top) and corresponding Drifter and Radial Standard Deviation plots vs. MLML Radar Look Angle (middle). Bold lines represent measured data and thin lines represent ideal data. The lower plot indicates the number of drifter/radar point matches/observations that occurred vs. MLML Radar Look Angle. The thin blue bar represents the measured pattern and the wide yellow bar represents the ideal pattern. First experiment only.

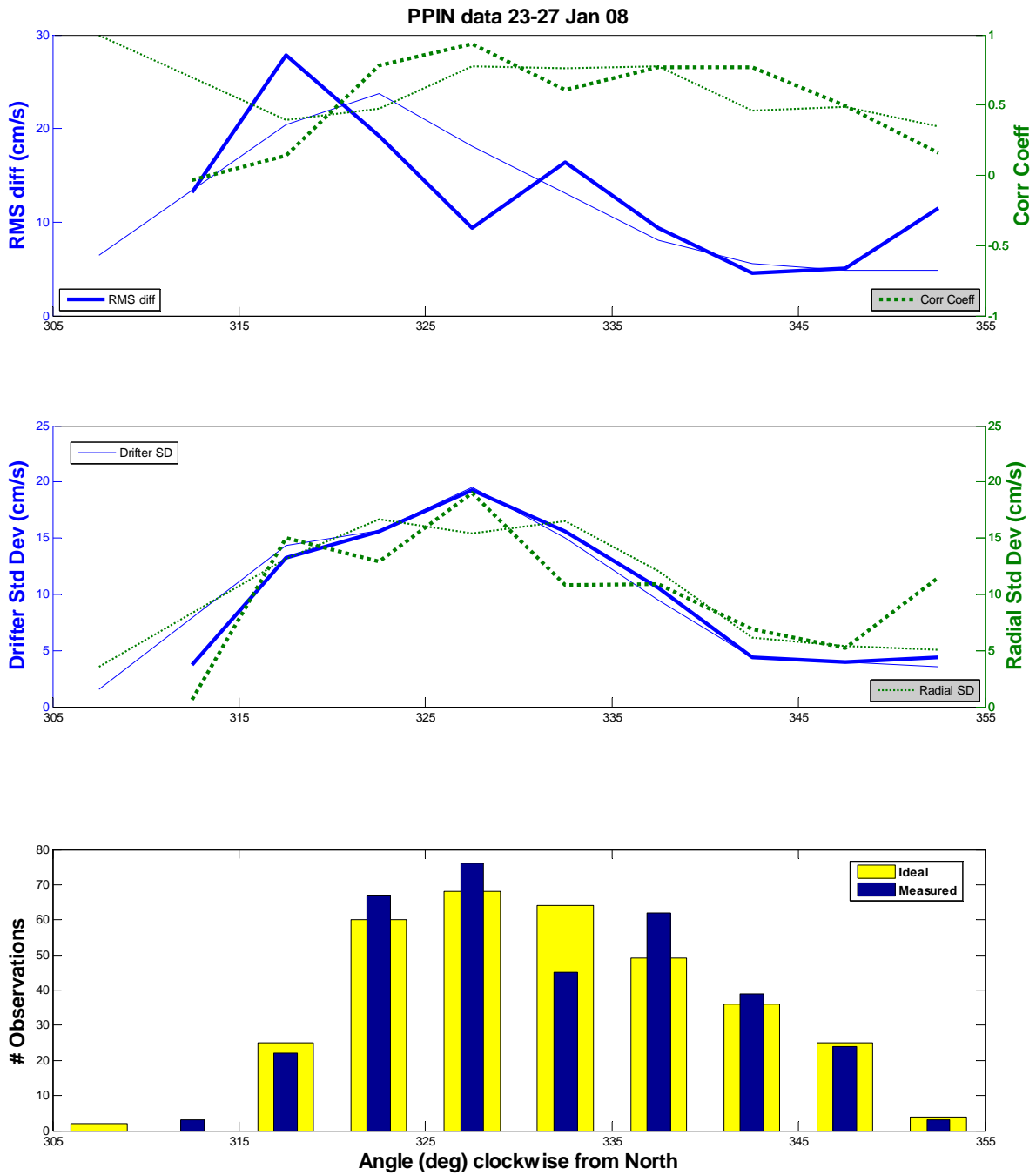


Figure 48. Correlation Coefficient and RMS difference plots vs. PPIN Radar Look Angle (top) and corresponding Drifter and Radial Standard Deviation plots vs. PPIN Radar Look Angle (middle). Bold lines represent measured data and thin lines represent ideal data. The lower plot indicates the number of drifter/radar point matches/observations that occurred vs. PPIN Radar Look Angle. The thin blue bar represents the measured pattern and the wide yellow bar represents the ideal pattern. First experiment only.

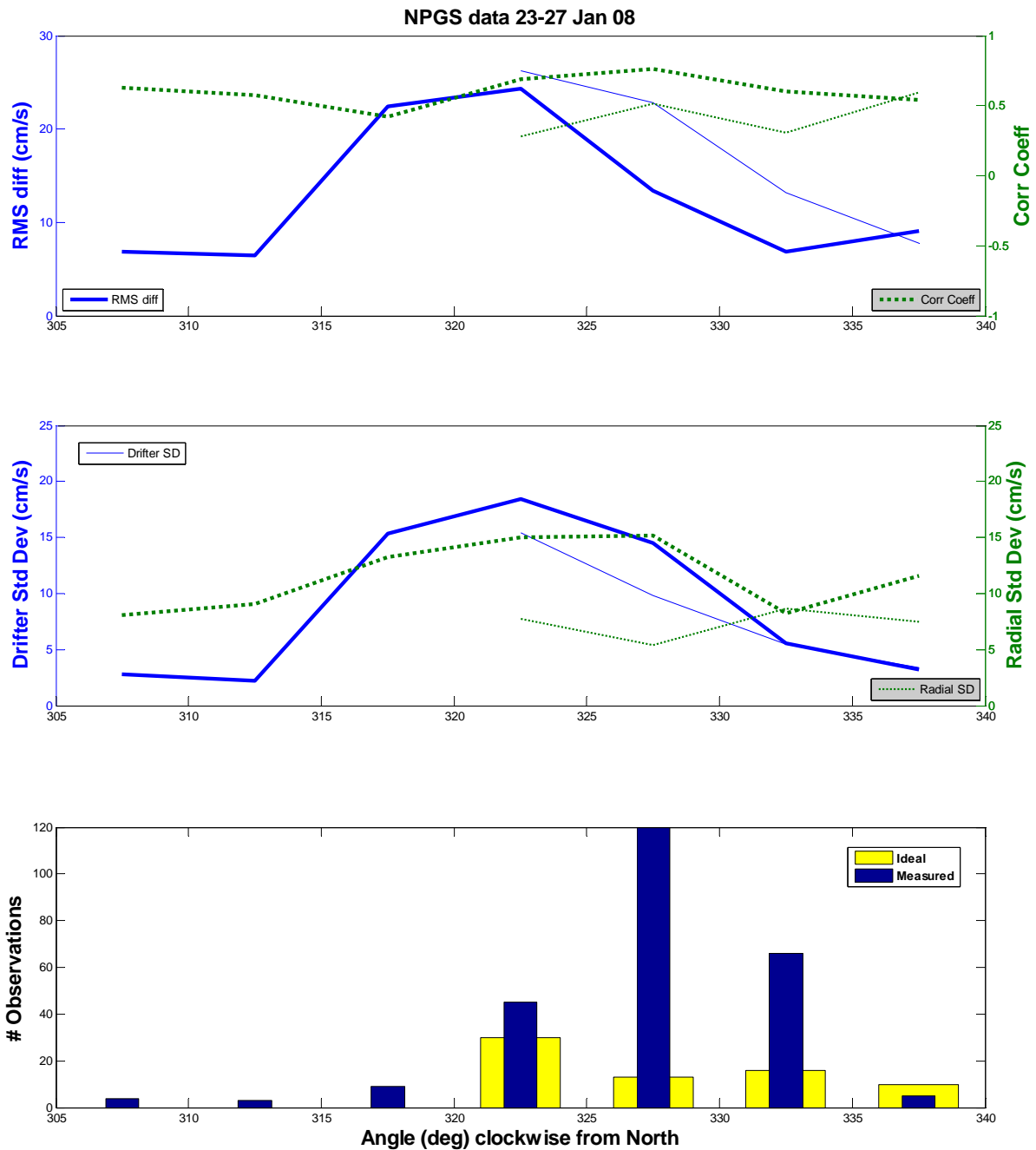


Figure 49. Correlation Coefficient and RMS difference plots vs. NPGS Radar Look Angle (top) and corresponding Drifter and Radial Standard Deviation plots vs. NPGS Radar Look Angle (middle). Bold lines represent measured data and thin lines represent ideal data. The lower plot indicates the number of drifter/radar point matches/observations that occurred vs. NPGS Radar Look Angle. The thin blue bar represents the measured pattern and the wide yellow bar represents the ideal pattern. First experiment only.

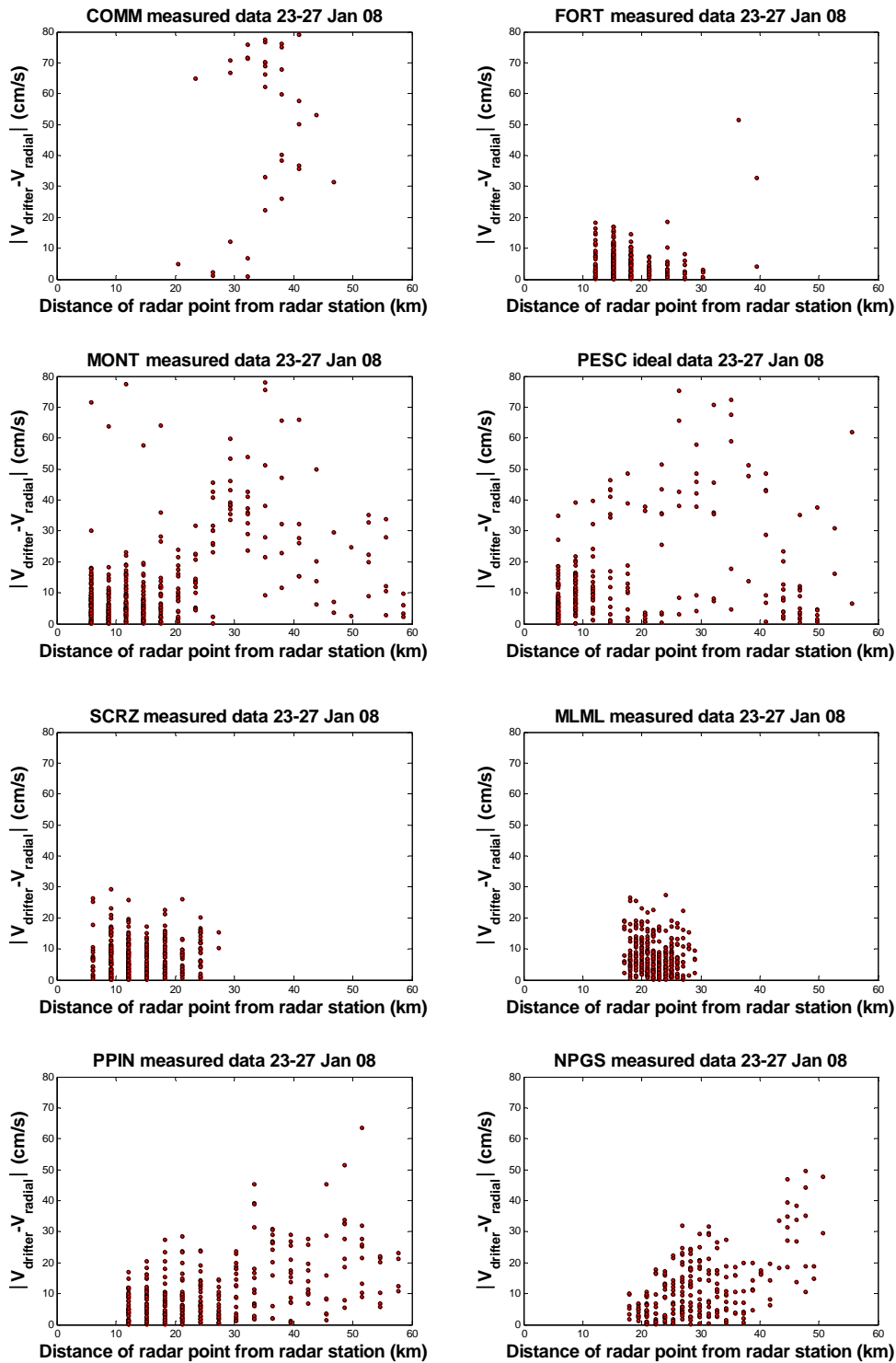


Figure 50. Plot of absolute value of (Drifter Radial Velocity minus Radar Radial Velocity) vs. Distance of radar point from radar station for each radar station (North to South). The 3 kilometer spatial range separation of each radar station's data is evident in the vertical groupings of the data. First experiment only.

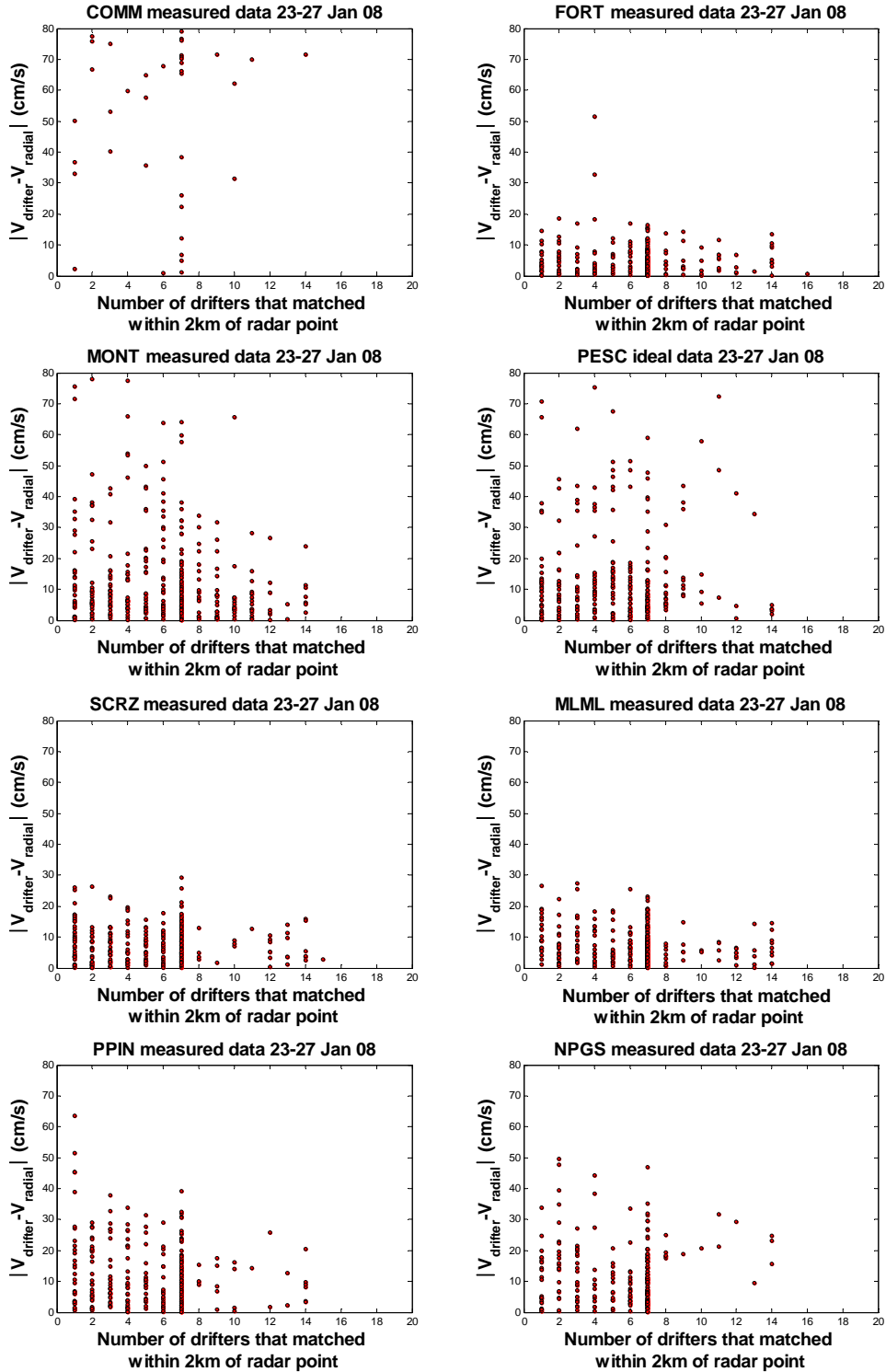


Figure 51. Plot of absolute value of (Drifter Radial Velocity minus Radar Radial Velocity) vs. the # of drifters that matched within 2km of a radial point for each radar station (North to South). Vertical groupings at intervals of 7 are indicative of the predominance of having a full range of drifter data (+/- 30 min) per hourly radar point. First experiment only.

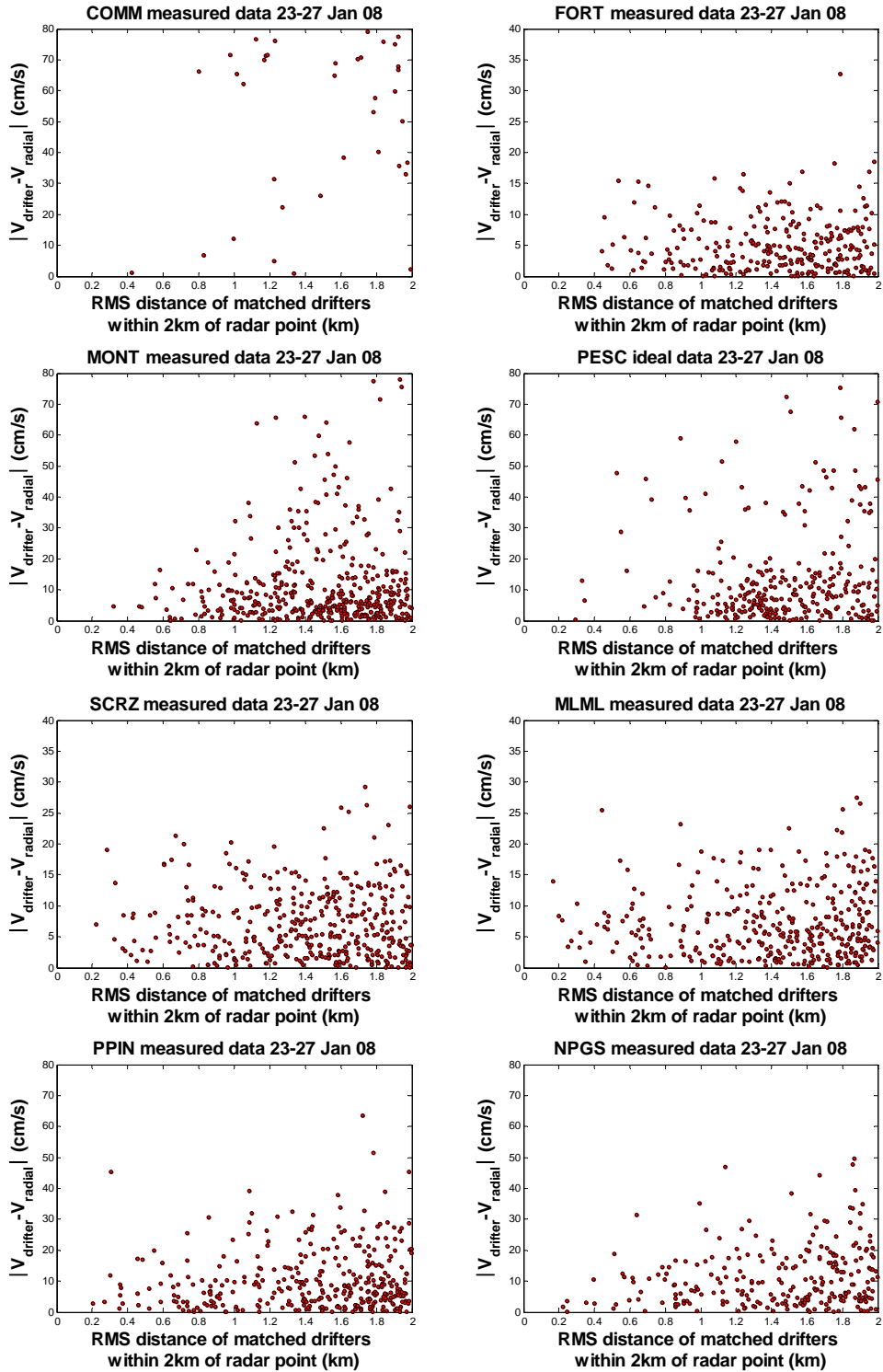


Figure 52. Plot of absolute value of (Drifter Radial Velocity minus Radar Radial Velocity) vs. the RMS distance of matched drifters within 2km of a radial point. First experiment only.

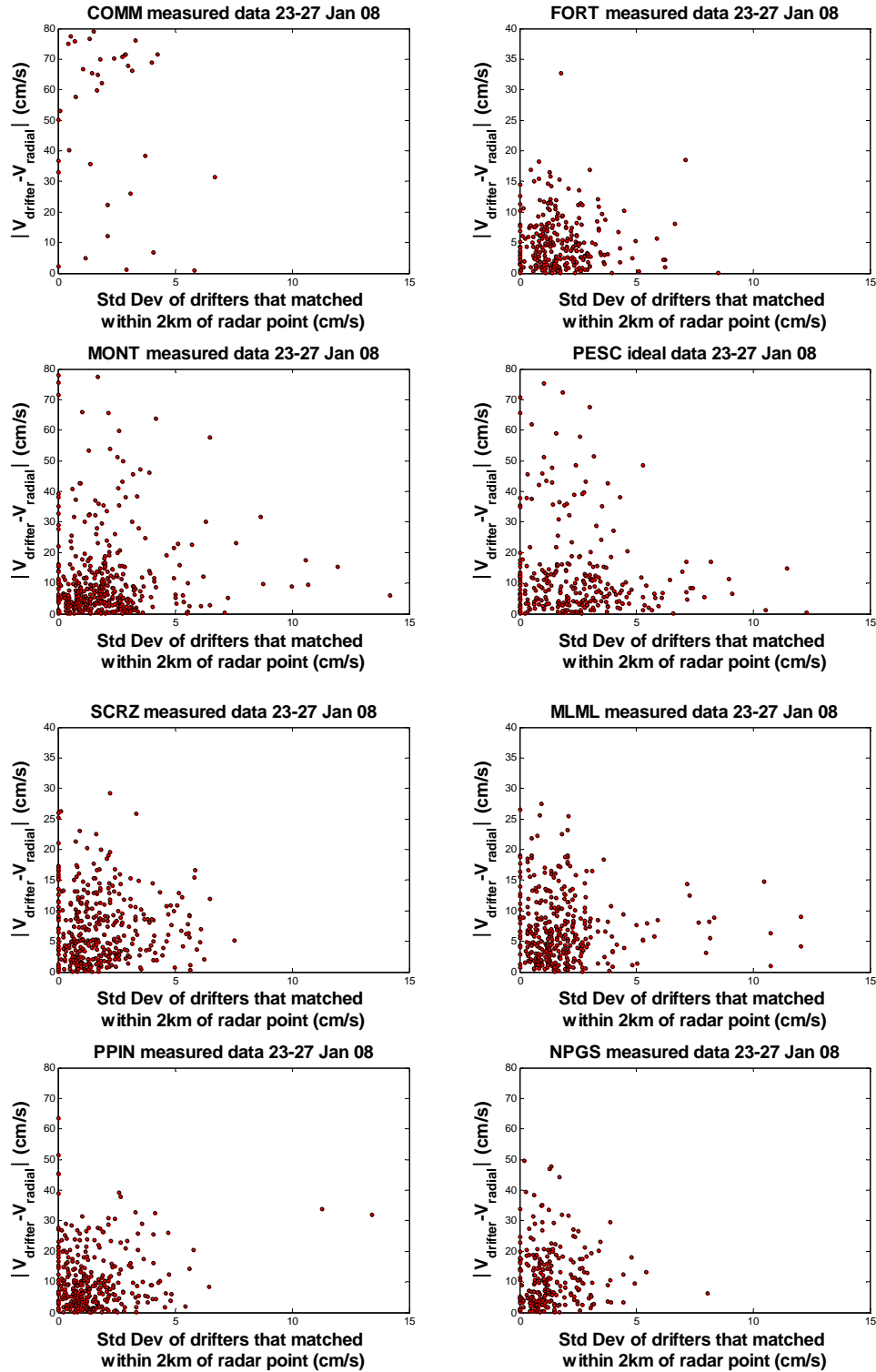


Figure 53. Plot of absolute value of (Drifter Radial Velocity minus Radar Radial Velocity) vs. the Standard Deviation of the drifters that matched within 2km of a radial point. Second experiment only.

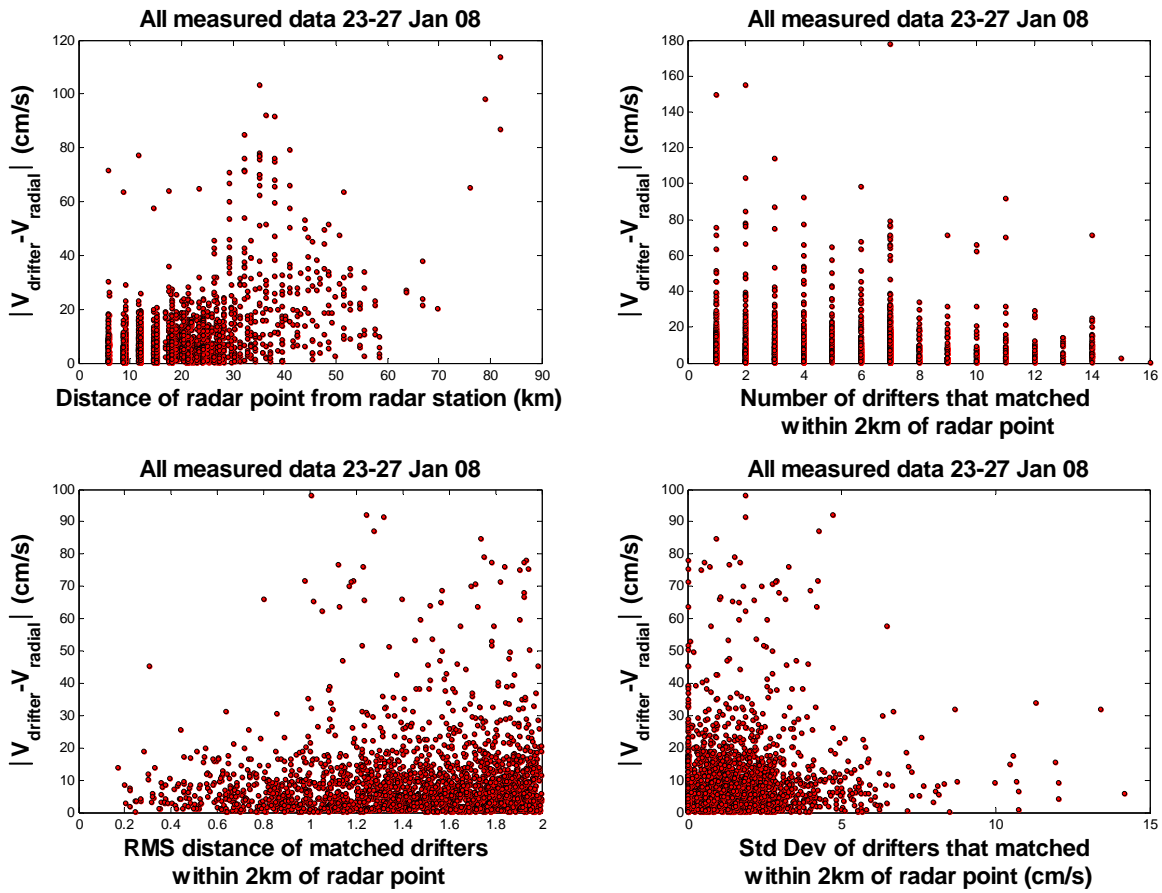


Figure 54. Plot of combined measured radar data for the second experiment vs. various queries.

<b>DRAK Measured data 1-10 Apr 08</b>				
<b>Weighted temporal Quality Range</b>	<b>Number of Values</b>	<b>% Cumulative Sum</b>	<b>Cumulative RMS difference</b>	<b>Cumulative R<sup>2</sup></b>
0<1	178	7.76	8.7630	0.7234
1<2	574	32.78	8.5862	0.7289
2<3	553	56.89	9.1904	0.6897
3<4	369	72.97	9.5258	0.6657
4<5	227	82.87	9.8592	0.6421
5<6	143	89.10	10.0076	0.6345
6<7	88	92.94	10.0739	0.6282
7<8	51	95.16	10.1408	0.6254
8<9	37	96.77	10.1735	0.6238
9<10	38	98.43	10.3803	0.6111
10<11	14	99.04	10.4080	0.6102
11<12	6	99.30	10.4379	0.6079
12<13	4	99.48	10.4472	0.6069
13<14	7	99.78	10.5109	0.6027
14<15	0	99.78	10.5109	0.6027
15<16	3	99.91	10.5348	0.6012
16<17	1	99.96	10.5325	0.6012
17<18	1	100.00	10.5370	0.6012

Table 5. Summary of DRAK weighted temporal quality results

<b>COMM Measured data 1-10 Apr 08</b>				
<b>Weighted temporal Quality Range</b>	<b>Number of Values</b>	<b>% Cumulative Sum</b>	<b>Cumulative RMS difference</b>	<b>Cumulative R<sup>2</sup></b>
0<1	435	13.54	6.5473	0.7205
1<2	1028	45.55	7.0106	0.6689
2<3	731	68.31	7.1636	0.654
3<4	449	82.29	7.4328	0.6288
4<5	257	90.29	7.7362	0.6022
5<6	110	93.71	7.8963	0.5933
6<7	77	96.11	7.9313	0.5912
7<8	54	97.79	8.0103	0.5847
8<9	22	98.47	8.0613	0.5811
9<10	15	98.94	8.0653	0.5807
10<11	14	99.38	8.0925	0.5794
11<12	7	99.60	8.1017	0.5788
12<13	8	99.84	8.1071	0.5777
13<14	3	99.94	8.1150	0.5771
14<15	0	99.94	8.1150	0.5771
15<16	0	99.94	8.1150	0.5771
16<17	0	99.94	8.1150	0.5771
17<18	1	99.97	8.1153	0.5771
18<19	1	100.00	8.1448	0.5771

Table 6. Summary of COMM weighted temporal quality results

<b>SLID Measured data 1-10 Apr 08</b>				
<b>Weighted temporal Quality Range</b>	<b>Number of Values</b>	<b>% Cumulative Sum</b>	<b>Cumulative RMS difference</b>	<b>Cumulative R<sup>2</sup></b>
0<1	203	6.51	7.0605	0.6342
1<2	788	31.76	7.7684	0.5998
2<3	810	57.72	8.3827	0.5569
3<4	544	75.16	8.8111	0.5202
4<5	341	86.09	9.0942	0.4946
5<6	201	92.53	9.2720	0.4826
6<7	94	95.54	9.4442	0.4694
7<8	48	97.08	9.5161	0.4672
8<9	43	98.46	9.6168	0.4611
9<10	14	98.91	9.6950	0.4546
10<11	14	99.36	9.6879	0.4565
11<12	7	99.58	9.7129	0.4545
12<13	1	99.62	9.7113	0.4545
13<14	4	99.74	9.7378	0.4523
14<15	3	99.84	9.7364	0.4539
15<16	4	99.97	9.7371	0.4538
16<17	1	100.00	9.7412	0.4538

Table 7. Summary of SLID weighted temporal quality results

<b>FORT Measured data 1-10 Apr 08</b>				
<b>Weighted temporal Quality Range</b>	<b>Number of Values</b>	<b>% Cumulative Sum</b>	<b>Cumulative RMS difference</b>	<b>Cumulative R<sup>2</sup></b>
0<1	183	9.78	11.3907	0.2731
1<2	488	35.86	10.5541	0.3437
2<3	385	56.44	10.8063	0.3329
3<4	286	71.73	11.2653	0.2996
4<5	212	83.06	11.3235	0.304
5<6	106	88.72	11.4999	0.2886
6<7	75	92.73	11.5154	0.2858
7<8	53	95.56	11.7411	0.2661
8<9	32	97.27	11.7748	0.2631
9<10	19	98.29	11.8038	0.2605
10<11	14	99.04	11.8356	0.2566
11<12	8	99.47	11.8339	0.257
12<13	4	99.68	11.8264	0.2585
13<14	2	99.79	11.8220	0.2584
14<15	2	99.89	11.8166	0.2586
15<16	1	99.95	11.8147	0.2586
16<17	1	100.00	11.8147	0.2586

Table 8. Summary of FORT weighted temporal quality results

<b>MONT Measured data 1-10 Apr 08</b>				
<b>Weighted temporal Quality Range</b>	<b>Number of Values</b>	<b>% Cumulative Sum</b>	<b>Cumulative RMS difference</b>	<b>Cumulative R<sup>2</sup></b>
0<1	67	4.93	14.3821	0.3409
1<2	246	23.01	14.1899	0.3214
2<3	215	38.82	14.9979	0.2889
3<4	208	54.12	15.0355	0.276
4<5	141	64.49	14.9177	0.2843
5<6	127	73.82	15.2009	0.255
6<7	104	81.47	15.0922	0.2529
7<8	63	86.10	15.2730	0.2473
8<9	52	89.93	15.3039	0.2453
9<10	34	92.43	15.3829	0.241
10<11	41	95.44	15.4970	0.2341
11<12	18	96.76	15.5629	0.235
12<13	14	97.79	15.6501	0.227
13<14	10	98.53	15.6662	0.2273
14<15	4	98.82	15.6625	0.2265
15<16	7	99.34	15.6793	0.2248
16<17	4	99.63	15.6989	0.2234
17<18	2	99.78	15.7077	0.224
18<19	1	99.85	15.7254	0.224
19<20	2	100.00	15.7154	0.2221

Table 9. Summary of MONT weighted temporal quality results

<b>PILR Measured data 1-10 Apr 08</b>				
<b>Weighted temporal Quality Range</b>	<b>Number of Values</b>	<b>% Cumulative Sum</b>	<b>Cumulative RMS difference</b>	<b>Cumulative R<sup>2</sup></b>
0<1	11	3.21	11.0073	0.5222
1<2	36	13.70	9.1903	0.6345
2<3	47	27.41	10.2846	0.5705
3<4	50	41.98	12.1091	0.5036
4<5	49	56.27	13.3584	0.4663
5<6	31	65.31	13.7033	0.4277
6<7	22	71.72	13.5626	0.4331
7<8	21	77.84	13.7331	0.4173
8<9	16	82.51	13.5050	0.424
9<10	14	86.59	13.8973	0.4054
10<11	11	89.80	14.3901	0.3705
11<12	11	93.00	14.7092	0.3465
12<13	6	94.75	14.9460	0.3334
13<14	7	96.79	15.1911	0.3234
14<15	3	97.67	15.1241	0.3236
15<16	4	98.83	15.4723	0.3082
16<17	0	98.83	15.4723	0.3082
17<18	2	99.42	15.7432	0.2968
18<19	2	100.00	15.7801	0.2938

Table 10. Summary of PILR weighted temporal quality results

<b>PESC Measured data 1-10 Apr 08</b>				
<b>Weighted temporal Quality Range</b>	<b>Number of Values</b>	<b>% Cumulative Sum</b>	<b>Cumulative RMS difference</b>	<b>Cumulative R<sup>2</sup></b>
0<1	42	5.65	12.7723	0.3124
1<2	117	21.37	14.2765	0.2016
2<3	133	39.25	14.4198	0.1711
3<4	120	55.38	14.0117	0.1658
4<5	96	68.28	14.1208	0.1828
5<6	73	78.09	14.4803	0.1569
6<7	44	84.01	14.4581	0.1529
7<8	48	90.46	14.3739	0.1574
8<9	15	92.47	14.6883	0.1436
9<10	23	95.56	14.8088	0.1376
10<11	12	97.18	14.9556	0.1305
11<12	9	98.39	15.0200	0.1338
12<13	1	98.52	15.0910	0.1338
13<14	5	99.19	15.1551	0.1272
14<15	2	99.46	15.1693	0.127
15<16	1	99.60	15.1821	0.127
16<17	1	99.73	15.1718	0.127
17<18	0	99.73	15.1718	0.127
18<19	1	99.87	15.2207	0.127
19<20	1	100.00	15.2105	0.127

Table 11. Summary of PESC weighted temporal quality results

<b>BIGC Ideal data 1-10 Apr 08</b>				
<b>Weighted temporal Quality Range</b>	<b>Number of Values</b>	<b>% Cumulative Sum</b>	<b>Cumulative RMS difference</b>	<b>Cumulative R<sup>2</sup></b>
0<1	13	9.63	13.4289	0.5146
1<2	21	25.19	18.7001	0.2623
2<3	24	42.96	21.2116	0.2123
3<4	20	57.78	21.2190	0.1724
4<5	17	70.37	20.4605	0.1797
5<6	9	77.04	20.3923	0.2124
6<7	11	85.19	19.8347	0.2344
7<8	9	91.85	19.7024	0.2366
8<9	1	92.59	19.6375	0.2366
9<10	7	97.78	19.9010	0.2392
10<11	0	97.78	19.9010	0.2392
11<12	0	97.78	19.9010	0.2392
12<13	2	99.26	19.8039	0.2463
13<14	0	99.26	19.8039	0.2463
14<15	0	99.26	19.8039	0.2463
15<16	0	99.26	19.8039	0.2463
16<17	0	99.26	19.8039	0.2463
17<18	0	99.26	19.8039	0.2463
18<19	0	99.26	19.8039	0.2463
19<20	1	100.00	19.8285	0.2463

Table 12. Summary of BIGC weighted temporal quality results

THIS PAGE INTENTIONALLY LEFT BLANK

## LIST OF REFERENCES

- Barrick, D.E., M.W. Evans and B.L. Weber, 1977: Ocean surface currents mapped by radar. *Science*, **198**, 138-144.
- Chapman, R.D., L.K. Shay, H.C. Graber, J.B. Edson, A. Karachintsev, C.L. Trump, and D.B. Ross, 1997: On the accuracy of HF radar surface current measurements: Inter-comparison with ship-based sensors. *J. Geophys. Res.*, **102** (C8), 18,737-18,748.
- CODAR Ocean Sensors, 2007: LonLatUVFormat, [http://www.codaros.com/Manuals/SeaSonde/Docs/GuidesToFileFormats/File\\_LonLatUV\\_RDL\\_TOT\\_ELP.pdf](http://www.codaros.com/Manuals/SeaSonde/Docs/GuidesToFileFormats/File_LonLatUV_RDL_TOT_ELP.pdf) (accessed on September 8, 2008).
- Crombie, D.D., 1955: Doppler spectrum of sea echo at 13.56 Me/s. *Nature*, **175**, 681-682.
- Devore, J.L., 2004: *Probability and Statistics*. Brooks/Cole, Toronto, 795 pp.
- Emery, B. M., L. Washburn, and J. A. Harlan, 2004: Evaluating radial current measurements from CODAR high-frequency radars with moored current meters. *J. Atmos. Oceanic Technol.*, **21**, 1259–1271.
- Holbrook, J. R., and A. S. Frisch, 1981: A comparison of near-surface CODAR and VACM measurements in the Strait of Juan de Fuca, August 1978. *J. Geophys. Res.*, **86**, 10 908–10 912.
- Kaplan, D. M., J. Largier, and L. W. Botsford, 2005: HF radar observations of surface circulation off Bodega Bay (northern California, USA). *J. Geophys. Res.*, **110**, C10020, doi:10.1029/2005JC002959.
- Kim, K.C., 2004: calibration and validation of high frequency radar for ocean surface current mapping. Master's Thesis, Naval Postgraduate School, Monterey, CA.
- Kohut, J.T., and S.M. Glenn, 2003: Improving HF radar surface current measurements with measured antenna beam patterns. *Journal of Atmospheric and Oceanic Technology*. **20**, 1303.
- Niiler, P. P., R. Davis and H. White, 1987: Water-following characteristics of a mixed-layer drifter. *Deep-Sea Res.* **34**, 1867-1882.
- Ohlmann, C., P.White, L. Washburn, E. Terrill, B. Emory, M. Otero, 2006: Interpretation of coastal HF radar – derived surface currents with high-resolution drifter data. *Journal of Atmospheric and Ocean Technology*. **24**, 666-680.

- Paduan, J.D., K.C. Kim, M.S. Cook, and F.P. Chavez, 2006: Calibration and validation of direction-finding high frequency radar ocean surface current observations. *IEEE J. Oceanic Engineering*, 10.1109/JOE.2006.886195, 862-875.
- \_\_\_\_\_, and H.C. Graber, 1997: Introduction to High-Frequency radar: Realty and myth. *Oceanography*, **10**, 36-39.
- \_\_\_\_\_, and L.K. Rosenfeld, 1996: Remotely sensed surface currents in Monterey Bay from shore-based HF radar (Coastal Ocean Dynamics Application Radar). *J. Geophys. Res.*, **101**, 20 669–20 686.
- Prandle, 1991: A new view of near-shore dynamics based on observations from HF radar. *Progr. Oceanogr.*, **27**, 403-438.
- Schott, F. A., S. A. Frisch and J. C. Larsen, 1986: Comparison of surface currents measured by HF Doppler Radar in the western Florida straits during November 1983 to January 1984 and Florida current transports. *J. Geophys. Res.*, **91**, 8451–8460.
- Stewart, R.H. and J.W. Joy, 1974: HF radar measurement of surface current. *Deep-Sea Res.*, **21**, 1039-1049.

## INITIAL DISTRIBUTION LIST

1. Defense Technical Information Center  
Ft. Belvoir, Virginia
2. Dudley Knox Library  
Naval Postgraduate School  
Monterey, California
3. Dr. Jeffrey D. Paduan  
Department of Oceanography, OC/PD  
Naval Postgraduate School  
Monterey, California
4. Dr. Mary L. Batteen  
Department of Oceanography, OC/BV  
Naval Postgraduate School  
Monterey, California
5. Dr. Leslie Rosenfeld  
Department of Oceanography, OC/RO  
Naval Postgraduate School  
Monterey, California
6. Dr. Curtis A. Collins  
Department of Oceanography, OC/CO  
Naval Postgraduate School  
Monterey, California
7. Dr. Donald Barrick, President  
Codar Ocean Sensors, Ltd.  
Los Altos, California
8. Dr. Newell Garfield, Director  
Romberg Tiburon Center  
San Francisco State University  
Tiburon, California
9. Dr. Jack Harlan  
NOAA IOOS Program  
Silver Springs, Maryland

10. Dr. Glenn Watabushy  
NOAA ERD  
Seattle, Washington
11. Dr. Carter Ohlmann  
University of California  
Santa Barbara, California